VOL. 107 NO. HY4. APRIL 1981

JOURNAL OF THE HYDRAULICS DIVISION

PROCEEDINGS OF
THE AMERICAN SOCIETY
OF CIVIL ENGINEERS

VOL.107 NO.HY4. APRIL 1981

JOURNAL OF THE HYDRAULICS DIVISION

PROCEEDINGS OF THE AMERICAN SOCIETY OF CIVIL ENGINEERS

Copyright© 1981 by
American Society
of Civil Engineers
All Rights Reserved
ISSN 0044-796X

AMERICAN SOCIETY OF CIVIL ENGINEERS

BOARD OF DIRECTION

President
Irvan F. Mendenhall

Past President
Joseph S. Ward

President Elect
James R. Sims

Vice Presidents
Robert D. Bay
Francis J. Connell
Lyman R. Gillis
Albert A. Grant

Directors
Martin G. Abegg
Floyd A. Bishop
L. Gary Byrd
Larry J. Feeser
John A. Focht, Jr.
Sergio Gonzalez-Karg
James E. Humphrey, Jr.
Richard W. Karn
Leon D. Luck
Arthur R. McDaniel
Paul R. Munger
William R. Neuman
Leonard S. Oberman
John D. Parkhurst
Celestino R. Pennoni
Robert B. Rhode
S. Russell Stearns
William H. Taylor
Stafford E. Thornton
Robert E. Whiteside
Richard S. Woodruff

EXECUTIVE OFFICERS

Eugene Zwoyer, *Executive Director*
Julie E. Gibouleau, *Assistant to the Executive Director*
Louis L. Meier, *Washington Counsel/Assistant Secretary*
William H. Wisely, *Executive Director Emeritus*
Michael N. Salgo, *Treasurer*
Elmer B. Isaak, *Assistant Treasurer*

STAFF DIRECTORS

Donald A. Buzzell, *Managing Director for Education and Professional Affairs*
Robert A. Crist, Jr., *Managing Director for Publications and Technical Affairs*
Alexander Korwek, *Managing Director for Finance and Administrative Services*
Alexandra Bellow, *Director, Human Resources*
David Dresia, *Director, Publications Production and Marketing*
Barker D. Herr, *Director, Membership*
Richard A. Jeffers, *Controller*
Carl E. Nelson, *Director, Field Services*
Don P. Reynolds, *Director, Policy, Planning and Public Affairs*
Bruce Rickerson, *Director, Legislative Services*
James M. Shea, *Director, Public Communications*
Albert W. Turchick, *Director, Technical Services*
George K. Wadlin, *Director, Education Services*
R. Lawrence Whipple, *Director, Engineering Management Services*

COMMITTEE ON PUBLICATIONS

Stafford E. Thornton, *Chairman*
Martin G. Abegg
John A. Focht, Jr.
Richard W. Karn
Paul R. Munger
William R. Neuman

HYDRAULICS DIVISION

Executive Committee
Ronald E. Nece, *Chairman*
Rudolph P. Savage, *Vice Chairman*
George E. Hecker
Ralph M. Weaver
Charles S. Mifkovic, *Secretary*
John J. Cassidy, *Management Group D Contact Member*

Publications Committee
Melvin W. Anderson, ***Chairman***
John A. Hoopes, ***Vice Chairman***
Philip H. Burgi, *Hydraulic Structures*
Richard H. (Pete) Hawkins, *Surface Water Hydrology*
John A. Hoopes, *Hydromechanics, General*
Gerhard H. Jirka, *Hydraulic Transport and Dispersion*
Chintu Lai, *Hydromechanics, Open Channels*
Frederick A. Locher, *Hydromechanics, Open Channels*
Donn G. DeCoursey, *Sedimentation*
Bryan R. Pearce, *Tidal Hydraulics*
John A. Roberson, *Hydromechanics, Closed Conduits*
John L. Wilson, *Groundwater Hydrology*
George E. Hecker, *Exec. Comm. Contact Member*

PUBLICATION SERVICES DEPARTMENT

David Dresia, *Director, Publications Production and Marketing*

Technical and Professional Publications

Richard R. Torrens, *Manager*
Joseph P. Cerami, *Chief Copy Editor*
Linda Ellington, *Copy Editor*
Thea C. Feldman, *Copy Editor*
Meryl Mandle, *Copy Editor*
Joshua R. Spieler, *Copy Editor*
Shiela Menaker, *Production Co-ordinator*
Richard C. Scheblein, *Draftsman*

Information Services

Elan Garonzik, *Editor*

PERMISSION TO PHOTOCOPY JOURNAL PAPERS

Permission to photocopy for personal or internal reference beyond the limits in Sections 107 and 108 of the U.S. Copyright Law is granted by the American Society of Civil Engineers for libraries and other users registered with the Copyright Clearance Center, 21 Congress Street, Salem, Mass. 01970, provided the appropriate fee is paid to the CCC for all articles bearing the CCC code. Requests for special permission or bulk copying should be addressed to the Manager of Technical and Professional Publications, American Society of Civil Engineers.

CONTENTS

Self-Formed Straight Channels in Sandy Beds
by Syunsuke Ikeda 389

Variation of Karman Constant in Sediment-Laden Flow
by Shang-yi Wang 407

Performance of Baffled Chute with 90° Bend
by David T. Higgins 419

Unstable Turbulent Flow in Open Channels
by Jean E. Berlamont and Nicole Vanderstappen 427

Separated Flow Through Large Sudden Expansions
by Prabhulal R. Mehta 451

Simulating Mass Transport in Unconfined Aquifers
by Varuttamadhira Guvanasen and Raymond E. Volker 461

Mathematical Model of Shallow Water Flow over Porous Media
by Ali Osman Akan and Ben Chie Yen 479

This Journal is published monthly by the American Society of Civil Engineers. Publications office is at 345 East 47th Street, New York, N.Y. 10017. Address all ASCE correspondence to the Editorial and General Offices at 345 East 47th Street, New York, N.Y. 10017. Allow six weeks for change of address to become effective. Subscription price to members is $16.50. Nonmember subscriptions available; prices obtainable on request. Second-class postage paid at New York, N.Y. and at additional mailing offices. HY.

The Society is not responsible for any statement made or opinion expressed in its publications.

TECHNICAL NOTES

Proc. Paper 16154

Scales for Circular Jets in Cross-Flow
by Nallamuthu Rajaratnam and Thimmaiah Gangadharaiah 497

Sand-Water Slurry Experiment
by M. R. Carstens and Graeme Addie 501

New Design Equations for Scour Around Bridge Piers
by Christopher James Baker 507

DISCUSSION

Proc. Paper 16151

Estimation of Direct Runoff from Urban Watersheds, by Aolad Hossain, A. Ramachandra Rao, and Jacques W. Delleur (Feb., 1978. Prior Discussion: Aug., 1980).
errata 515

Estimating Average Velocity in Gravel-Bed Rivers, by Dale I. Bray (Sept., 1979. Prior Discussions: Sept., Oct., 1980).
closure 515

Hydraulic Geometry of Active Gravel Rivers, by Gary Parker (Sept., 1979. Prior Discussions: July, Oct., 1980).
closure 517

Approximate Flood Routing Methods: A Review, by P. Erwin Weinmann and Eric M. Laurenson (Dec., 1979. Prior Discussions: Nov., Dec., 1980).
errata 519

Log Pearson Type 3 Distribution: A Generalized Evaluation,[a] by Donthamsetti Veerabhadra Rao (May, 1980).
by M. Riazul Hasan 519

[a]Discussion period closed for this paper. Any other discussion received during this discussion period will be published in subsequent Journals.

Heat Loss from Sidearms of Cooling Lakes,* by Terry W. Sturm and John F. Kennedy (May, 1980).
by Subhash C. Jain and Nevzat Yildirim 521

Characteristics of Low Flows,* by the Task Committee on Low-Flow Evaluation and Needs of the Committee on Surface-Water Hydrology of the Hydraulics Division (May, 1980).
by Michel North 523

Composite Roughness of Natural Channels,* by Asok K. Motayed and Muthusamy Krishamurthy (June, 1980).
by James Grant Mac Broom 526

Boundary Layers in Developing Open Channel Flow,* by Edward Silberman (July, 1980).
by Edward H. Wilson 527

Scour Velocities in Ephemeral Channels,* by William C. Hughes (Sept., 1980).
by Subhash C. Mehrotra 529

Submerged Horizontal Jet over Erodible Bed,* by S. S. Chatterjee and S. N. Ghosh (Nov., 1980).
by Subhash C. Mehrotra 530

INFORMATION RETRIEVAL

The key words, abstract, and reference "cards" for each article in this Journal represent part of the ASCE participation in the EJC information retrieval plan. The retrieval data are placed herein so that each can be cut out, placed on a 3 × 5 card and given an accession number for the user's file. The accession number is then entered on key word cards so that the user can subsequently match key words to choose the articles he wishes. Details of this program were given in an August, 1962 article in CIVIL ENGINEERING, reprints of which are available on request to ASCE headquarters.

*Discussion period closed for this paper. Any other discussion received during this discussion period will be published in subsequent Journals.

16195 SELF-FORMED CHANNELS IN SANDY BEDS

KEY WORDS: **Channel beds; Channel flow;** Geometry; Laboratory tests; Regime theory; **Sands; Secondary flow; Stream flow;** Stream meandering

ABSTRACT: The hydraulic geometry and the local features of straight, relatively wide self-formed channels composed of sandy bed are studied in laboratory flumes. Introduction of one loose and the other rigid bank in experiments excludes the tendency toward meanders and provides good examples to test hydraulic regime relations. The experiments support a few regime relations derived rationally. The transverse bed shapes in equilibrium have a universal profile regardless of initially-molded cross section, discharge of flow, and sand diameter within the scope of the experiments. A theoretical analysis of secondary currents in straight channels provides reasonable interpretation of the local features of self-formed channels such as the longitudinal sand ridges, and this analysis suggests the insignificant effect of secondary currents on the size of self-formed channels.

REFERENCE: Ikeda, Syunsuke, "Self-Formed Straight Channels in Sandy Beds," *Journal of the Hydraulics Division,* ASCE, Vol. 107, No. HY4, **Proc. Paper 16195**, April, 1981, pp. 389-406

16184 KARMAN CONSTANT IN SEDIMENT-LADEN FLOW

KEY WORDS: **Channels (waterways); Coefficients; Fluid flow; Hydraulics;** Rivers; **Sedimentation; Sediment production;** Shear stress; Streams; Velocity

ABSTRACT: Based on the principle of energy balance and the effective power of suspension-load, a formula for calculating the Karman Constant K in sediment-laden flow is presented. The calculating formula may be used in practice. According to the variablity of sediment effective power, W_e, the influence of the characteristics of suspension-load on K is as follows: when W_e is greater than zero, the value of K decreases with the increase of concentration of suspension-load C (mean value); when the value of $W_e<0$, the value of K increases with the increase of C (mean value); and when the value of $W_e = 0$, the variablity of K has no relation with the value of C (mean value) directly.

REFERENCE: Wang, Shang-yi, "Variation of Karman Constant in Sediment-Laden Flow," *Journal of the Hydraulics Division,* ASCE, Vol. 107, No. HY4, **Proc. Paper 16184**, April, 1981, pp. 407-417

16187 PERFORMACE OF BAFFLED CHUTE WITH 90° BEND

KEY WORDS: Aprons; **Baffles; Chutes; Chute spillways;** Energy dissipation; Mathematical models; Scour; **Spillways;** Splash

ABSTRACT: The effects of a 90° bend on scour and splash in a baffled chute have been studied in a 1:12 model. The model design followed recommended United States Bureau of Reclamation practice except for the square bend. Various combinations of guide vanes and bend floor elevations were examined in 12-ft and 24-ft (3.7-m and 7.3m) wide chutes carrying 40 cfs/ft (3.7 $m^3/s/m$). The simplest, plain, square bend caused 2.3 ft (0.7 m) more scour depth than does a standard, straight chute. The additional scour may be eliminated by using guide vanes or lowering the bend floor. Sever splash beyond the bend and lower chute walls may require slope protection.

REFERENCE: Higgins, David T., "Performance of Baffled Chute with 90° Bend," *Journal of the Hydraulics Division,* ASCE, Vol. 107, No. HY4, **Proc. Paper 16187**, April, 1981, pp. 419-426

16191 UNSTABLE TURBULENT FLOW IN OPEN CHANNELS

KEY WORDS: Flow measurement; **Flumes; Friction; Hydraulics;** Hydrodynamic configurations; **Hydrodynamics;** Open channel flow; **Open channels;** Supercritical flow; Theories; **Turbulent flow; Unsteady flow**

ABSTRACT: Controversy on the determination of the friction factor, f, for turbulent flow in open channels of rectangular cross section has existed among previous investigators. A number of them found that the Froude number affects the value of the friction factor, while others did not find such a dependence. In this study, the theoretical expression for the critical Froude number is first derived. Given a value of the Reynolds number, the flow becomes unstable above the critical Froude number. This critical Froude number, which appears to be strongly dependent upon the channel width, is then introduced in an equation by Rouse to calculate the values of the friction factor under unstable flow conditions. The influence of the Froude number on the friction factor appears to be important, but the channel width is a determinating factor as well.

REFERENCE: Berlamont, Jean E., and Vanderstappen, Nicole, "Unstable Turbulent Flow in Open Channels," *Journal of the Hydraulics Division,* ASCE, Vol. 107, No. HY4, **Proc. Paper 16191**, April, 1981, pp. 427-449

16206 FLOW THROUGH LARGE SUDDEN EXPANSIONS

KEY WORDS: **Expansion; Flow characteristics;** Flow measurement; **Flow patterns;** Reynolds number; Shear flow; **Turbulence;** Uniform flow

ABSTRACT: Flow patterns for large, sudden expansions have been obtained experimentally. The experimental studies reveal that flow patterns for large expansions are highly asymmetric and unsteady. Two distinct types of flow have been observed in which the flow characteristics are essentially mirror images of each other. Turbulence develops peak values earlier and decays faster with increasing expansion ratios. Because of the increased turbulent mixing with increased expansion ratio, the mean flow pattern becomes steady and uniform more rapidly with increased expansion ratios. For the Reynolds number range 0.5×10^5 to 1.0×10^5, there is no Reynolds number influence on these flow patterns.

REFERENCE: Mehta, Prabhulal R., "Separated Flow Through Large Sudden Expansions," *Journal of the Hydraulics Division,* ASCE, Vol. 107, No. HY4, **Proc. Paper 16206**, April, 1981, pp. 451-460

16209 MASS TRANSPORT IN UNCONFINED AQUIFERS

KEY WORDS: **Aquifers;** Dispersion; Experimental data; Finite elements; **Flow rate;** Free surfaces; Ground water; **Mass transfer; Mathematical models; Water pollution**

ABSTRACT: The weighted residual technique in conjunction with the finite element method is employed to formulate numerical models to solve flow and transport problems in a nonstationary saturated ground-water zone. Through the formulation presented, elements are allowed to move to accommodate the nonstationary saturated domain without the necessity for interpolation when proceeding from one time step to the next in the solution of the mass transport equation. The models can simulate the flow of water and the movement of a pollutant in the saturated zone of a homogeneous isotropic aquifer. The moisture influx from the unsaturated zone can exert some influence over mass distribution in the neighborhood of the free surface.

REFERENCE: Guvanasen, Varuttamadhira, and Volker, Raymond E., "Simulating Mass Transport in Unconfined Aquifers," *Journal of the Hydraulics Division,* ASCE, Vol. 107, No. HY4, **Proc. Paper 16209**, April, 1981, pp. 461-477

16213 SHALLOW WATER FLOW OVER POROUS MEDIA

KEY WORDS: **Computation;** Drainage; **Fluid flow; Ground water;** Hydrography; Hydrology; **Infiltration (water); Mathematical models;** Numerical analysis; Open channel flow; Open channels; **Porous media;** Runoff; Seepage; Water flow

ABSTRACT: A conjunctive mathematical model for a surface-subsurface flow system is developed. The unsteady surface flow is explored by a set of one-dimensional dynamic wave equations for shallow water, which are solved by using a four-point implicit finite-difference scheme. The transient subsurface flow is two-dimensional, with potential gradients in the vertical direction as well as the surface flow direction. The porous medium may be saturated or unsaturated or both, and it can be nonhomogeneous and anisotropic. The subsurface flow equation is solved by employing a successive line over-relaxation implicit finite-difference scheme. The surface and subsurface flow components are coupled at the ground surface considering the mass conservation and pressure relationships. The model is verified by using existing experimental data and analytical solutions for special cases.

REFERENCE: Akan, Ali Osman, and Yen, Ben Chie, "Mathematical Model of Shallow Water Flow over Porous Media," *Journal of the Hydraulics Division,* ASCE, Vol. 107, No. HY4, **Proc. Paper 16213,** April, 1981, pp. 479-494

U.S. Customary-SI Conversion Factors

In accordance with the October, 1970 action of the ASCE Board of Direction, which stated that all publications of the Society should list all measurements in both U.S. Customary and SI (International System) units, the following list contains conversion factors to enable readers to compute the SI unit values of measurements. A complete guide to the SI system and its use has been published by the American Society for Testing and Materials. Copies of this publication (ASTM E-380) can be purchased from ASCE at a price of $3.00 each; orders must be prepaid.

All authors of *Journal* papers are being asked to prepare their papers in this dual-unit format. To provide preliminary assistance to authors, the following list of conversion factors and guides are recommended by the ASCE Committee on Metrication.

To convert	To	Multiply by
inches (in.)	millimeters (mm)	25.4
feet (ft)	meters (m)	0.305
yards (yd)	meters (m)	0.914
miles (miles)	kilometers (km)	1.61
square inches (sq in.)	square millimeters (mm^2)	645
square feet (sq ft)	square meters (m^2)	0.093
square yards (sq yd)	square meters (m^2)	0.836
square miles (sq miles)	square kilometers (km^2)	2.59
acres (acre)	hectares (ha)	0.405
cubic inches (cu in.)	cubic millimeters (mm^3)	16,400
cubic feet (cu ft)	cubic meters (m^3)	0.028
cubic yards (cu yd)	cubic meters (m^3)	0.765
pounds (lb) mass	kilograms (kg)	0.453
tons (ton) mass	kilograms (kg)	907
pound force (lbf)	newtons (N)	4.45
kilogram force (kgf)	newtons (N)	9.81
pounds per square foot (psf)	pascals (Pa)	47.9
pounds per square inch (psi)	kilopascals (kPa)	6.89
U.S. gallons (gal)	liters (L)	3.79
acre-feet (acre-ft)	cubic meters (m^3)	1,233

JOURNAL OF THE HYDRAULICS DIVISION

SELF-FORMED STRAIGHT CHANNELS IN SANDY BEDS

By Syunsuke Ikeda,[1] M. ASCE

INTRODUCTION

Water and sediment in alluvial rivers interact to yield self-formed channel geometry. The simplest but most essential morphological problem in self-formed channels is how to interpret rationally the process of side-bank erosion and the resulting stable channel formation in straight channels with noncohesive materials.

The river engineers in India established the regime theory on the basis of their experiences obtained in excavating and maintaining large canals with straight alinement. Any method based on dynamics has not succeeded in deriving the regime theory rationally. For a long time, the only analytical model has been the threshold theory, which assumes the critical tractive force everywhere in a canal section (see e.g., Refs. 5 and 10).

Experiments on the stable channels in coarse noncohesive sands were made by Wolman and Brush (16), and they showed that the concept of static equilibrium is not realistic. There exists a dynamic equilibrium for which the sediment is actively transported at least in the central bed region and bed load vanishes in the side-bank regions. The threshold theory cannot be applied to most rivers, because sediment transport occurs without widening their widths in the rivers.

A theory which allows for bed-load transport was first developed by Hirano (6). He treated analytically the process of widening straight channels where the sand grains are assumed to move down the bank to the center bed region. However, sediment transport seems to be incompatible with the stable channel concept. In order for the sediment constituting the bed to be transported, the shear stress must be greater than the critical stress in the center bed region. Since the bank region joins the center bed region smoothly, the shear stress must be above the critical stress somewhere in the bank region, and bank erosion will again occur. Thus, as long as the bed load exists, the channel must widen indefinitely. This is incompatible with the aforementioned concept of graded

[1]Assoc. Prof., Dept. of Foundation Engrg., Saitama Univ., Urawa, Saitama, Japan.

Note.—Discussion open until September 1, 1981. To extend the closing date one month, a written request must be filed with the Manager of Technical and Professional Publications, ASCE. Manuscript was submitted for review for possible publication on July 28, 1980. This paper is part of the Journal of the Hydraulics Division, Proceedings of the American Society of Civil Engineers, ©ASCE, Vol. 107, No. HY4, April, 1981. ISSN 0044-769X/81/0004-0389/$01.00.

rivers with nocohesive bed materials. This paradox is vividly described by Parker (12), and is termed the "stable channel paradox." He resolved the paradox by taking an account of the lateral momentum transfer due to turbulence, and succeeded in deriving several rational regime relations for straight reaches. The relations predict the gross profiles of stable rivers, such as the depth or the width if slope, discharge, and sediment characteristics are specified.

These works still leave several important phenomena, such as the process of self-formation of channels, the lateral stable bed profile, the effect of secondary flow on the formation of channels, and so on, to be explained more fully.

In the research described herein, the process of widening and hydraulic characteristics of self-formed straight channels with noncohesive sands were studied in two laboratory flumes which are different in size. The experiments were conducted under an idealized condition to exclude the effects of several disturbances such as ripples, dunes, and meanders. The secondary circulations found in the experiments are analyzed theoretically, and are proven to be consistent with the observations.

Experiments

Apparatus and Procedure.—Two flumes were used for the experiments. One flume (for the sake of simplicity termed the "large flume") is 15 m long and has a width of 50 cm; the slope and discharge are adjustable. The side walls of the flume are made of glass, which allows the convenience of visual observations. Water is circulated by a pump, and the discharge is measured with a triangular weir equipped at the bottom tank. An adjustable tailgate controls the flow depth at the downstream end, so as not to yield the drawdown backwater. A well-graded sand with median diameter, D_{50}, of 1.3 mm, and the gradation coefficient, σ, of 1.3 were used, because for this size ripples or dunes were not produced. The flume was covered by the sand in the reach between the 1-m section and 14-m section from the upstream end. The initial cross section was trapezoidal and molded by a template. Only one side bank was made mobile to exclude the tendency toward meanders. The molded flume was filled with still water before the start of experiments. Then the tailgate was opened and the water was recirculated.

The elevations of free surface and bed were measured by a point gage at the 9-m section and 11-m section from the entrance where the width and the depth of formed channels were uniform, and the effects of flume ends were minimized. Sand feeding was made at the entrance to prevent degradation in the upper reach. However, the degradation was not completely avoided, because sands were not supplied sufficiently from the side bank in the upper reach. The sediment transport rate was measured with a trap cage at every 1 cm along the traverse after a stable state was achieved (as revealed in a later figure). At the same time the distribution of flow velocity in a cross section was determined with a pitot tube for several runs. A series of 20 runs were conducted in the large flume, and it generally required 10 h to reach a stable state.

Small-flume runs were conducted in a 2-m long, 30-cm wide recirculatory, tilting flume. A well-graded sand which had a median diameter of 0.85 mm, and the gradation coefficient of 1.3, were used. The procedure of the experiments

was about the same as for the large-flume runs. The sediment transport rate and the flow velocity were not measured, because the flume was too small. Fourteen runs were performed in the small flume, and no ripples, dunes, or meanders were found throughout the total set of runs.

View of Representative Run.—A detailed description of a representative run will give a general overview of the series of experiments, because the features

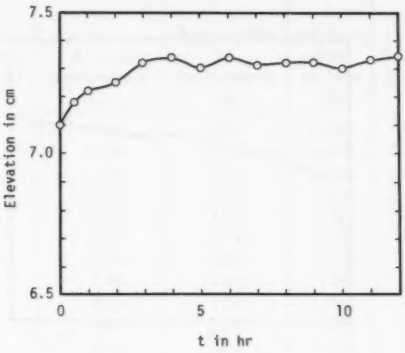

FIG. 1.—Variation of Free Surface Elevation with Time for Run 17 at $x = 11$ m

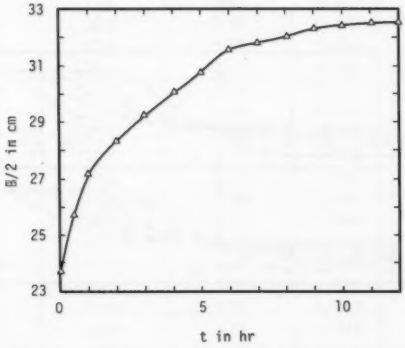

FIG. 2.—Variation of Free Surface Width with Time for Run 17 at $x = 11$ m

of the experiments did not differ essentially with each other. Since the total process necessary to reach a stable state was studied in detail for Run 17, it has been selected as the representative run. The initially-molded cross section was trapezoidal with a lateral slope of 30°, an 11-cm bottom width, 23.5-cm top width, and 7-cm depth. The experiment was continued for a total run time of 12 h until a dynamically stable state had been achieved. The discharge was

4,130 cm^3/s throughout the run. The water surface elevation was initially about 7 mm below the side bank, and it rose a little with time. The water surface height increased about 2.5 mm during the first 3 h, and then reached a stable level as is shown in Fig. 1. The massive fall of sands reported by Ashida, et al. (1) did not occur at the water margin. The sand particles at the margin fell one by one, and the width increased smoothly with time. A stable width was achieved after about 10 h had passed from the beginning (see Fig. 2).

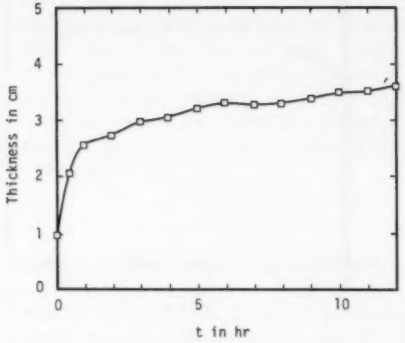

FIG. 3.—Variation of Sand Layer Thickness with Time for Run 17 at $x = 11$ m and $y = 0$

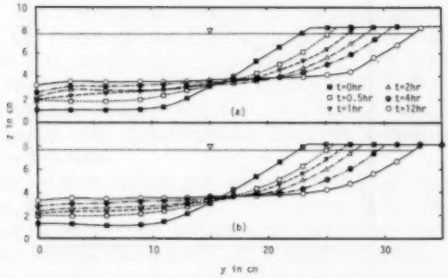

FIG. 4.—Variation of Lateral Bed Topography with Time for Run 17 at: (*a*) $x = 9$ m; (*b*) $x = 11$ m; Both Sections are Located at Lower Reach of Large Flume

Only one particle layer thickness was eroded during the next 2 h. The eroded particles moved down the side-bank slope to settle in the central bed region, and the bed aggraded very rapidly in the first hour (see Fig. 3). However, the aggradation was not sufficient in the reach between the 1-m section and 6-m section despite the sand feeding at the upstream end due to the shortage of supply from the side bank. A uniform flow depth and a uniform bed thickness

were established in the middle and lower reach of the stream. The sediment was actively transported in the central bed region and vanished in the side-bank region after a stable state was established.

TABLE 1.—Summary of Experimental Data

Run number (1)	$Q/2$, in cubic centimeters per second (2)	$B/2$, in centimeters (3)	Mean depth, in centimeters (4)	S, slope of free surface (5)	Reynolds number (6)	Total run time, in hours (7)
1	265	6.20	1.63	1/280	3,340	2.5
2	268	6.50	1.57	1/200	3,770	2
3	310	7.90	1.46	1/260	3,740	2
4	310	7.25	1.66	1/245	4,200	1.5
5	340	7.60	1.68	1/226	3,800	2
6	346	7.05	1.74	1/270	4,390	1.5
7	350	7.30	1.68	1/310	4,400	1.5
8	361	7.95	1.64	1/240	4,220	1.5
9	408	8.00	1.53	1/310	4,560	1.5
10	413	7.60	2.07	1/280	4,210	2
11	467	8.70	2.07	1/333	3,200	2
12	530	9.90	1.83	1/490	4,030	3
13	530	9.65	2.01	1/280	4,400	4
14	630	11.7	2.05	1/240	4,670	2
15	3,800	31.0	3.43	1/467	8,400	10.5
16	4,070	32.2	3.54	1/479	8,500	10
17	4,130	32.4	3.59	1/466	8,600	12
18	4,480	35.2	3.61	1/506	8,700	10
19	4,550	33.7	3.74	1/550	9,200	11
20	4,630	35.7	3.73	1/498	8,700	9
21	4,680	37.5	3.43	1/450	8,400	9
22	4,780	35.4	3.79	1/502	9,100	8.3
23	4,820	37.6	3.39	1/434	8,700	9
24	4,870	35.6	3.76	1/530	9,200	11.5
25	4,940	37.5	3.61	1/464	9,000	9
26	4,980	39.1	3.55	1/468	8,600	9
27	5,130	39.0	3.61	1/495	8,700	9
28	5,290	39.3	3.70	1/496	9,500	9.5
29	5,440	39.8	3.78	1/493	9,400	10
30	5,620	40.5	3.76	1/482	9,500	11
31	5,710	40.9	4.00	1/511	11,200	8
32	5,740	39.6	3.95	1/511	9,900	10
33	5,990	39.9	3.91	1/508	10,500	8.3
34	6,300	41.7	4.02	1/503	10,200	9

The variation of the lateral bed profile with time is shown in Figs. 4(*a*) and 4(*b*). The profiles are nearly identical, and it is concluded that a uniform and stable reach was established in the channel.

The experimental data are summarized in Table 1.

Data Analysis

It is known that the width is significantly correlated to discharge, and several empirical formulas expressed by power-law relations have been proposed:

$$B = aQ^b \quad \ldots\ldots\ldots\ldots\ldots\ldots\ldots\ldots\ldots\ldots\ldots\ldots\ldots\ldots\ldots\ldots\ldots\ldots\ldots\ldots\ldots\ldots (1)$$

in which B = width of free surface at dominant discharge. Variables a and b = numerical constants.

Leopold and Maddock (11) found that the exponent b has an average value of 0.5 based on extensive field data. To test whether the relation is applicable also to laboratory flume data, the measured values of width are plotted against the discharge in Fig. 5. Though there exist considerable scatters especially in flume data of Wolman and Brush (16), the aforementioned relation seems to hold at least for each kind of sand. The constant a, however, is different in each kind. The stable width seems to be less if the diameter of sand becomes large, even if discharges of flow are identical. The power law is therefore not

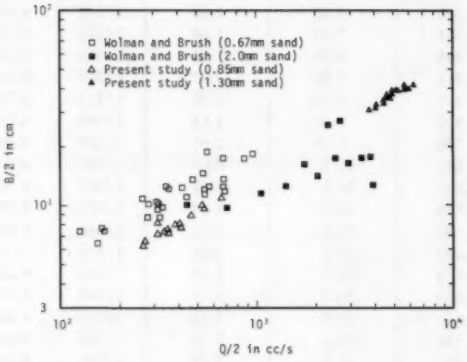

FIG. 5.—Half-Width Plotted Against Half-Discharge of Flow

rational in that it does not account for any effect of bed materials. The stable width of an active sandy channel should be determined by a combination of several hydraulic variables such as the shear stress and the diameter of sand particles.

Parker (12,13) obtained rational regime relations for active gravel rivers (ignoring secondary flows):

$$R = 0.0553\, S^{-1.01}; \quad \text{first regime relation} \ldots\ldots\ldots\ldots\ldots\ldots\ldots\ldots (2)$$

$$R = 0.866 \left(\frac{\tilde{Q}}{B^*}\right)^{0.830}; \quad \text{second regime relation} \ldots\ldots\ldots\ldots\ldots\ldots (3)$$

$$Q^* = 1.02 \times 10^{-5} R^{0.275} B^* \left(1 - \frac{4.52}{A}\right); \quad \text{third regime relation} \ldots\ldots\ldots (4)$$

in which $R = H/D_{50}$; H = center depth; D_{50} = median diameter size; S = water surface slope; $\bar{Q} = Q/[(FgD_{50})^{0.5}D_{50}^2]$; Q = discharge of flow; F = submerged specific gravity of sediment and is 1.65 for natural sands; $B^* = B/D_{50}$; A = aspect ratio; $Q^* = Q_s/[(FgD_{50})^{0.5}D_{50}^2]$; and Q_s = bed load discharge.

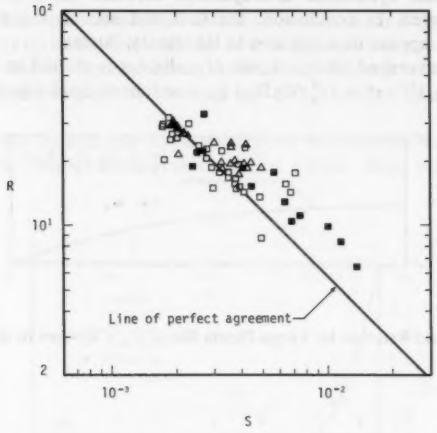

FIG. 6.—Test of Eq. 2 for Laboratory Data; Symbols as in Fig. 5

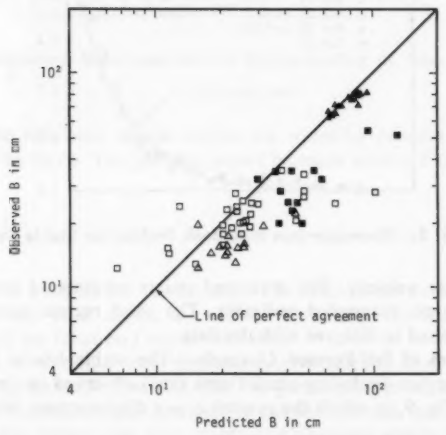

FIG. 7.—Test of Eq. 3 for Laboratory Data; Symbols as in Fig. 5

The first regime relation is tested in Fig. 6 with the same data as in Fig. 5. The theoretically predicted values of R agree fairly well with the laboratory data, and the agreement with the large-flume data is excellent.

The second regime relation is examined also for the same data (see Fig. 7). In predicting the stable width, B, R in Eq. 3 is calculated from the first regime relation, because three parameters, Q, S, and D_{50}, are thought to be independent and primary hydraulic variables in alluvial rivers. While considerable scatter is present, systematic discrepancies between the four kinds of sand cannot be detected. In conclusion, the first and second regime relations are reasonable, and appear to apply also to laboratory flumes.

The laterally averaged transport rate of sediment is plotted in Fig. 8 in which $q^* = q_B/(FgD_{50})^{0.5}$; $\tau^* = U_*^2/FgD_{50}$; q_B = sediment discharge per unit width;

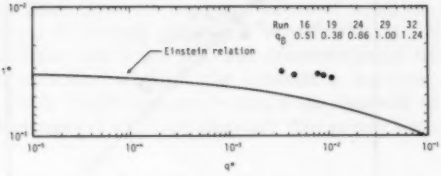

FIG. 8.—Bed-Load Relation for Large-Flume Runs; q_B is Written in Grams per Minute Centimeters

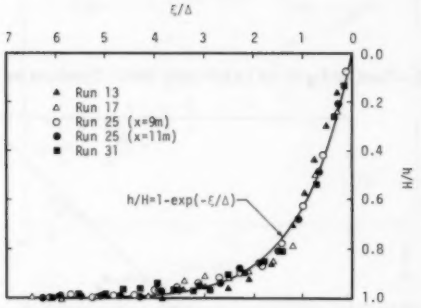

FIG. 9.—Dimensionless Side-Bank Profiles for Stable State

and U_* = shear velocity. The measured points correspond to low transport rates, implying no suspended sediment. The third regime relation (bed-load relation) was found to disagree with the data.

Local Features of Self-Formed Channels.—The stable lateral bed shapes in the side-bank region (including small-flume runs) observed in the present work are plotted in Fig. 9, in which the symbol Δ = a displacement thickness defined by

$$\Delta = \frac{1}{H}\int_0^{B/2} (H-h)\,d\xi \quad \ldots\ldots\ldots\ldots\ldots\ldots\ldots\ldots\ldots\ldots\ldots\ldots\ldots\ldots (5)$$

in which h = local depth; H = center depth; and ξ = lateral coordinate from the water margin. The shapes thus nondimensionalized are roughly similar

regardless of discharge, scale of flume, and kind of sand. It is well-expressed by an exponential function defined by

$$\frac{h}{H} = 1 - \exp\left(-\frac{\xi}{\Delta}\right) \quad \ldots \ldots \ldots

scheme of the secondary currents inferred from the bed topography is shown in the figure.

A minute observation of Fig. 9 reveals that for Runs 13, 17, and 31, where the sand ridges were formed, there are systematic discrepancies between the exponential profile and the experimental values. The local depths are larger

FIG. 11.—View of Longitudinal Sand Ridges Formed in Run 17; Arrows Indicate Ridges which Extend Unbroken From Upstream to Downstream End

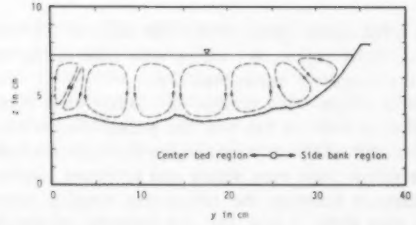

FIG. 12.—Lateral Bed Profile Corresponding to Fig. 11; Measurements were Made at $t = 12$ h and $x = 11$ m; Broken Lines Indicate Secondary Currents Inferred From Bed Topography; Note That Vertical Scale is Exaggerated

than the solid line around $\xi/\Delta = 2$, and they are shallower at $\xi/\Delta = 3 - 4$, where the sand ridges were yielded. For Run 25, in which the sand ridges were not observed, the experimental values can be simulated with sufficient accuracy by the exponential function. We can therefore imagine the existence of pair vortices also in the sloping side-bank region.

The velocity distributions were measured for Runs 16, 19, 24, 29, and 32. The isovels show marked lateral undulations in Runs 16 and 32 (see Fig. 13), and they are thought to be due to the secondary currents. Indeed, a comparison of the bed topography of Run 17 (see Fig. 12) with the isovels of Run 16 reveals that the longitudinal fluid velocity is slow immediately above the ridges and swift between them (both runs are identical within the error of measurements).

Corresponding to the undulations, the lateral distributions of bed-load transport show wavy profiles. The bed-load transports are diminished in the side-bank region for all runs.

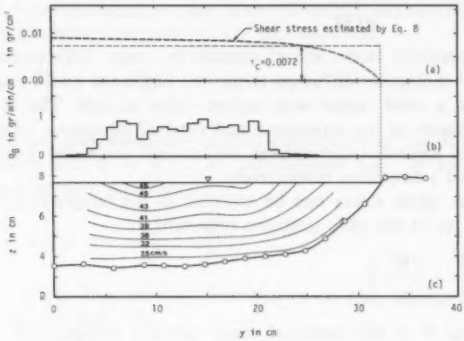

FIG. 13.—Lateral Distributions of: (*a*) Bottom Shear Stress; (*b*) Sediment Transport Rate; (*c*) Isovels for Run 16 at $x = 11$ m

A first estimate of the lateral distributions of the bottom shear stress can be obtained from the normal depth method defined by (see, e.g., Ref. 15)

$$\tau = \rho g S \frac{dA}{ds} \quad \ldots\ldots\ldots\ldots\ldots\ldots\ldots\ldots\ldots\ldots\ldots\ldots\ldots\ldots\ldots\ldots\ldots\ldots\ldots\ldots\ldots\ldots (8)$$

in which ρ = mass density of fluid; dA = area of cross-sectional segment between adjacent straight lines normal to bottom; and ds = wetted perimeter corresponding to the segment. The calculated bottom shear stress is described with a broken line in Fig. 13, in which the threshold shear stress for level and flat boundaries is also estimated with the Shields curve. While the lateral inclination of the bed naturally affects the incipient motion, the estimation may give reasonable values at least in the central bed region. The bed-load transport rates are diminished or show abrupt decreases at the critical points thus estimated. The bottom shear stresses exceed the critical by about 20% in the major parts

of the central bed region for the runs, which is exactly one of the constraints imposed in applying the regime relations Eqs. 2, 3, and 4.

Secondary Currents and Their Effects

As described already, the secondary currents seem to affect at least the local features of the hydraulic variables such as the local depth, the isovels, and the sediment transport rate. Analysis of the secondary flows should provide a more rational explanation of the local features, especially of the sand ridges. The analysis will moreover provide useful information for the adequateness of the rational regime relations (the effect of secondary currents is neglected).

Equations of Motions.—It can be shown that for steady uniform turbulent flows in straight channels the Reynolds equations of motions reduce to (see Refs. 3 and 7)

$$\left(\frac{\partial^2}{\partial y^2} - \frac{\partial^2}{\partial z^2}\right)\overline{vw} = \frac{\partial^2(\overline{vv} - \overline{ww})}{\partial y \partial z} \quad \ldots\ldots\ldots\ldots\ldots\ldots\ldots\ldots (9)$$

in which the pressure terms are eliminated by cross differentiation, and the convective and molecular diffusion terms are neglected as Gessner and Jones (4) indicated in a wind tunnel with square cross section. The symbols y and z = the coordinates of the transverse and vertical directions, respectively; $\overline{vw}$ = the kinematic Reynolds shear stress; and $\overline{vv}$ and $\overline{ww}$ = the Reynolds normal stresses of y and z directions respectively.

The Reynolds shear stress can be equated to the temporal mean velocities with a component of the eddy diffusion tensor, ϵ_{yz}

$$-\overline{vw} = \epsilon_{yz}\left(\frac{\partial V}{\partial z} + \frac{\partial W}{\partial y}\right) \quad \ldots\ldots\ldots\ldots\ldots\ldots\ldots\ldots (10)$$

in which V and W = the temporal mean velocity components of the y and z directions, respectively. Introduction of a stream function of the secondary currents Ψ gives a simpler form of Eq. 10

$$-\overline{vw} = \epsilon_{yz} L\Psi \quad \ldots\ldots\ldots\ldots\ldots\ldots\ldots\ldots (11)$$

in which $L = \partial^2/\partial z^2 - \partial^2/\partial y^2$. Using the Brundrett and Baines (2) measurements on the Reynolds shear stress and the secondary flow, ϵ_{yz} is estimated to be crudely identical to (see Ref. 7)

$$\epsilon_{yz} = \frac{\kappa U_* H}{6} \quad \ldots\ldots\ldots\ldots\ldots\ldots\ldots\ldots (12)$$

in which κ = the Karman constant; and U_* = spatially-averaged boundary shear stress. If the very crude assumption of constant eddy viscosity is allowed, then substitution of Eq. 11 into Eq. 9 gives a secondary flow equation

$$L^2\Psi = \frac{1}{\epsilon_{yz}} \frac{\partial^2(\overline{vv} - \overline{ww})}{\partial y \partial z} \quad \ldots\ldots\ldots\ldots\ldots\ldots\ldots\ldots (13)$$

The secondary flows in corners of square ducts (a similar pair of vortices is seen in the left corner of Fig. 11) were examined based on Eq. 13, which

was shown to give a reasonable estimation of the actual secondary flow field (see Refs. 3 and 7). So, it can be postulated that Eq. 13 interprets the secondary flows in straight channels at least at the lowest order.

Secondary Currents in Wide-Open Channels.—As mentioned previously, steady uniform secondary currents exist also in turbulent flows of wide-open channels. It is impossible to suppose that the driving force of the secondary flow, $\overline{vv} - \overline{ww}$ in Eq. 13 is distributed uniformly along the traverse, and a slight fluctuation of it will produce the secondary flow. The distribution of $\overline{vv} - \overline{ww}$ along the traverse thus can be assumed to take the form

$$\frac{\overline{vv} - \overline{ww}}{U_*^2} = \alpha \left(1 + \delta \cos k \frac{y}{H}\right) \hat{f}\left(\frac{Z}{H}\right) \quad \ldots\ldots\ldots\ldots\ldots\ldots \quad (14)$$

in which α = coefficient shown to be approximately unit by Perkins (14); δ = amplitude of the perturbation, much smaller than unity; k = dimensionless lateral wave number; and $\hat{f}(z/H)$ = dimensionless vertical distribution of the driving force. Corresponding to the aforementioned expression, the stream function of the secondary currents should take the form

$$\hat{\Psi} = \hat{\psi}\left(\frac{z}{H}\right) \sin k \frac{y}{H} \quad \ldots\ldots\ldots\ldots\ldots\ldots\ldots\ldots\ldots\ldots \quad (15)$$

in which $\hat{\psi}(z/H)$ = dimensionless vertical distribution of the stream function, to be determined; and $\hat{\Psi} = \Psi/U_*H$. Substituting Eqs. 14 and 15 into Eq. 13 yields a dimensionless equation

$$\frac{d^4\hat{\psi}}{d\hat{z}^4} + 2k^2 \frac{d^2\hat{\psi}}{d\hat{z}^2} + k^4\hat{\psi} = -\frac{U_*H\delta k}{\epsilon_{yz}} \frac{d\hat{f}}{d\hat{z}} \quad \ldots\ldots\ldots\ldots\ldots\ldots \quad (16)$$

in which $\hat{z} = z/H$. The vertical distribution of the driving force can be approximated by (see Ref. 14)

$$\hat{f}(\hat{z}) = 1 - \hat{z} \quad \ldots\ldots\ldots\ldots\ldots\ldots\ldots\ldots\ldots\ldots\ldots\ldots \quad (17)$$

Eq. 16 can be solved under the following constraints: (1) $\hat{\psi}(\hat{z})$ must be real; and (2) $\hat{\psi}(\hat{z}) = 0$ at $\hat{z} = 1$, because the stream function should be zero at the free surface and the bottom. The solution for Ψ is given by

$$\frac{\Psi}{U_*H} = \frac{6\delta}{\kappa k^3} \sin \frac{ky}{H} \left[\left(2\frac{z}{H} - 1\right) \cos \frac{kz}{H} + 1\right] \quad \text{for} \quad k = (2m-1)\pi \ldots\ldots \quad (18)$$

$$\frac{\Psi}{U_*H} = \frac{6\delta}{\kappa k^3} \sin \frac{ky}{H} \left(1 - \cos \frac{kz}{H}\right) \quad \text{for} \quad k = 2m\pi \quad \ldots\ldots\ldots\ldots \quad (19)$$

in which m = 1, 2, and so on. It is apparent that the largest cell corresponding to $k = \pi$ is predominant, and other smaller cells contribute little to Ψ. The higher modes thus can be neglected, and the velocity components of the secondary circulation can be approximated by

$$\frac{V}{U_*} = \frac{6\delta}{\kappa\pi^3} \sin \frac{\pi y}{H} \left[2 \cos \frac{\pi z}{H} - \pi \left(2\frac{z}{H} - 1\right) \sin \frac{\pi z}{H}\right] \ldots\ldots\ldots\ldots \quad (20)$$

$$\frac{W}{U_*} = -\frac{6\delta}{\kappa\pi^2}\cos\frac{\pi y}{H}\left[\left(2\frac{z}{H}-1\right)\cos\frac{\pi z}{H}+1\right] \quad \ldots\ldots\ldots\ldots\ldots (21)$$

Relations with Longitudinal Ridges and Isovels.—The theory thus obtained predicts the depth-scale secondary currents with opposite directions of rotation. Once a series of such pair vortices is set in array, sand ridges will be formed where the flows converge. The sand ridges thus formed will next distort the field of the Reynolds normal stresses along the traverse, which will, in turn, maintain the secondary currents. The mutual interaction will thus reach a stable state. Unfortunately, any functional relationship between the characteristic scales of the ridges (e.g., height of the ridges), and the distortion of the Reynolds

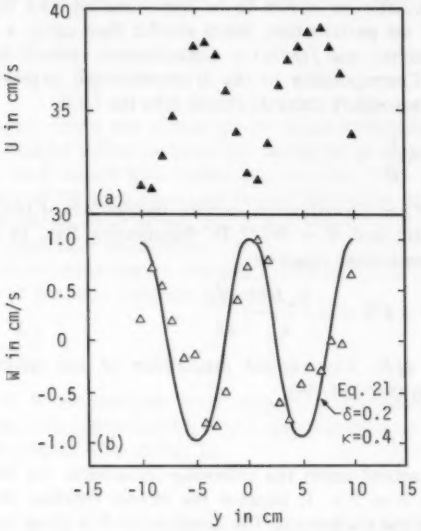

FIG. 14.—Lateral Distributions of U and W at $z/H = 0.5$ in Flume with Artificial Sand Ridges; Measurements were Made by Kuroki and Kishi (9)

stresses is not yet established, and further analysis of this instability mechanism is impossible at present. If δ of Eq. 14 can be correlated to the height of the ridges, then the instability problem would be resolved completely.

The distortion of the mean flow fields with the boundaries simulating the sand ridges were studied by Kuroki and Kishi (9) in a tilting flume 8 m long and 0.8 m wide. Spacing artificial ridges at an interval of twice the depth, they measured the transverse distribution of the longitudinal velocity component, U, the vertical secondary flow component, W, and the Reynolds shear stress, $\overline{uw}$. The mean flow fields show relatively regular undulations with a wavelength of the interval of the ridges, and the W field is described fairly well if δ of

0.2 is selected in Eq. 25 (see Fig. 14). The W velocity component transports a longitudinal momentum deficit upward at the crests, resulting in low fluid velocity above the crests. The situation is exactly the same as that found in Runs 16 and 17 of the present study. Moreover, they noticed that the regular waviness of the W field was broken if the interval-depth ratio was changed from 2.

Experimental data on the distance between the adjacent ridges were presented by Kinoshita (8) and Wolman and Brush (16). Their data are compared with the prediction that the spacing of sand ridges should be twice the depth (see Fig. 15). It is apparent that the ratio maintains the nearly constant value of two regardless of the Froude number and the Reynolds number (3,300–19,100).

Effects on General Profiles.—The secondary flows are thus cellular and composed of depth-scale pair vortices in the central bed region. The local bed topography reveals the existence of a pair vortices also in the side-bank region. We can therefore conclude qualitatively that the secondary currents exchange

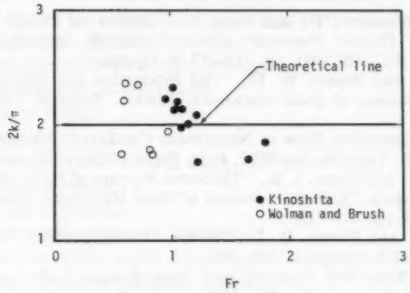

FIG. 15.—Test of Eq. 18 ($m = 1$)

the longitudinal momentum only in the scale of depth, and the lateral momentum transfer is insignificant. This qualitative examination supports the assumption of Parker (12,13), and this may be the reason why the regime relations describe the actual well.

Conclusion

The size and the shape of self-formed channels in uniform noncohesive sands were studied in two laboratory flumes where the center of the channel cross sections was replaced by a vertical side wall; the resulting half-channel helped suppress meandering tendencies.

These experiments revealed the following: (1) Corresponding to a combination of the hydraulic variables, a stable channel which allows bed-load transport in the central bed region exists; (2) the transverse bed shapes in equilibrium have a universal one in the side-bank region regardless of the initial shape, the discharge, and the sand diameter. The side-bank region keeps the universal shape also in the widening process, and it is well-described by an exponential

function, rather than cosine; (3) equilibrium depth and width depend not only on discharge, but also slope and bed materials; and (4) secondary currents affect the local features of the self-formed straight channels, but seem not to influence the general features such as the equilibrium depth or width.

A crude theoretical argument on the secondary currents was made based on the Reynolds equations of motions, and it explained fairly well the local features of the self-formed channels.

Acknowledgments

K. Ashida of Kyoto University provided a useful comment and conversation. M. Kuroki and T. Kishi of Hokkaido University allowed the use of their data. H. Amano and T. Otomo assisted with the experiments. Financial support was provided by the National Sciences Foundation, Ministry of Education, Japan.

Appendix I.—References

1. Ashida, K., Muramoto, Y., and Narai, S., "Studies on Fluvial Process of Stream Channels (2)," *Disaster Prevention Research Institute Annuals*, Kyoto University, Kyoto, Japan, No. 14B, 1971, pp. 275–297 (in Japanese).
2. Brundrett, E., and Baines, W. D., "The Production and Diffusion of Vorticity in Duct Flow," *Journal of Fluid Mechanics*, London, England, Vol. 19, Part 3, 1964, pp. 375–394.
3. Gerard, R., "Secondary Flow in Noncircular Conduits," *Journal of the Hydraulics Division*, ASCE, Vol. 104, No. HY5, Proc. Paper 13764, 1978, pp. 755–773.
4. Gessner, F. G., and Jones, J. B., "On Some Aspects of Fully Developed Turbulent Flow in Rectangular Channels," *Journal of Fluid Mechanics*, London, England, Vol. 23, Part 4, 1965, pp. 689–713.
5. Glover, R. E., and Florey, Q. L., "Stable Channel Profiles," *Hydraulics*, United States Bureau of Reclamation, 325, 1951.
6. Hirano, M., "River Bed Variation with Bank Erosion," *Proceedings of the Japan Society of Civil Engineers*, No. 210, 1973, pp. 13–20 (in Japanese).
7. Kikkawa, H., and Ikeda, S., "Fundamental Study on the Velocity Distribution in Straight Channels with Square Cross Section," *Proceedings of the Japan Society of Civil Engineers*, No. 250, 1976, pp. 63–71 (in Japanese).
8. Kinoshita, R., "An Analysis of the Movement of Flood Flows by Aerial Photography," *Photogrammetry*, Vol. 7, No. 1, 1967, pp. 1–17 (in Japanese).
9. Kuroki, M., and Kishi, T., "Structures of Longitudinal Vortices on Sand Waves," *Proceedings of the Annual Conference of the Japan Society of Civil Engineers*, Vol. 2, 1979, pp. 299–300 (in Japanese).
10. Lane, E. W., "Design of Stable Channels," *Transactions*, ASCE, Vol. 120, Paper No. 2276, 1955, pp. 1234–1279.
11. Leopold, L. B., and Maddock, T., Jr., "The Hydraulic Geometry of Stream Channels and Some Physiographic Implications," *Professional Paper 252*, United States Geological Survey, 1953.
12. Parker, G., "Self-Formed Straight Rivers with Equilibrium Banks and Mobile Bed: Part II, The Gravel River," *Journal of Fluid Mechanics*, London, England, Vol. 89, Part 1, 1978, pp. 127–146.
13. Parker, G., "Hydraulic Geometry of Active Gravel Rivers," *Journal of the Hydraulics Division*, ASCE, Vol. 105, No. HY9, Proc. Paper 14841, 1979, pp. 1185–1201.
14. Perkins, H. J., "The Formation of Streamwise Vorticity in Turbulent Flow," *Journal of Fluid Mechanics*, London, England, Vol. 44, Part 4, 1970, pp. 721–740.
15. Sawai, K., and Ashida, K., "Erosion and Cross Section on the Cohesive Stream Bed," *Proceedings of the Japan Society of Civil Engineers*, No. 266, 1977, pp. 73–86 (in Japanese).
16. Wolman, M. G., and Brush, L. M., "Factors Controlling the Size and Shape of

Stream Channels in Coarse Non-cohesive Sands," *Professional Paper No. 282-G*, United States Geological Survey, 1961.

Appendix II.—Notation

The following symbols are used in this paper:

A = aspect ratio;
a = numerical constant in Eq. 1;
B = width of free surface;
B_s = width of side-bank region;
B^* = B/D_{50} = dimensionless width;
b = numerical constant in Eq. 1;
D_{50} = median diameter size;
dA = segmented area;
ds = wetted perimeter corresponding to dA;
e = thickness of sand layer at center bed region;
F = $(\rho_s/\rho) - 1$ = submerged specific gravity of sand;
f = functional relationship in Eq. 7;
$\hat{f}$ = dimensionless vertical distribution of $\overline{vv} - \overline{ww}$;
g = gravitational acceleration;
H = center depth;
h = local depth;
k = dimensionless vertical wave number of cell;
m = positive integer;
Q = water discharge;
Q_s = volumetric sediment discharge;
$\bar{Q}$ = dimensionless water discharge;
Q^* = dimensionless sediment discharge;
q_B = sediment discharge per unit width;
q^* = dimensionless sediment discharge per unit width;
R = H/D_{50} = dimensionless depth;
S = water surface slope;
t = time;
U, V, W = longitudinal, lateral, and vertical temporal mean velocity, respectively;
U_* = laterally averaged shear velocity;
$\overline{uw}, \overline{vw}$ = the kinematic Reynolds stress;
$\overline{vv}, \overline{ww}$ = the kinematic Reynolds normal stress;
x = longitudinal coordinate from the entrance of flume;
y = lateral coordinate from the center of channel;
z = vertical coordinate;
$\hat{z}$ = z/H = dimensionless vertical coordinate;
α = numerical constant in Eq. 14;
Δ = displacement thickness of side bank profile;
δ = dimensionless amplitude of perturbation in Eq. 14;
ϵ_{yz} = component of eddy diffusion tensor;
κ = the Karman constant;
ξ = lateral coordinate from water margin;

ρ = water density;
ρ_s = sediment density;
σ = $(D_{84}/D_{50} + D_{50}/D_{16})/2$ = gradation coefficient;
τ = bottom shear stress;
τ_c = critical bottom shear stress (Shields);
τ^* = dimensionless bottom shear stress;
Ψ = stream function of secondary flow;
$\hat{\Psi}$ = dimensionless stream function; and
$\hat{\psi}$ = vertical distribution of dimensionless stream function.

JOURNAL OF THE HYDRAULICS DIVISION

VARIATION OF KARMAN CONSTANT IN SEDIMENT-LADEN FLOW

By Shang-yi Wang[1]

INTRODUCTION

The study of the law of velocity distribution in open-channel flow carrying sediment load is one of the basic problems in the exploration of river bed development. Practice has shown that velocity distribution along the depth in sediment-laden open-channel is supposed to follow approximately the logarithmic formula of velocity distribution. In the formula there is a very important factor (K) called the von Karman coefficient. A vast amount of research works have been done by different workers on the study of the value of K (2,3,4,5,6,7,9,10, 11,12,14).

Besides the characteristics of suspended load, the factors which have an influence on the variation of the coefficient K should also include the bottom regime of stream flow. In the study of the influence of suspension-load characteristics on the value of K, many researchers had attempted to conduct experiments under controlled bottom conditions. Owing to the complexity of the problem, however, such attempts have not been successful.

In this paper, based on the energy balance in a movable bed model without suspension load and the principle of effective power of suspension load, the following formula is presented for calculating the Karman constant K in the region of main flow in an open channel carrying sediment load as given in Eq. 17 in the following.

Where the first term on the right-hand side of the equation expresses the influence of the bottom condition on the value of K, and the second term expresses the influence of characteristics of suspension load on K. Through an analysis of data in the laboratory and natural open-channel flow, a value of the coefficient β_* together with a method for calculating the numerical value of K_w has finally been proposed. Equation 17 calculates the value of K which

[1]Assoc. Prof., Dept. of Hydr. Engrg., Tianjin Univ., Tianjin, China.

Note.—Discussion open until September 1, 1981. To extend the closing date one month, a written request must be filed with the Manager of Technical and Professional Publications, ASCE. Manuscript was submitted for review for possible publication on June 4, 1980. This paper is part of the Journal of the Hydraulics Division, Proceedings of the American Society of Civil Engineers, ©ASCE, Vol. 107, No. HY4, April, 1981. ISSN 0044-796X/81/0004-0407/$01.00.

is given, and is verified reasonably well with some data observed both in the laboratory and in the field.

Theoretical Analysis

From the viewpoint of energy balance (1), it may be shown that the energy expended to support the sediment load in suspension is not taken directly from the effective potential energy, but is only a part of the total frictional loss in stream flow.

The velocity distribution reflects intrinsically the resistance drag in stream flow. For open channels, the resistance drag not only depends on the characteristics of sediment load, but also more closely on the bottom conditions which consist of the bed form and the characteristics of the bed load (2). We must consider, therefore, the influence of bottom conditions of the stream flow when studying the effect of the suspension load on the velocity distribution. Owing to the complexity of bed material motion which is acted on by the bottom regime directly, it is extremely difficult to rule out the influence of bottom conditions throughout the experiment even if the bed form is fixed and the sediment is controlled without siltation.

In order to facilitate analysis, by considering the sediment-laden open-channel flow as a whole a model is suggested in which the effect of suspension load on the velocity distribution in the region of main flow is differentiated from that caused by bottom conditions.

Suppose that in a model of open-channel flow with no suspension load but with the same movable bottom conditions there is a depth of flow and hydraulic gradient as an actual sediment-laden open channel. We may then write:

$$-(U - U_w)\, d\tau_w = \tau_w d(U - U_w) - d\,[\tau_w(U - U_w)] \quad \ldots\ldots\ldots\ldots\ldots (1)$$

in which U = the velocity at an arbitrary point Z measured from the water surface in sediment-laden open-channel flow; and τ_w and U_w = the shearing stress and velocity at the corresponding point Z in the model, respectively.

Based on the principle of energy balance in sediment-laden open-channel flow, it may be seen that in the term of $(U - U_w)\, d\tau_w$ in Eq. 1, part of the differential is caused by the difference in velocities due to the suspension load and induced by the effective potential energy supplied by the stream flow, while the other part is caused by the differential shearing stresses. The term $\tau_w d(U - U_w)$ is the corresponding differential, part of which is caused by the difference in velocities and is a part of the local energy dissipated while the other part of the energy dissipated is caused by the difference in shearing stresses; the term $d\,[\tau_w(U - U_w)]$ is the corresponding differential, part of which is caused by the difference in velocities and is induced from the transmitted energy, and for the same reason, the other part of transmitted energy is also caused by the difference in shearing stresses. In the previous analysis, all of the higher order differential parts are being neglected.

In the sense of the aforementioned energy of stream flow and the principle of effective power of sediment, three suppositions could be mentioned as follows:

First Supposition.—The changed portion of the effective potential energy caused by the difference in velocities at an arbitrary point is proportional to the effective potential energy supplied by the suspension load. It may be put as

$$-(U - U_w)\, d\tau_w = -\alpha_1(\gamma_s - \gamma_w)\, C\, U\, J\, dZ \quad \ldots\ldots\ldots\ldots\ldots\ldots (2)$$

in which α_1 = a proportional coefficient; the term $(\gamma_s - \gamma_w)\ CUJ$ denotes the effective potential energy supplied by suspensionload per unit volume at an arbitrary point per second; C = the concentration in specific volume at the arbitrary point; U = the velocity at the arbitrary point; J = the hydraulic gradient; and γ_s and γ_w = the specific weights of sediment and clean water, respectively.

Second Supposition.—The transmitted energy $d[\tau_w(U - U_w)]$ previously mentioned is proportional to the power of suspension load. It may be put as

$$-d[\tau_w(U - U_w)] = -\alpha_2(\gamma_s - \gamma_w)\, C\, W\, dZ \quad \ldots\ldots\ldots\ldots\ldots\ldots (3)$$

in which α_2 = a proportional coefficient; $(\gamma_s - \gamma_w)\ C\ W$ denotes the power of suspension load per unit volume at arbitrary point; and w = the settling velocity of sediment in still water.

Substituting Eq. 2 and Eq. 3 into Eq. 1, we obtain

$$-\alpha_1(\gamma_s - \gamma_w)\, C\, U\, J\, dZ = \tau_w d(U - U_w) - \alpha_2(\gamma_s - \gamma_w)\, C\, W\, dZ \quad \ldots\ldots (4)$$

Putting $\tau_w = \gamma_w\, ZJ$ and substituting into Eq. 4, we obtain

$$Z\frac{dU}{dZ}\, dZ - Z\frac{dU_w}{dZ}\, dZ = \frac{(\gamma_s - \gamma_w)}{\gamma_w}(\alpha_2 w - \alpha_1 U J)\, C\, dZ \quad \ldots\ldots\ldots\ldots (5)$$

Integrating the aforementioned equation along the depth of turbulent region in stream flow, may have

$$\int_o^h Z\frac{dU}{dZ}\, dZ - \int_o^h Z\frac{dU_w}{dZ}\, dZ = \frac{(\gamma_s - \gamma_w)}{\gamma_w^J}\int_o^h (\alpha_2 w - \alpha_1 UJ)\, C\, dZ \quad \ldots\ldots (6)$$

in which $h = H - \delta$ = the depth of turbulent region in stream flow; H = the depth of stream flow; and δ = the thickness of bed layer.

Third Supposition.—The proportional coefficient α_1 is equal to α_2 and they have a constant value α_* along the depth of stream flow. It may be put as

$$\alpha_1 = \alpha_2 = \alpha_* \quad \ldots\ldots\ldots\ldots\ldots\ldots\ldots\ldots\ldots\ldots\ldots\ldots (7)$$

Substituting into Eq. 7 may obtain

$$\int_o^h Z\frac{dU}{dZ}\, dZ - \int_o^h Z\frac{dU_w}{dZ}\, dZ = \frac{(\gamma_s - \gamma_w)}{\gamma_w^J}\int_o^h (w - UJ)\, C\, dz \quad \ldots\ldots\ldots (8)$$

in which the term $(w - UJ)$ denoted in Eq. 8 = the effective power of sediment (17); and h = the depth of main stream flow.

Ordinarily, we may write the equation of velocity distribution along the depth of stream flow as the following:

$$U_w = \bar{U}_w + \frac{U_{*b}}{K_w}\left(1 + 2.3\log\frac{H - Z}{H}\right) \quad \ldots\ldots\ldots\ldots\ldots\ldots (9)$$

and $$U = \bar{U} + \frac{U_{*b}}{K}\left(1 + 2.3\log\frac{H - Z}{H}\right) \quad \ldots\ldots\ldots\ldots\ldots\ldots (10)$$

in which K_w and K = the von Karman constant of two kinds of channels

previously mentioned, respectively; U_{*b} = the frictional velocity; $\bar{U}_w$ and $\bar{U}$ = the mean velocities along the depth of stream flow in the two kinds of channels previously mentioned, respectively:

$$\frac{dU_w}{dZ} = -\frac{2.3\,U_{*b}}{K_w}\left(\frac{1}{H-Z}\right) \quad \ldots\ldots\ldots\ldots\ldots\ldots\ldots\ldots\ldots\ldots (11)$$

and $$\frac{dU}{dZ} = -\frac{2.3\,U_{*b}}{K}\frac{1}{H-Z} \quad \ldots\ldots\ldots\ldots\ldots\ldots\ldots\ldots\ldots\ldots (12)$$

Substituting into Eq. 8, we have

$$\frac{1}{K} = \frac{1}{K_w} - \frac{1}{2.3A_*}\alpha_*\frac{(\gamma_s-\gamma_w)}{U_{*b}J}\frac{1}{H}\int_o^h (w-UJ)\,C\,dZ \quad \ldots\ldots\ldots\ldots (13)$$

in which $$A_* = 2.3\log\frac{H-h}{H} + \frac{h}{H} \quad \ldots\ldots\ldots\ldots\ldots\ldots\ldots\ldots (14)$$

and $$\frac{1}{H}\int_o^h (w-UJ)\,C\,dZ \simeq \sigma_*(\bar{w}-\bar{U}J)\,\bar{C} \quad \ldots\ldots\ldots\ldots\ldots\ldots (15)$$

where σ_* = a correction factor; $\bar{w}$, $\bar{U}$ and $\bar{C}$ = the mean values of the corresponding factors along the depth of stream flow; and $(\bar{w}-\bar{U}J)$ denotes the mean value of the effective power of sediment along the depth of stream flow. Setting

$$\beta_* = \frac{\alpha_*\sigma_*}{2.3A_*} \quad \ldots\ldots\ldots\ldots\ldots\ldots\ldots\ldots\ldots\ldots\ldots\ldots (16)$$

and substituting Eqs. 15 and 16 into Eq. 13, then

$$\frac{1}{K} = \frac{1}{K_w} + \beta_*\frac{(\gamma_s-\gamma_w)}{\gamma_w}\frac{(\bar{w}-\bar{U}J)}{U_{*b}J}\bar{C} \quad \ldots\ldots\ldots\ldots\ldots\ldots (17)$$

Eq. 17 denotes the variation of von Karman constant K in the region of main stream flow in open channels. According to the analysis previously mentioned, the term $1/K_w$ is a part of the influence caused by the bottom conditions on the velocity distribution. The second term which lies in the right-hand side of Eq. 17 is caused by the characteristics of suspended load.

According to the variability of effective power of sediment and from Eq. 17, three conclusions can be drawn as follows: (1) When $\bar{w}-\bar{U}J > 0$; the value of K decreases with the increase of $\bar{C}$; (2) when $\bar{w}-\bar{U}J < 0$, the value of K increases with the increase of $\bar{C}$; and (3) when $\bar{w}-\bar{U}J = 0$, the variability of K has not relation with the value of $\bar{C}$ directly.

Calculation of von Karman Constant K

In the calculating of the value of K using Eq. 17, it is necessary that the coefficient β_* and K_w be determined beforehand.

Determination of β_*.—According to Eq. 16, we know that β_* is a function of three variables α_*, σ_*, and A_*. It is almost impossible that the value of β_* can be obtained by theoretical analysis. When we want to obtain the value

of β_* by Eq. 17 directly, it is necessary also to know the value of K_w which is yet unknown. As it is practically impossible to make a model of open channel having exactly the same values of H, J, and the bottom conditions with the prototype, approximate methods must be employed to solve the problem.

In Ref. 2 it may be found that there are some experiment data which show the characteristics of the two kinds of sediment-laden open channels in which the difference between their depths of stream flow ($\Delta H < 0.1$ cm) between their hydraulic gradients ($\Delta J \leq 0.2$ ‰), the formation and the form of bed, and the physical characteristics of sediment are approximately the same. In our analysis, the values of K_w are considered the same in the two sediment-laden

TABLE 1.—Calculating Results of Coefficient β_*

Number (1)	H, in centimeters (2)	J, (‰) (3)	C, as a percentage (4)	K (5)	U_{*b}, in centimeters per second (6)	$\bar{U}$, in centimeters per second (7)	Bed pattern (8)	β_* (9)
III 5	7.84	2.06	0.261	0.223	0.946	73.5	Smooth	
III 5a	7.77	2.06	0.305	0.219	0.946	72.8	Smooth	1.03
IV 8a	7.74	2.59	0.0192	0.345	1.98	81.8	Smooth	
IV 8b	7.70	2.57	0.0532	0.330	1.98	79.9	Smooth	1.41
IV 8a	7.74	2.59	0.0192	0.345	1.98	81.1	Smooth	
IV 8c	7.70	2.57	0.0920	0.319	1.98	79.9	Smooth	1.21
IV 8a	7.74	2.59	0.0192	0.345	1.98	81.1	Smooth	
IV 8d	7.70	2.59	0.1230	0.310	1.98	80.5	Smooth	1.16
IV 8b	7.70	2.57	0.0532	0.330	1.98	79.9	Smooth	
IV 8c	7.70	2.57	0.092	0.319	1.98	79.9	Smooth	1.00
IV 8b	7.70	2.57	0.0532	0.330	1.98	79.9	Smooth	
IV 8d	7.70	2.59	0.1230	0.310	1.98	80.5	Smooth	1.05
IV 8c	7.70	2.59	0.092	0.319	1.98	79.9	Smooth	
IV 8d	7.70	2.59	0.1230	0.310	1.98	80.5	Smooth	1.02

open channels previously mentioned; we may obtain

$$\beta_* = \frac{\dfrac{1}{K_1} - \dfrac{1}{K_2}}{\dfrac{(\gamma_s - \gamma_w)}{\gamma_w} \dfrac{(\bar{w} - \bar{U}_1 J_1)\,\bar{C}_1 - (\bar{w} - \bar{U}_2 J_2)\,\bar{C}_2}{U_{*b}\,\bar{J}}} \quad \ldots\ldots\ldots\ldots (18)$$

The subscripts "1" and "2" denote the corresponding factors of two similar channels previously mentioned, respectively, and the mean value of hydraulic gradient $\bar{J}$ is equal to $(1/2)(J_1 + J_2)$. Using Eq. 23 and calculating with the data of Ref. 2, we may obtain the results as shown in Table 1. From these results, it may be seen that the values of β_* are invariable and we may take its mean value as

$$\beta_* = \bar{\beta}_* \simeq 1.14 \quad \ldots \quad (19)$$

Determination of K_w.—Substituting Eq. 19 into Eq. 17, we then obtain

$$\frac{1}{K_w} = \frac{1}{K} - 1.14 \frac{(\gamma_s - \gamma_w)}{w} \frac{(\bar{w} - \bar{U} J)}{U_{*b} J} \bar{C} \quad \ldots \quad (20)$$

According to Eq. 20, we have calculated with a set of practical data which has 95 runs and vary in the following regions, such as the depths of stream flow, $H = 7.0 \sim 195$ cm; velocities, $\bar{U} = 30 \sim 250$ cm/s; hydraulic gradient,

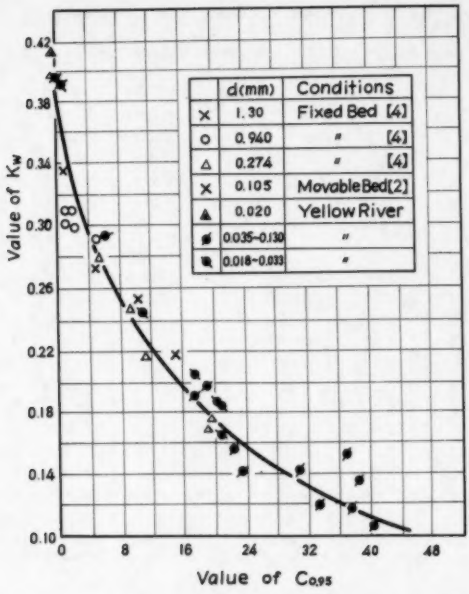

FIG. 1.—Variability of K_w Relative to Value of $C_{0.95}$

$J = (1.2 \sim 255)$ ‰; the concentrations of sediment, $\bar{C} = 0.02 \sim 0.396$ and the mid-diameters of sediment, $d_{50} = 0.018 \sim 1.3$ mm.

To calculate the settling velocity, we use the following equation in collective system (16):

$$\bar{w} = \bar{w}_o (1 - B_*) \bar{C}^{2.5} \quad \ldots \quad (21)$$

in which $\bar{w}_o$ = the mean settling velocity without concerning the influence of concentration of sediment along the depth of stream flow. The value of B_* is determined by the following equation (17):

$$B_* = \frac{1}{0.755 + 0.222 \log d_{50}} \quad \ldots\ldots\ldots\

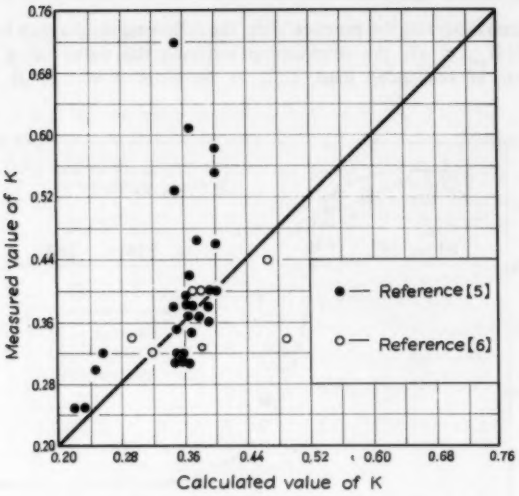

FIG. 4.—Calculated Results for Data in References 5 and 6

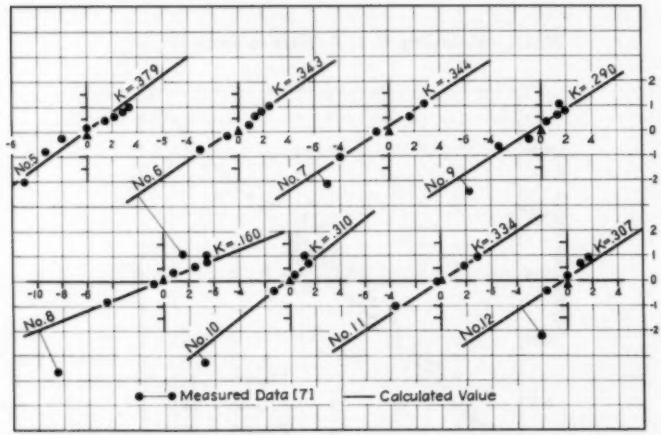

FIG. 5.—Comparison between Results Calculated by Equation 23 and Data Measured in Reference 7

(Fig. 1). When $\bar{U}/U_{*b} \geq 17$, K_w decreases as $\bar{U}/U_{*b}$ increases. At the conditions $17 \leq \bar{U}/U_{*b} < 24$, K_w varies from 0.4–0.2 widely, and until $\bar{U}/U_{*b} \geq 24$, K_w approaches a constant value 0.2 (Fig. 2).

For the purpose of contract, the value of K in clean-water stream flow with a fixed bed is shown also in Fig. 2.

Calculating Equation of K.—According to the relationship of Eq. 20, we may write

$$\frac{1}{K} = \frac{1}{K_w} + 1.14 \frac{(\gamma_s - \gamma_w)}{\gamma_w} \frac{(w - \bar{U}J)}{U_{*b}J} \bar{C} \ldots\ldots\ldots\ldots\ldots\ldots (23)$$

This is the equation for calculating the value of K and its standard deviation is about $\sigma_g = \pm 0.025$ (Fig. 3).

Verification of Equation 23

We have used the experimental data in Refs. 5, 6, and 7 for verifying Eq. 23. The acquired results are shown in Fig. 4 and Fig. 5.

Summary

1. Besides the characteristics of suspended load, the factors which have influence on the variability of Karman constant K may be the bottom regime of stream flow. Ordinarily, the later is more important than the former, as pointed out by Vanani and Nomicos in Ref. 2.

2. The first term on the right-hand side of Eq. 17 expresses the influence of the bottom conditions on the value of K and the second term expresses the influence of characteristics of suspended load on K.

3. According to the variability of the effective power of sediment we may conclude the influence of the characteristics of suspension load on K as in the following: (1) When $\bar{w} - \bar{U}J > 0$, the value of K decreases with the increase of $\bar{C}$; (2) when $\bar{w} - \bar{U}J < 0$, the value of K increases with the increase of $\bar{C}$; and (3) when $\bar{w} - \bar{U}J = 0$, the variability of K has no relation with the value of $\bar{C}$ directly.

4. The calculation for Eq. 23 may be used in practice. Its standard deviation is about $\sigma_g = \pm 0.025$. The primary results to calculate with the data of Refs. 5, 6, and 7 are shown in Fig. 4 and Fig. 5.

Acknowledgment

The writer wishes to thank C. Tao-Hung and Y. Chaoxi for their encouragement and help during this study.

Appendix I.—References

1. Bakmeteff, B. A., and Allan, W., "The Mechanism of Energy in Fluid Friction," *Transactions*, ASCE, Vol. 111, Paper No. 2288, 1946, pp. 1043–1102.
2. Vanoni, V. A., and Nomicos, G. N., "Resistance Properties of Sediment-Laden Stream," *Journal of the Hydraulics Division*, ASCE, Vol. 85, No. HY5, Proc. Paper 2020, 1959, pp. 77–105.

3. Vanoni, V. A., "Transportation of Suspended Sediment by Water," *Transactions*, ASCE, Vol. 111, Paper No. 2267, 1946, pp. 67–133.
4. Chien, Ning, and Wan, Z. H., "The Effects of Sediment Concentration Gradient on the Characteristics of Flow and Sediment Motion," *Journal of Hydraulic Engineering*, No. 4, 1965, pp. 1–20 (in Chinese).
5. Broton, J. R., and Lin, P. N., "A study of Sediment Transport in Alluvial Stream," Colorado A & M College, 1955.
6. Hsia, C. H., "A Study of Transportation of the Fine Sediments by Flowing Water," Graduate College of the State University of Iowa, Ames, Iowa, July, 1943.
7. Fan, J., "A Primary Experiment of Suspended Load," *Special Publication 1*, Peijin Hydraulic Academy of Sciences, Peijin, China, May, 1958, pp. 1–30 (in Chinese).
8. Brush, H., and Singamsetti, "A Study of Sediment in Suspension," *IASH Publication No. 59*, 1962.
9. Shevelev, F. A., "Velocity Distribution in Pipes," *Research on the Major Hydraulic Regularity of Turbulent Flow in Pipes*, National Building and Architectural Press, Moscow, Russia, 1953, pp. 49–77 (in Russian).
10. Sayre, W. W., and Albertson, M. I., "Roughness Spacing in Rigid Open Channels," *Journal of the Hydraulics Division*, ASCE, Vol. 87, No. HY3, Proc. Paper 2823, May, 1961, pp. 121–150.
11. Toichiro T., "On the Effects on Suspended Sediment on the Flow Characteristics," *Journal of the Japan Society of Civil Engineers*, Vol. 40, No. 9, 1955, pp. 1–6 (in Japanese).
12. Elata, C., and Ippen, A. T., "The Dynamics of Open Channel Flow with Suspension of Neutrally Buoyant Particle," *Hydraulic Laboratory Report*, No. 45, Massachusetts Institute of Technology, Jan., 1961.
13. Chou, T.-I., discussion of "Resistance Properties of Sediment-Laden Streams," by V. A. Vanoni, *Journal of the Sanitary Engineering Division*, ASCE, Vol. 85, No. SA5, Proc. Paper 2181, Sept., 1959, pp. 57–60.
14. Ismail, H. M., "Turbulent Transfer Mechanism and Suspended Sediment in Closed Channels," *Transactions*, ASCE, Vol. 117, Paper No. 2500, 1952, pp. 409–446.
15. Chien, N., "The Present Status of Research of Sediment Transport," *Transactions*, ASCE, Vol. 121, Paper No. 2824, 1956, pp. 833–884.
16. Wang, S., "The Settling of Fine Particles in Still Water," *Journal of Hydraulic Engineering*, No. 5, 1964, pp. 20–29 (in Chinese).
17. Wang, S., "A Review on the Effective Power of Sediment Suspension in Open Channel Flow on the Criteria of Distinguishing Bed Material Load from Wash Load," *Bulletin of Science*, Vol. 24, No. 9, pp. 410–413 (in Chinese).

Appendix II.—Notation

The following symbols are used in this paper:

A_* = $2.3 \log [(H - h)/(H)] + h/H$;
B_* = $1/(0.755 + 0.222 \log d_{50})$;
$c, \bar{c}$ = concentration in specific volume at arbitrary point and its mean value along depth of stream flow, respectively;
d_{50} = mid-diameter of sediment, in millimeters;
h = $H - \delta$, depth of turbulent region in stream flow;
H = depth of stream flow;
$J, \bar{J}$ = hydraulic gradient and its mean value of two, J_1 and J_2, respectively;
K = Karman constant;
K_w = part of K, determined by bottom regime of stream flow;
$U, \bar{U}$ = velocity at arbitrary point and its mean value along depth of stream flow, respectively;

$U_w, \bar{U}_w$ = velocity at arbitrary point and its mean value along depth of modeling stream flow, respectively;
U_{*b} = frictional velocity;
$W, \bar{W}$ = settling velocity of sediment in still water at arbitrary point and its mean value along depth of stream flow, respectively;
$\alpha_1, \alpha_2, \alpha_*$ = three proportional coefficients;
A_* = $(\alpha_*, \sigma_*)/(2.3\, A_*)$;
γ_s, γ_w = specific weight of sediment and clear water, respectively;
δ = thickness of bed layer;
σ_* = correction factor;
σ_g = standard deviation; and
τ_w = $\gamma_w Z J$.

JOURNAL OF THE HYDRAULICS DIVISION

PERFORMANCE OF BAFFLED CHUTE WITH 90° BEND

By David T. Higgins,[1] M. ASCE

INTRODUCTION

The baffled chute is a spillway-type structure that carries water to lower elevations with relatively low terminal velocity and no need for a constructed stilling basin. The Water and Power Resources Service (formerly the United States Bureau of Reclamation and referred to in this paper as the USBR) operates many such chutes on its irrigation projects. It has developed general guidelines for their design provided they are straight in plan. However it is not difficult to imagine situations where topography or interfering structures would make a baffled chute with one or more horizontal bends desirable.

Questions about the performance of a chute with a bend led to the exploratory studies reported in this paper. The results, mostly about scour and splash, may provide a design engineer with sufficient information to decide whether such a structure is a practical solution to his problem and whether further model tests are in order.

MODEL DESCRIPTION

Numerical information about the model will be stated in terms of prototype magnitude wherever it is reasonable to do so. The model is shown in Fig. 1. It included a reach of approach channel, an upper chute, a bend, a lower chute and a reach of outlet channel. Details of the upper and lower chutes followed the recommendations of the USBR (2) for a 24-ft (7.3-m) wide chute carrying 40 cfs/ft (3.7 $m^3/s/m$) at a scale of 1:12. The discharge and scale were similar to those of straight chute models reported by the USBR (1).

Outside of the bend, the model geometry was held constant except for changing the width to 12 ft (3.7 m) in four tests and dropping the approach channel

[1] Assoc. Prof., Dept. of Civ. and Environmental Engrg., Washington State Univ., Pullman, Wash. 99164.

Note.—Discussion open until September 1, 1981. To extend the closing date one month, a written request must be filed with the Manager of Technical and Professional Publications, ASCE. Manuscript was submitted for review for possible publication on June 26, 1980. This paper is part of the Journal of the Hydraulics Division, Proceedings of the American Society of Civil Engineers, ©ASCE, Vol. 107, No. HY4, April, 1981. ISSN 0044-769X/81/0004-0419/$01.00.

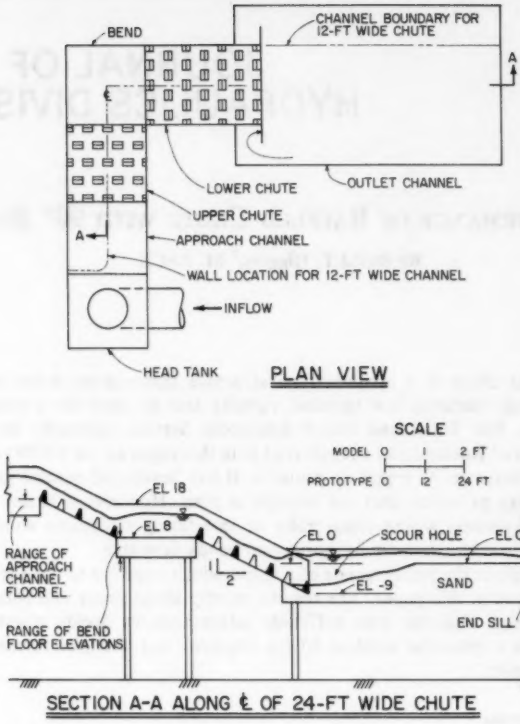

FIG. 1.—Plan and Section of Model (1 ft = 0.3 m)

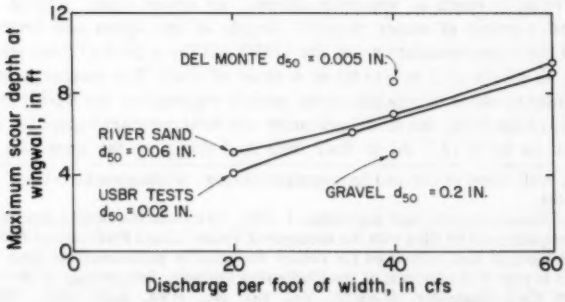

FIG. 2.—Scour Depths for Four Sands at the Base of Straight Baffled Chute (1 ft = 0.3 m, 1 in. = 25 mm, 1 cfs = 0.028 m^3)

floor 5 ft (1.5 m) in two tests. Discharge for all tests was 40 cfs/ft (3.7 $m^3/s/m$). Baffles were 3 ft (1 m) high and were arranged in five rows in the upper chute and in seven rows in the longer, lower chute. A sill with crest at elevation zero controlled tailwater stage and sand bed elevation. It was located 72 ft (22 m) downstream of the lower chute exit.

Model Calibration.—The Froude law was used to determine model discharge. But scaling scour is a different matter. For these exploratory tests it seemed appropriate to relate bend-model scour to the scour tests of the USBR (1).

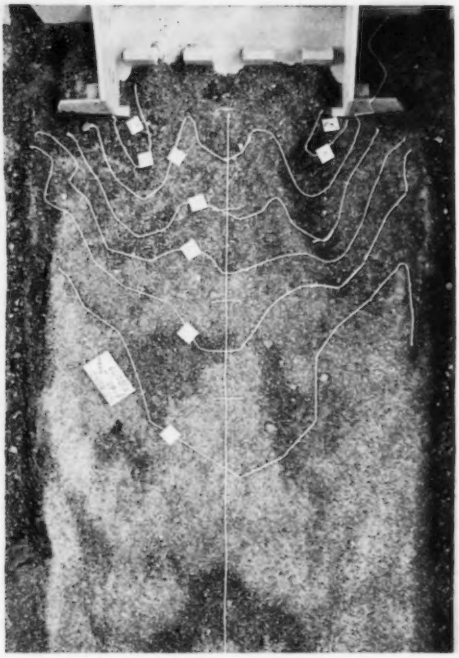

FIG. 3.—Scour Pattern below Straight Baffled Chute (Test No. 2) (1 ft = 0.3 m, 40 cfs/ft = 3.7 $m^3/s/m$)

The model was temporarily modified to operate as a straight chute with 11 rows of baffles. Several locally available sands were tested in order to find one that would scour in about the same way as that reported by the USBR. Results of the tests are shown in Fig. 2. The scour behavior of the river sand was sufficiently close to that of the USBR to proceed with it in the bend-model tests. The anomaly between scour depths and relative d_{50} is probably due to the inability of the simple d_{50} to correlate uniquely with complex scour phenomena.

Test Program

Scope.—The test program was devoted mostly to examining scour depth as a function of geometry within the bend. Guide vane arrangement and bend floor elevation were the principle variables. A few tests looked at surge height, splash against and over the chute walls, and pressures on the bend walls.

Procedures.—Before each scour test the sand lost during the previous test was replaced and the entire sand bed surface, including that within the lower end of the chute, was brought to elevation zero. The model was then operated

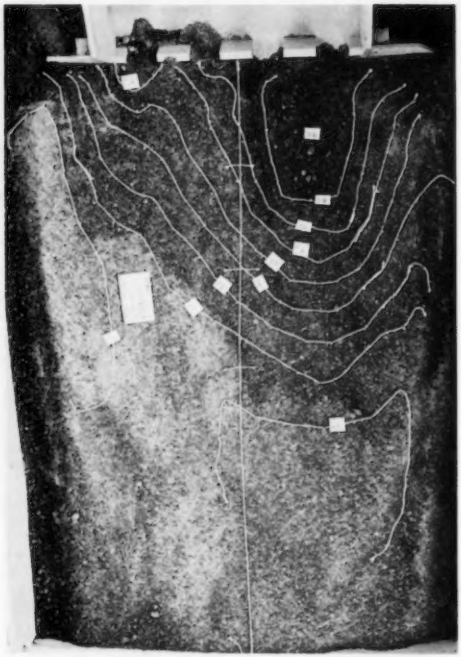

FIG. 4.—Scour Pattern below a Baffled Chute with 90° Bend (Test No. 6) (1 ft = 0.3m , 40 cfs/ft = 3.7 $m^3/s/m$)

for 30 min (model time), drained, and the scoured area marked with contour lines at 1-ft (0.3-m) intervals.

Some interesting features of the scour behavior were noted during these tests. Scour patterns closely duplicated themselves under identical test conditions. As test duration increased beyond 30 min the region of bed degradation extended farther downstream, but the scour depth at the chute exit remained constant. If the scour hole was deepened by hand after a 30-min run, a few more minutes' running time saw the scour hole refilled to its 30-min equilibrium level.

More water splashes over the walls in the bend model than in straight chute models. To record how high the splash went, chute and bend walls were extended vertically by adding panels of brown chipboard against which splash marks showed vividly. To record lateral splash extent, chute wall height was held at 9 ft (2.7 m) normal to the chute floor and chipboard panels were installed at that height outboard of the chute and parallel to the chute floor.

In the event that guide vanes might be a practical design feature of chute bends, orifices for pressure transducers were installed in the wall of the 12-ft

TEST NO. (1)	PLAN VIEW OF BEND 0 12 24 FT (2)	ELEV. OF APPROACH CHANNEL (FT) (3)	BEND FLOOR ELEV. (FT) (4)	MAXIMUM SCOUR DEPTH (FT) (5)	REMARKS (6)
1	NO BEND	20	-	7.0	12-FT WIDTH
2	NO BEND	20	-	6.7	24-FT WIDTH
3	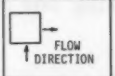	15	2	7.3	SIMPLE BEND IN 12-FT CHUTE
4		15	8	7.3	
5		20	8	7.5	
6	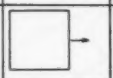	20	8	9.0	SIMPLE BEND IN 24-FT CHUTE
7			6	8.5	
8			4	8.0	
9			2	7.0	
10		20	8	7.0	THIN SHEET METAL VANES 11-FT HIGH
11			3	7.5	
12	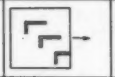	20	8	7.0	0.75-FT THICK GUIDE VANES 8-FT HIGH
13			6	7.6	
14	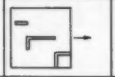	20	8	7.5	
15	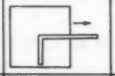	20	8	7.1	1.5-FT THICK GUIDE VANE 8-FT HIGH
16	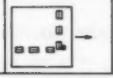	20	8	10.3	STANDARD PIERS

FIG. 5.—Summary of Scour Tests (1 ft = 0.3 m)

(3.7-m) wide chute bend. The 12-ft (3.7-m) bend wall would experience about the same surging pressure environment as a guide vane in a wider bend.

Tests Results and Considerations

Scour.—The effect of the bend on scour is to make it deeper and asymmetric with respect to the lower chute centerline. This effect is shown in Figs. 3 and 4 which, respectively, show scour contours below a straight chute (test 2) and a chute with a bend (test 6).

The complete set of scour test results is summarized in Fig. 5. The additional scour depth due to the bend varied from 0.3 ft (0.1 m)–3.6 ft (1.1 m) and was influenced largely by variations in geometry within the bend itself. The effect of entrance velocity to the upper chute is shown to be minor in tests 3, 4, and 5.

Tests 1, 3, 4, and 5 (Fig. 5) show that a square, 90° bend without guide vanes in a 12-ft (3.7-m) chute causes less than 0.5 ft (0.2 m) additional scour. Tests 6–16 in the 24-ft (7.3-m) chute show additional scour depths of from 0.3 ft (0.1 m)–3.6 ft (1.1 m).

Tests 6–9 demonstrate the effect of varying floor elevation in a plain, square bend. The lower the floor, the less the scour. But for some reason this trend does not exist when guide vanes are present. See tests 10 and 11, and 12 and 13.

The curved sheet metal vanes in tests 10 and 11 were not a practical prototype alternative. They were installed simply as a limiting case of flow guidance.

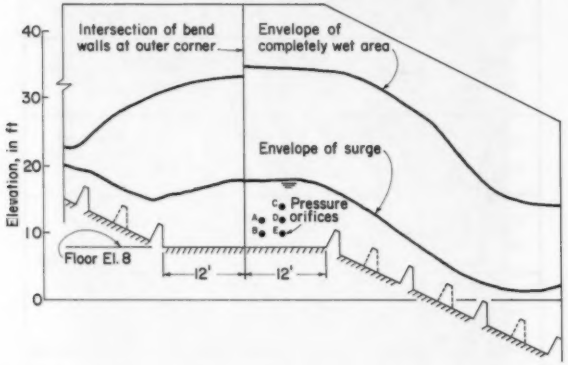

FIG. 6.—Surge and Splash Profiles along Outer Walls of 12-ft Chute and Bend (1 ft = 0.3 m)

The baffles of test 16 *were* thought to be a practical alternative and, surprisingly, caused the deepest scour of all.

Of the several arrangements of plane, segmented vanes (tests 12–15) the single vane of test 15 may be the most practical.

However, all consideration of vane patterns is largely academic. Their contribution to scour reduction would probably not repay their cost. Instead the simple bend designs of tests 5 and 6 would be appropriate design choices. An additional row of baffles at the bottom of the chute would protect against the added scour.

Splash.—The agitated flow in the upper chute around and over the baffles is a prolific source of splashing water. The trajectories of most of the drops are parallel to the chute center line. On the usual straight chute these drops will land harmlessly farther down in the chute or in the stream below. But in the bend model a significant quantity of water is thrown beyond the bend

as shown in Figs. 6 and 7. If prototype splash is at all like the splash in the model, then splash and its overbank erosion potential become an item of concern for the designer.

Surge.—On tests 5 and 6 the usual stage of the choppy water surface in the bend was about elevation 16 ft (4.9 m). Surges along the wall rose about 2 ft (0.7 m) above this level. Fig. 6 shows the envelope of maximum surge height along the bend and lower chute walls for the 12-ft (3.7-m) chute. Surges were a bit lower in the 24-ft (7.3-m) chute. The surge height envelope along the right wall of the lower chute was about 0.5 ft (0.2 m) lower than along the outer wall.

Pressure.—Pressures against the 12-ft (3.7-m) chute bend wall may be a good approximation to pressures acting on guide vanes in wider bends. Pressures were recorded at the five locations shown in Fig. 6 for the bend of test 5. They suggest that the lower 8 ft (2.9 m) of vane will be subjected to a uniform

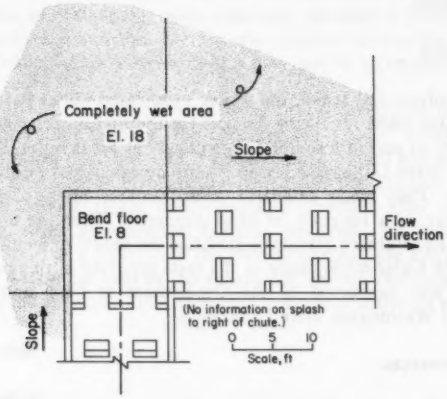

FIG. 7.—Lateral Distribution of Completely Wet Splashed Area to Left of Chute (1 ft = 0.3 m)

unbalanced thrust of 4 ft (1.2 m) of water. This includes the effect of flow separation behind the vane. The frequency of the oscillating pressure against the bend wall *in the model* was about 7 Hz.

Summary and Conclusions

The straight, baffled chute has proven to be a useful hydraulic structure. The incorporation of horizontal bends would widen its field of application if performance were not seriously degraded. This empirical study explored the consequences of a single, 90° bend in chutes of 12 ft and 24 ft widths (3.7 and 7.3 m) discharging 40 cfs/ft (3.7 $m^3/s/m$).

Except for details of flow guidance within the bend, the model design followed USBR recommendations for straight, baffled chutes. The effects of several

guidance schemes on scour were measured. A few splash tests were also made. The results may be summarized as follows:

1. A simple, square, 90° bend in a standard baffled chute carrying 40 cfs/ft (3.7 $m^3/s/m$) increases the scour depth 0.5 ft (0.2 m) in a 12-ft (3.7-m) wide chute, and 2.3 ft (0.7 m) in a 24-ft (7.3-m) wide chute.
2. The additional scour below the 24-ft (7.3-m) chute may be virtually eliminated by placing guide vanes in the bend or by lowering the bend floor. Alternatively, one more row of baffles may be installed at the bottom of the lower chute to protect against the additional scour.
3. Splash beyond the bend and lower chute walls may require slope protection.

From these tests the writer concludes that for flow rates at least up to 40 cfs/ft (3.7 $m^3/s/m$), there is no important reason based on performance why a designer should not consider a baffled chute with a bend where it could solve his problem.

Acknowledgments

During a professional leave, the writer speculated about the effect of bends in baffled chutes while reviewing designs for thermal power plant cooling water systems. Later, as part of a senior design course at Washington State University, Robert Dyer, Steve Gallo, and James Hamre designed and built the first version of this model. They made extensive measurements of the flow conditions in the lower chute as a function of bend geometry. Then, as a special project, Dennis Burns and Bernard Hargrave modified the model to include scour effects. Finally, Nadira Kabir made many of the tests reported in this paper. The entire test program was supported by the Department of Civil and Environmental Engineering at Washington State University.

Appendix.—References

1. Peterka, A. J., *Hydraulic Design of Stilling Basins and Energy Dissipators, Engineering Monograph No. 25*, United States Department of the Interior, Bureau of Reclamation, 1958; revised Jan., 1978, pp. 153–188.
2. *Design of Small Dams*, 2nd ed., United States Department of the Interior, Bureau of Reclamation, 1973, pp. 363–367.

JOURNAL OF THE HYDRAULICS DIVISION

UNSTABLE TURBULENT FLOW IN OPEN CHANNELS

By Jean E. Berlamont[1] and Nicole Vanderstappen[2]

INTRODUCTION

A review of the literature dealing with the determination of the friction factor for turbulent flow in rectangular open channels, revealed a controversial fact; a number of authors found that the Froude number affects the value of the friction factor, while others asserted that it may not be an important parameter after all.

In this study, the critical Froude number is first theoretically derived. Given a value of the Reynolds number, the flow for the Froude number above the critical value becomes unstable with the appearance of roll waves. The critical Froude number tends to be strongly dependent on the channel width. Then, the value of the friction factor under unstable turbulent flow conditions can be calculated by using an empirical formula developed by Rouse. Formulas for the friction factor as a function of the Froude number, the Reynolds number, and the channel width can thus be developed for smooth channels. The present study will clarify the apparently contradictory findings of different experimenters.

GOVERNING EQUATIONS

Equations of Motion

The general two-dimensional Reynolds equations for turbulent flow in open channels, taking into account the vertical velocity and acceleration, are:

$$\frac{1}{\rho}\frac{\partial p}{\partial x} = -\left(\frac{\partial u}{\partial t} + u\frac{\partial u}{\partial x} + v\frac{\partial u}{\partial y}\right) + g\sin\theta + \frac{1}{\rho}\frac{\partial \tau_{xx}}{\partial x} + \frac{1}{\rho}\frac{\partial \tau_{xy}}{\partial y} \quad \ldots\ldots (1)$$

$$\frac{1}{\rho}\frac{\partial p}{\partial y} = -\left(\frac{\partial v}{\partial t} + u\frac{\partial v}{\partial x} + v\frac{\partial v}{\partial y}\right) - g\cos\theta + \frac{1}{\rho}\frac{\partial \tau_{yx}}{\partial x} + \frac{1}{\rho}\frac{\partial \tau_{yy}}{\partial y} \quad \ldots\ldots (2)$$

[1]Prof. of Hydr., Dept. of Civ. Engrg., Univ. of Leuven, Leuven, Belgium.
[2]Civ. Engr., Dept. of Civ. Engrg., Univ. of Leuven, Leuven, Belgium.

Note.—Discussion open until September 1, 1981. To extend the closing date one month, a written request must be filed with the Manager of Technical and Professional Publications, ASCE. Manuscript was submitted for review for possible publication on January 4, 1980. This paper is part of the Journal of the Hydraulics Division, Proceedings of the American Society of Civil Engineers, ©ASCE, Vol. 107, No. HY4, April, 1981. ISSN 0044-796X/81/0004-0427/$01.00.

in which the x-axis is chosen along the channel bottom and the y-axis is perpendicular to it; and g = acceleration of gravity; $p(x,y,t)$ = pressure at point (x,y), at time t; $u(x,y,t)$ = velocity component in the x direction; $v(x,y,t)$ = velocity component in the y direction; θ = slope angle of the channel; ρ = mass density of the fluid; and τ_{xx}, τ_{xy}, τ_{yy}, τ_{yx} = Reynolds stresses.

Continuity Equation

$$\frac{\partial u}{\partial x} + \frac{\partial v}{\partial y} = 0 \quad \text{for an incompressible fluid} \quad \ldots\ldots\ldots\ldots\ldots\ldots (3)$$

Integrating Eq. 3 over the cross-sectional area, A, with the help of the kinematic surface condition gives the continuity equation for the mean flow

$$\frac{\partial (UH)}{\partial x} + \frac{\partial H}{\partial t} = 0 \quad \ldots\ldots\ldots\ldots\ldots\ldots\ldots\ldots\ldots\ldots\ldots\ldots (4)$$

in which $U(x,t)$ = mean velocity over the cross section at x at time t; and $H(x,t)$ = water depth at x at time t.

Eqs. 1 and 2 may be integrated over a cross section by assuming the following.

1. The flow is gradually varied, i.e., $\partial \tau_{xy} / \partial x = 0$.
2. $\tau_{xx} = \tau_{yy}$.
3. The expression for the mean shear stress on the channel walls is, even in unsteady flow:

$$(\tau_{xy})_{y=0} = \tau = \rho \frac{U^2}{8} f(U,H) \quad \ldots\ldots\ldots\ldots\ldots\ldots\ldots\ldots\ldots\ldots (5)$$

in which f = the Darcy-Weisbach friction factor.

4. The velocity profiles are similar in all cross sections:

$$u(x,y,t) = F(z)\, U(x,t) \quad \ldots\ldots\ldots\ldots\ldots\ldots\ldots\ldots\ldots\ldots\ldots\ldots (6)$$

in which $z = y/H$. This assumption is valid both in the case of laminar flow (parabolic profile) and turbulent flow (logarithmic profile). From $\int_H u(x,y,t)\, dH = UH$, it follows that $\int_0^1 F(z)\, dz = 1$.

5. Products of lower derivatives of U and H, with respect to x and t, are small, as compared with the higher derivatives (11).

From Eqs. 3 and 6 it follows that

$$v = -\int_0^y \frac{\partial (FU)}{\partial x}\, dy = -\int_0^y \left(F \frac{\partial U}{\partial x} - \frac{U}{H} z \frac{\partial H}{\partial x} \frac{\partial F}{\partial z} \right) dy \quad \ldots\ldots\ldots\ldots (7)$$

Eq. 2 becomes, with assumption 1:

$$\frac{\partial v}{\partial t} + u \frac{\partial v}{\partial x} + v \frac{\partial v}{\partial y} = -\frac{1}{\rho} \frac{\partial (p - \tau_{yy})}{\partial y} - g \cos \theta \quad \ldots\ldots\ldots\ldots\ldots (8)$$

Substituting Eq. 7 into Eq. 8, with the help of Eq. 4 and assumption 5, one obtains, after integrating Eq. 8 between y and H:

$$\frac{p-\tau_{yy}}{\rho} = g(H-y)\cos\theta + \frac{\partial^2 H}{\partial t^2}\int_y^H dy\int_0^z F\,dz$$
$$+ U\frac{\partial^2 H}{\partial x\,\partial t}\int_y^H dy\left(\int_0^z F\,dz + \int_0^z \frac{\partial F}{\partial z}\,z\,dz + F\int_0^z F\,dz\right)$$
$$+ U^2\frac{\partial^2 H}{\partial x^2}\int_y^H dy\left(F\int_0^z F\,dz + F\int_0^z \frac{\partial F}{\partial z}\,z\,dz\right) \quad \ldots\ldots\ldots\ldots\ldots\ldots (9)$$

After integrating Eq. 1 over the cross section, A, substituting Eq. 9, and taking assumption 2 into account, one obtains the momentum equation:

$$\frac{\partial U}{\partial t} + \alpha U\frac{\partial U}{\partial x} + (1-\alpha)\frac{U}{H}\frac{\partial H}{\partial t} + g\frac{\partial H}{\partial x}\cos\theta$$
$$+ \frac{HU^2}{3}\left(\frac{C_1}{U^2}\frac{\partial^3 H}{\partial x\,\partial t^2} + \frac{C_2}{U}\frac{\partial^3 H}{\partial x^2\,\partial t} + C_3\frac{\partial^3 H}{\partial x^3}\right) = g\sin\theta - \frac{\tau}{\rho R} \quad \ldots\ldots (10)$$

in which R = the hydraulic radius; and C_1, C_2, and C_3 = constants, the value of which depends upon the shape of the velocity profile $F(z)$, and is defined by

$$C_1 = 3\int_0^1 dz\int_z^1 dz\int_0^z F\,dz \quad \ldots\ldots\ldots\ldots\ldots\ldots\ldots\ldots\ldots (11)$$

$$C_2 = 3\int_0^1 dz\int_z^1 dz\left(\int_0^z F\,dz + \int_0^z \frac{\partial F}{\partial z}\,z\,dz + F\int_0^z F\,dz\right) \quad \ldots\ldots\ldots (12)$$

$$C_3 = 3\int_0^1 dz\int_z^1 F\,dz\left(\int_0^z F\,dz + \int_0^z \frac{\partial F}{\partial z}\,z\,dz\right) \quad \ldots\ldots\ldots\ldots\ldots (13a)$$

$$\alpha = \frac{\int_0^1 u^2\,dz}{U^2} = \int_0^1 F^2\,dz = \text{the velocity distribution coefficient.} \quad \ldots\ldots (13b)$$

Dropping the third derivatives, Eq. 10 reduces to the "shallow water" equation. Eq. 9 then reduces to the hydrostatic law.

On the contrary, assuming a uniform velocity distribution [$F(z) = 1$, $\alpha = 1$, $C_1 = C_3 = 1$, and $C_2 = 2$], but taking the higher derivatives into account, one finds the momentum equation, obtained by Keulegan (11). Eq. 9 then reduces to:

$$\frac{p-\tau_{yy}}{\rho} = g(H-y)\cos\theta$$
$$+ U^2\frac{H}{2}(1-z^2)\left(\frac{1}{U^2}\frac{\partial^2 H}{\partial t^2} + \frac{2}{U}\frac{\partial^2 H}{\partial x\,\partial t} + \frac{\partial^2 H}{\partial x^2}\right) \quad \ldots\ldots\ldots\ldots (14)$$

The coefficients C_1, C_2, and C_3 can be calculated for different values of α, if the turbulent velocity profile is approximated by a "trapezoidal" one:

$$F(z) = \frac{a}{b} z \quad \text{for} \quad 0 \le z \le b; \quad F(z) = a \quad \text{for} \quad b \le z \le 1;$$

$$\text{or} \quad F(z) = \left\langle \frac{a}{b} z \right\rangle_0^b + \langle a \rangle_b^1 \quad \ldots\ldots\ldots\ldots\ldots\ldots\ldots\ldots \quad (15)$$

$$\text{Since} \quad \int_0^1 F(z)\,dz = 1, \quad \text{one obtains:} \quad a = \frac{2}{2-b} \quad \ldots\ldots\ldots\ldots \quad (16)$$

$$\text{Furthermore} \quad \alpha = \int_0^1 F(z)^2\,dz = \frac{4}{3}\frac{(3-2b)}{(2-b)^2} \quad \ldots\ldots\ldots\ldots\ldots \quad (17)$$

$$\frac{C_1}{3} = \frac{2}{(2-b)}\left[\frac{b^3}{8} + \frac{b(1-b^2)}{4} + \frac{(1-b)^2(2+b)}{6}\right] \quad \ldots\ldots\ldots \quad (18)$$

$$\frac{C_2}{3} = \frac{1}{(2-b)}\left[\frac{(14-5b)}{10(2-b)} b^3 + b\frac{(3-b)}{(2-b)}(1-b^2) + \frac{(4-b)}{(2-b)}\frac{(1-b)^2}{3}(2+b)\right] \quad \ldots\ldots\ldots\ldots\ldots\ldots\ldots \quad (19)$$

$$\frac{C_3}{3} = \frac{4}{(2-b)^2}\left[\frac{b^3}{5} + \frac{b(1-b^2)}{2} + \frac{(1-b)^2}{6}(2+b)\right] \quad \ldots\ldots\ldots \quad (20)$$

TABLE 1.—Typical Values of Constants C_1, C_2, and C_3

Velocity profile (1)	b (2)	α (3)	C_1 (4)	C_2 (5)	C_3 (6)
Parabolic	—	1.20	0.825	2.496	1.864
Uniform	0	1	1	2	1
Trapezoidal	0.088	1.03	0.977	2.068	1.094
	0.145	1.05	0.961	2.113	1.161
	0.281	1.10	0.921	2.227	1.341
Triangular	1	1.33	0.750	2.700	2.400

Typical values of the constants C_1, C_2, and C_3 for various velocity profile assumptions are listed in Table 1.

Stability Criterion

When searching for a stability criterion, one should find out under which conditions an infinitesimal small amplitude disturbance wave will grow or decay with time. Eqs. 4 and 10 can be linearized by putting: $U = U_0 + U'(U' << U_0)$; $H = H_0 + H'(H' << H_0)$; $R = R_0 + R'(R' << R_0)$; and $\tau = \tau_0 + \tau'(\tau' << \tau_0)$, in which the subscript 0 refers to values in uniform flow. Thus

$$\frac{\partial U'}{\partial t} + \alpha\,(U_0 + U')\frac{\partial U'}{\partial x} + (1-\alpha)\frac{(U_0 + U')}{(H_0 + H')}\frac{\partial H'}{\partial t}$$

$$+ g\frac{\partial H'}{\partial x}\cos\theta + \frac{(H_0+H')(U_0+U')^2}{3}\left[\frac{C_1}{(U_0+U')^2}\frac{\partial^3 H'}{\partial x\,\partial t^2}\right.$$

$$\left. + \frac{C_2}{(U_0+U')}\frac{\partial^3 H'}{\partial x^2\,\partial t} + C_3\frac{\partial^3 H'}{\partial x^3}\right] = g\sin\theta - \frac{(\tau_0+\tau')}{\rho(R_0+R')} \quad \ldots\ldots\ldots \quad (21)$$

$$\frac{\partial\,[(H_0+H')(U_0+U')]}{\partial x} + \frac{\partial H'}{\partial t} = 0 \quad \ldots\ldots\ldots\ldots\ldots\ldots \quad (22)$$

Neglecting the product $U'H'$, Eq. 22 becomes:

$$H_0\frac{\partial U'}{\partial x} + U_0\frac{\partial H'}{\partial x} + \frac{\partial H'}{\partial t} = 0 \quad \ldots\ldots\ldots\ldots\ldots\ldots\ldots\ldots \quad (23)$$

Differentiating Eq. 21 with respect to x, and neglecting products and powers of U' and H' greater than 1, one obtains, with the help of assumption 5 and Eq. 23:

$$\left(g\cos\theta - \alpha\frac{U_0^2}{H_0}\right)\frac{\partial^2 H'}{\partial x^2} - 2\alpha\frac{U_0}{H_0}\frac{\partial^2 H'}{\partial x\,\partial t} - \frac{1}{H_0}\frac{\partial^2 H'}{\partial t^2}$$

$$+ \frac{H_0U_0^2}{3}\left(\frac{C_1}{U_0^2}\frac{\partial^4 H'}{\partial x^2\,\partial t^2} + \frac{C_2}{U_0}\frac{\partial^4 H'}{\partial x^3\,\partial t} + C_3\frac{\partial^4 H'}{\partial x^4}\right)$$

$$= -\frac{1}{\rho R_0}\frac{\partial\tau}{\partial x} + \frac{\tau_0}{\rho R_0^2}\frac{\partial R}{\partial x} \quad \ldots\ldots\ldots\ldots\ldots\ldots\ldots\ldots \quad (24)$$

Applying a Taylor series to $\tau(U,H)$ and $R(H)$, and dropping the higher order terms, the right side of the equal sign in Eq. 24 may be written as:

$$-\frac{1}{\rho R_0}\left(\frac{\partial\tau}{\partial U}\right)_0\frac{\partial U'}{\partial x} - \frac{1}{\rho R_0}\left(\frac{\partial\tau}{\partial H}\right)_0\frac{\partial H'}{\partial x} + \frac{\tau_0}{\rho R_0^2}\left(\frac{\partial R}{\partial H}\right)_0\frac{\partial H'}{\partial x}$$

By introducing Eq. 23, one obtains:

$$= \frac{1}{\rho R_0}\left(\frac{\partial\tau}{\partial U}\right)_0\left(\frac{U_0}{H_0}\frac{\partial H'}{\partial x} + \frac{1}{H_0}\frac{\partial H'}{\partial t}\right)$$

$$- \frac{1}{\rho R_0}\left(\frac{\partial\tau}{\partial H}\right)_0\frac{\partial H'}{\partial x} + \frac{\tau_0}{\rho R_0^2}\left(\frac{\partial R}{\partial H}\right)_0\frac{\partial H'}{\partial x}$$

$$= \left[\frac{U_0}{\rho H_0 R_0}\left(\frac{\partial\tau}{\partial U}\right)_0 - \frac{1}{\rho R_0}\left(\frac{\partial\tau}{\partial H}\right)_0 + \frac{\tau_0}{\rho R_0^2}\left(\frac{\partial R}{\partial H}\right)_0\right]\frac{\partial H'}{\partial x}$$

$$+ \frac{1}{\rho R_0 H_0}\left(\frac{\partial\tau}{\partial U}\right)_0\frac{\partial H'}{\partial t}$$

The linear differential equation, Eq. 24, has a solution of the form:

$$H' = \eta\exp\left[\beta\, i(x-ct)\right] \quad \ldots\ldots\ldots\ldots\ldots\ldots\ldots\ldots \quad (25)$$

in which $\beta = 2\pi/\lambda$, the wave number; λ = the wave length; $c = c_r + i$

c_i; $i = \sqrt{-1}$; and η = the infinitesimal small amplitude of the disturbance wave.

Introducing Eq. 25 in Eq. 24, one obtains, when putting both the real and the imaginary part equal to zero:

$$\left(g\cos\theta - \alpha\frac{U_0^2}{H_0}\right)\beta + 2\alpha\frac{U_0}{H_0}\beta\, c_r + \frac{\beta}{H_0}(c_i^2 - c_r^2)$$
$$- \frac{H_0 U_0^2}{3}\beta^3\left[C_3 - C_2\frac{c_r}{U_0} + \frac{C_1}{U_0^2}(c_r^2 - c_i^2)\right] + \frac{c_i}{\rho H_0 R_0}\left(\frac{\partial\tau}{\partial U}\right)_0 = 0 \quad \ldots\ (26)$$

$$- 2\alpha\frac{U_0}{H_0}\beta\, c_i + 2\, c_i c_r\frac{\beta}{H_0} + \frac{H_0 U_0^2}{3}\beta^3\left(-\frac{C_2 c_i}{U_0} + \frac{C_1}{U_0^2}2\, c_i c_r\right)$$
$$- \left[\frac{U_0}{\rho H_0 R_0}\left(\frac{\partial\tau}{\partial U}\right)_0 - \frac{1}{\rho R_0}\left(\frac{\partial\tau}{\partial H}\right)_0 + \frac{\tau_0}{\rho R_0^2}\left(\frac{\partial R}{\partial H}\right)_0\right]$$
$$+ \frac{c_r}{\rho H_0 R_0}\left(\frac{\partial\tau}{\partial U}\right)_0 = 0 \quad \ldots\ (27)$$

Introducing the dimensionless variables:

$$\mathsf{F} = \frac{U_0}{\sqrt{g\, H_0\cos\theta}},\quad \text{the Froude number;}$$

$$C_i = \frac{c_i}{U_0},\quad \text{and}\quad C_r = \frac{c_r}{U_0},\quad \text{the dimensionless wave celerity; and}$$

$$\mathsf{B} = \beta\, H_0 = \frac{2\pi}{\Lambda},\quad \text{the dimensionless wave number;}$$

$$\Lambda = \frac{\lambda}{H_0},\quad \text{the dimensionless wave length,}$$

and multiplying Eq. 26 by $H_0/(\beta\, U_0^2)$, and Eq. 27 by H_0^2/U_0^2, one obtains:

$$\left(\alpha - \frac{1}{\mathsf{F}^2}\right) - 2\alpha\, C_r - C_i^2 + C_r^2$$
$$+ \frac{\mathsf{B}^2}{3}\left[C_3 - C_2 C_r + C_1(C_r^2 - C_i^2)\right] - \frac{1}{\mathsf{B}}\left(\frac{H_0}{R_0}\right)\left[\frac{1}{\rho U_0}\left(\frac{\partial\tau}{\partial U}\right)_0\right] C_i = 0 \quad (28)$$

and
$$2\, C_i(C_r - \alpha)\,\mathsf{B} + \frac{\mathsf{B}^3}{3}(2\, C_1 C_r - C_2)\, C_i$$
$$- \left[\frac{1}{\rho U_0}\left(\frac{\partial\tau}{\partial U}\right)_0\right]\frac{H_0}{R_0} + \frac{H_0}{R_0}\left[\frac{1}{\rho}\frac{H_0}{U_0^2}\left(\frac{\partial\tau}{\partial H}\right)_0\right]$$
$$- \left(\frac{H_0}{R_0}\right)^2\left(\frac{\partial R}{\partial H}\right)_0\left(\frac{1}{\rho}\frac{\tau_0}{U_0^2}\right) + \frac{H_0}{R_0}\left[\frac{1}{\rho U_0}\left(\frac{\partial\tau}{\partial U}\right)_0\right] C_r = 0 \quad \ldots\ (29)$$

Since, with assumption 3:

$$\tau = \rho \frac{U^2}{8} f(U, H); \quad \left(\frac{\partial \tau}{\partial U}\right)_0 = \rho \frac{U_0^2}{8} \left(\frac{\partial f}{\partial U}\right)_0 + \rho \frac{U_0}{4} f_0;$$

$$\left(\frac{\partial \tau}{\partial H}\right)_0 = \rho \frac{U_0^2}{8} \left(\frac{\partial f}{\partial H}\right)_0 \quad \ldots\ldots\ldots\ldots\ldots\ldots\ldots\ldots\ldots\ldots \quad (30)$$

in which f_0 = value of f in uniform flow.

The friction losses are best taken into account by using the White-Colebrook-Thijsse formula (18):

$$\frac{1}{\sqrt{f}} = -2.03 \log_{10} \left(\frac{\frac{ks}{R}}{12.20} + \frac{3.03}{\mathsf{R}\sqrt{f}} \right) \quad \ldots\ldots\ldots\ldots\ldots\ldots\ldots\ldots \quad (31)$$

in which k_s/R = the equivalent relative roughness of the channel; R = the hydraulic radius; $\mathsf{R} = 4\,(U\,R/\nu)$, the Reynolds number; and ν = the kinematic viscosity of the liquid.

TABLE 2.—$(\partial f/\partial U)_0$ and $(\partial f/\partial H)_0$ for Different Friction Formulas

Friction formula (1)	$(\partial f/\partial U)_0$ (2)	$(\partial f/\partial H)_0$ (3)
Chézy: f = constant = $8\,g/C^2$	0	0
Manning: $f = 8\,g\,n^2/R^{1/3}$	0	$-(1/3)(f_0/R_0)(\partial R/\partial H)_0$
White-Colebrook-Thijsse (Eq. 31)	$(-\phi/1+\phi)\,2(f_0/U_0)$	$(-\phi/1+\phi)2(f_0/R_0)(\partial R/\partial H)_0$
Laminar: $f = 64/\mathsf{R}$	$-f_0/U_0$	$-f_0/R_0\,(\partial R/\partial H)_0$

In a smooth channel ($k_s = 0$), Eq. 31 reduces to:

$$\frac{1}{\sqrt{f}} = 2.03 \log_{10} \mathsf{R}\sqrt{f} - 0.977 \quad \ldots\ldots\ldots\ldots\ldots\ldots\ldots\ldots \quad (32)$$

The expressions for $(\partial f/\partial U)_0$ and $(\partial f/\partial H)_0$ are summarized in Table 2 for different friction formulas.

Using the White-Colebrook-Thijsse formula, a function ϕ is introduced:

$$\phi = \frac{2.671}{\left(\frac{\frac{k_s}{R}}{12.20} + \frac{3.03}{\mathsf{R}\sqrt{f_0}} \right) \mathsf{R}} \quad \ldots\ldots\ldots\ldots\ldots\ldots\ldots\ldots \quad (33)$$

For hydraulic smooth surfaces:

$$\phi = 0.882\sqrt{f_0} \quad \ldots\ldots\ldots\ldots\ldots\ldots\ldots\ldots\ldots\ldots \quad (34)$$

The stability criterion is obtained by putting $C_i = 0$ in Eqs. 28 and 29. It yields the critical Froude number, F_c, and the celerity, $C_{r,c}$, of an infinitesimal

small amplitude disturbance wave at $F = F_c$. The flow will be unstable if $F > F_c (C_i > 0)$. Then the amplitude of the disturbance wave will increase with time.

Taking Eq. 30 into account, one obtains:

$$\left(\alpha - \frac{1}{F_c^2}\right) - 2\alpha C_{r,c} + C_{r,c}^2 + \frac{B^2}{3}(C_3 - C_2 C_{r,c} + C_1 C_{r,c}^2) = 0 \quad \ldots\ldots (35)$$

$$\frac{U_0}{8}\left(\frac{\partial f}{\partial U}\right)_0 - \frac{H_0}{8}\left(\frac{\partial f}{\partial H}\right)_0 + \left[2 + \left(\frac{H_0}{R_0}\right)\left(\frac{\partial R}{\partial H}\right)_0\right]\frac{f_0}{8}$$

$$= \left[\frac{U_0}{8}\left(\frac{\partial f}{\partial U}\right)_0 + \frac{f_0}{4}\right] C_{r,c} \quad \ldots\ldots (36)$$

To solve Eq. 36 for $C_{r,c}$, a function M is defined:

$$M = 1 - R_0\left(\frac{\partial P}{\partial A}\right)_0 \quad \ldots\ldots (37)$$

in which P = the wetted perimeter.

TABLE 3.—Values of Critical Dimensionless Wave Celerity, $C_{r,c}$, for Different Friction Formulas

Friction formula (1)	$C_{r,c}$ (2)
Chézy	$1 + (M/2)$
Manning	$1 + (2/3)\,M$
White-Colebrook	$1 + (M/2)(3\,\phi + 1)$
Laminar	$1 + 2\,M$

Since for a rectangular section of width B:

$$P = B + \frac{2A}{B} \quad \text{and} \quad \left(\frac{\partial P}{\partial A}\right) = \frac{\partial\left(\frac{P}{B}\right)}{\partial H} = \frac{\partial\left(\frac{H}{R}\right)}{\partial H} = \frac{1}{R} - \frac{H}{R^2}\frac{\partial R}{\partial H}$$

Eq. 37 reduces to:

$$M = \frac{H_0}{R_0}\left(\frac{\partial R}{\partial H}\right)_0 = \frac{1}{\frac{1 + 2H_0}{B}} \quad 0 < M < 1 \quad \ldots\ldots (38)$$

For a channel of infinite width, $M = 1$. The value of $C_{r,c}$ depends upon the friction formula chosen and is computed from Eq. 36 as given in Table 3.

The critical Froude number, F_c, can be obtained from Eq. 35, by substituting the results of Table 3. One obtains, using the White-Colebrook formula:

$$\frac{1}{F_c^2} = \alpha\left(1 + \frac{C_3}{\alpha}\frac{B^2}{3}\right) - 2\alpha\left(1 + \frac{C_2}{2\alpha}\frac{B^2}{3}\right)\left[1 + \frac{M}{2}(3\,\phi + 1)\right]$$

$$+\left[1+\frac{M}{2}(3\phi+1)\right]^2\left(1+C_1\frac{B^2}{3}\right) \quad \ldots\ldots\ldots\ldots\ldots\ldots\ldots\ldots\ldots\ldots \quad (39)$$

It is seen that the critical Froude number depends upon: (1) The shape of the velocity profile (α, C_1, C_2, C_3); (2) the Reynolds number, R, and a parameter

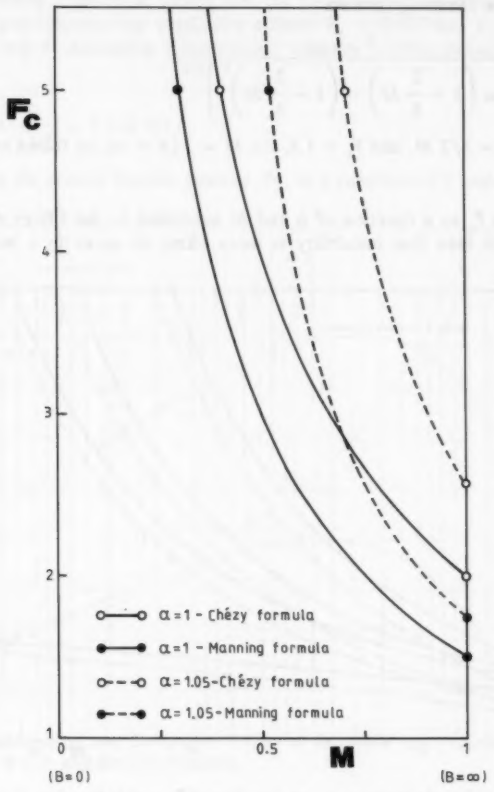

FIG. 1.—Critical Froude Number, F_c, as Function of M for Different Values of α According to Resistance Laws by Chézy and Manning

signifying the relative roughness, ϕ; (3) a parameter representing the channel width, M; and (4) the dimensionless wave number, B. For B = 0 (initial disturbance with infinite wave length), one finds:

1. Using the Chézy formula

$$F_c = \frac{1}{\left[\alpha - 2\alpha\left(1 + \frac{M}{2}\right) + \left(1 + \frac{M}{2}\right)^2\right]^{1/2}}$$

If $\alpha = 1$, $F_c = 2/M$, and $F_c = 2$, for $M = 1$ ($B = \infty$), as found by Jeffreys (7).

2. With the Manning formula

$$F_c = \frac{1}{\left[\alpha - 2\alpha\left(1 + \frac{2}{3}M\right) + \left(1 + \frac{2}{3}M\right)^2\right]^{1/2}}$$

If $\alpha = 1$, $F_c = 3/2\,M$, and $F_c = 1.5$, for $M = 1$ ($B = \infty$), as found by Keulegan (10).

Fig. 1 shows F_c as a function of α and M according to the Chézy or Manning formula. It is seen that instability is more likely to occur in a wide section.

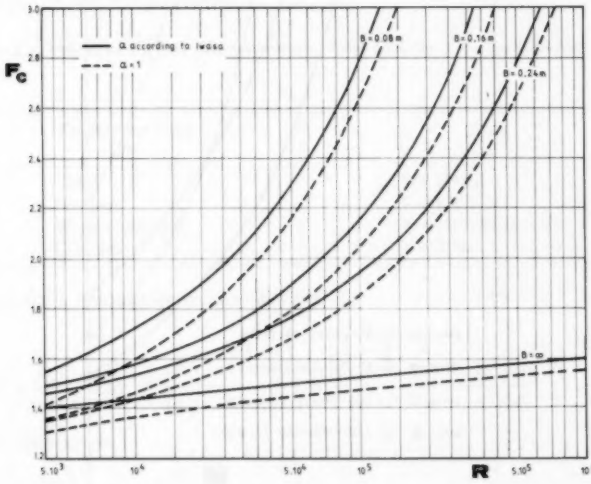

FIG. 2.—Critical Froude Number, F_c, as Function of Reynolds Number, R, and Channel Width, B, for Smooth Channel and B = 0

Using the White-Colebrook formula, Eq. 39, for B = 0, becomes

$$F_c = \frac{1}{\left\{\alpha - 2\alpha\left[1 + \frac{M}{2}(3\phi + 1)\right] + \left[1 + \frac{M}{2}(3\phi + 1)\right]^2\right\}^{1/2}} \quad \ldots\ldots\ldots (40)$$

Since its derivation was general, Eq. 35 indeed holds true for *laminar* flows

in which $\alpha = 1.2$ (see Table 1 for parabolic velocity profile). One obtains:

$$F_c = \frac{1}{[1.2 - 2.4(1 + 2M) + (1 + 2M)^2]^{1/2}}$$

in which $F_c = 0.577$ for $M = 1$ ($B = \infty$) or $R_c = 4$ cotg θ, and $C_{r,c} = 3$, as found by Ishihara (4).

Yih (22), using a potential theory and the Orr-Sommerfeld equations found (not taking into account the capillarity effect): $F_c = 0.527$ and $C_{r,c} = 3$; and $R_c = 3.33$ cotg θ. Assuming a logarithmic velocity profile, Iwasa has shown (6) that:

$$\alpha = 1 + 6.25 \frac{\tau_0}{\rho U_0^2} = 1 + 0.781 f_0 \quad \ldots\ldots\ldots\ldots\ldots\ldots\ldots\ldots \quad (41)$$

Fig. 2 shows the critical Froude number, F_c, as a function of R and the channel

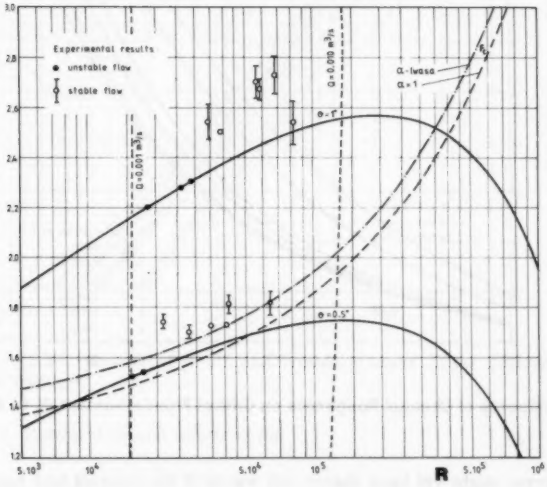

FIG. 3.—Experimental and Computed Values of Reynolds and Froude Number for $B = 0.24$ m, B = 0, and Smooth Channel

width, B, as computed with Eq. 40 for a smooth channel and B = 0 and both for $\alpha = 1$ and α computed according to Eq. 41 by Iwasa. For a given value of R, one obtains a marked increase of F_c for narrow channels, as compared with a channel of infinite width. It should be noted that, when a scale model is built at constant F, a stable flow in the model does not necessarily imply the same for the prototype.

In Fig. 3, some experimental results are shown for $B = 0.24$ m (10 ft) and a smooth channel (1). For this particular value of B, curves θ = constant can be drawn in the (R, F) plane. It is seen from Fig. 3 that for a given channel

width, a minimum slope exists below which no flow instability occurs. For a given discharge, the flow turns from a stable to an unstable regime at a critical Froude number obtained by increasing the channel slope. For a fixed channel slope, instability may disappear for large values of the discharge Q (or R).

The experimental results do not match the theoretical results completely. This can be explained (see Fig. 4) by the fact that a slight increase in channel roughness may increase F_c considerably (although the channel was reported to be smooth, k_s might have been of the order of a few tenths of millimeters), but especially because it takes some distance along the channel for developing roll waves (12,1), especially for the greater discharges and steeper slopes, so that flow conditions reported as being stable, i.e., with no (visual) development

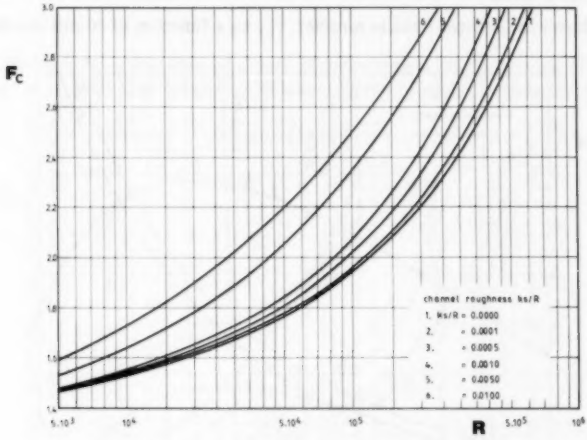

FIG. 4.—Influence of Channel Roughness on Critical Froude Number, F_c (α According to Iwasa)

of roll waves, might yet have shown roll waves if the channel had been longer than 12 m (40 ft) (1).

Friction Factor

According to a dimensional analysis by Rouse (15), the friction factor, f, should be a function not only of the Reynolds number, the relative channel roughness, and the shape of the flow section, but also of the Froude number. Since the few indications of gravitational influence found in the literature (3,8,13), were all obtained at Froude numbers well in excess of unity, Rouse assumed that the phenomenon was in some way connected with the surface instability involved in the formation of roll waves.

From experimental results obtained at Iowa (15,16), and experimental evidence

obtained by Nemec (2), Rouse found for smooth channels:

$$\frac{1}{\sqrt{f}} = 2.03 \log_{10} \frac{R\sqrt{f}}{\left(\frac{F}{F_c}\right)^{2/3}} - 0.99 \quad \text{for} \quad F > F_c \quad \ldots\ldots\ldots\ldots\ldots\ldots \quad (42)$$

If one puts $(F/F_c) = 1$ in Eq. 42 when $F \leq F_c$, Eq. 42 reduces to Eq. 32, except for a small difference in the constant value, which agrees with the laws by Blasius, Thijsse (18), Keulegan (9), Straub (17), and others.

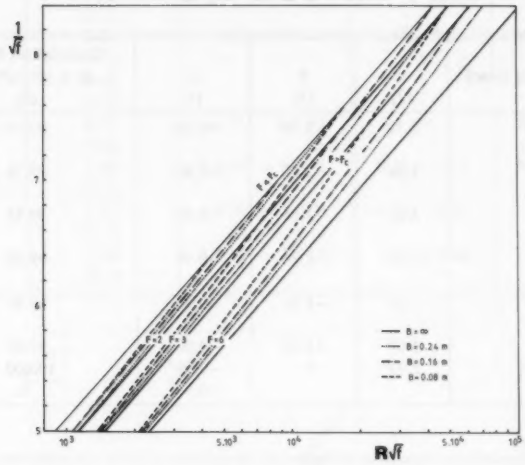

FIG. 5.—$1/\sqrt{f}$ as Function of $R\sqrt{f}$ and Froude number, F, for Different Values of Channel Width, *B*

Chen (2), Powell (13), and others wrote

$$\frac{1}{\sqrt{f}} = a \log_{10} R\sqrt{f} + b \quad \ldots\ldots\ldots\ldots\ldots\ldots\ldots\ldots\ldots\ldots \quad (43)$$

in which a and b are some function of F and F_c for $F > F_c$ and constants for $F \leq F_c$.

Introducing the value of F_c (see Eq. 40) into Eq. 42 by Rouse, one finds that f should not only be a function of R and F, but also a marked function of the channel width. The value $1/\sqrt{f}$, as computed with Eqs. 40 and 42, is represented in Fig. 5 as a function of $R\sqrt{f}$ and F for several channel widths. All stable flow situations ($F \leq F_c$) are situated on a straight line in the $(1/\sqrt{f}, R\sqrt{f})$ plane (see Eq. 32). Similar graphs can be drawn with $\sin\theta$ as a parameter instead of F. From Fig. 5 it can be seen that the influence of F on f is not negligible.

Since for a smooth channel, and a given channel width, B, F_c is a function

of R only (see Eq. 40), Eq. 42 can approximately be written as

$$\frac{1}{\sqrt{f}} = a(B) \log_{10} R \sqrt{f} + b(B) \log_{10} F + c(B) \quad \ldots \ldots \ldots \ldots \ldots \quad (44)$$

A linear regression on computed results similar to those presented in Fig. 5 yields, for the best straight line, according to Eq. 44, the values of a, b, and c given in Table 4 valid for $0.014 < f < 0.040$. From Table 4 it can be seen that c is nearly independent of the channel width.

TABLE 4.—Results of Linear Regression Analysis

B, in meters (feet) (1)	a (2)	b (3)	c (4)	Correlation factor, as a percentage (5)
0.08 (0.3)	2.32	−3.10	−0.89	99.75
0.16 (0.5)	2.24	−2.55	−0.93	99.51
0.24 (0.8)	2.21	−2.35	−0.91	99.51
0.40 (1.3)	2.17	−1.84	−0.99	99.64
1.00 (3.3)	2.12	−1.51	−0.98	99.80
∞	2.07	−1.34	−0.90	99.99
$F \leq F_c$	2.03	0	−0.99[a]	100.00
			−0.98[b]	

[a]See Eq. 42.
[b]See Eq. 32.

To obtain the value of the friction factor in hydraulically rough channels at Froude numbers in excess of F_c, Eqs. 40 and 41 should be used together with the formula by Rouse (16)

$$\frac{1}{\sqrt{f}} = 2 \log_{10} \frac{\dfrac{R}{k_s}}{\delta \left(\dfrac{F}{F_c}\right)^{2/3}} - 0.82 \quad \ldots \ldots \ldots \ldots \ldots \ldots \ldots \quad (45)$$

in which δ = the roughness concentration.

Comparison with Experimental Results

Experimental verification of the influence of the Froude number on the value of the friction factor, f, in hydraulically smooth channels, was obtained by Nemec (2,15), Jegorov (8), Powell (13), Iwagaki (5), and Wakhlu (21). Other experimenters (19), however, did not find any influence of the Froude number,

or attributed the measured differences to errors of the measurements, or both (2) (see Table 5).

TABLE 5.—Experimental Results Found in Literature

Reference (1)	B, in meters (feet) (2)	Reynolds interval (3)	Froude interval (4)	Influence of Froude	
				Yes (5)	No (6)
(8)	0.03 (0.1)	$8\ 10^3 - 5.6\ 10^4$	0.9 – 3.5	X	
(13,14)	0.20 (0.7)	$10^4 - 10^6$	2.49 – 3.28	X	
(5)	0.40 (1.3)			X	
(2,15)	0.76 (2.5)	$5.2\ 10^4 - 6.7\ 10^5$	~4	X	
(21)	1.00 (3.3)	$2.5\ 10^2 - 1.5\ 10^5$	0.50 – 12.5	X	
(19)	1.07 (3.5)	$6\ 10^4 - 7\ 10^5$	0.14 – 3.96		X
(2)	1.10 (3.6)	$8.8\ 10^4 - 2.4\ 10^5$	1.19 – 2.88		X

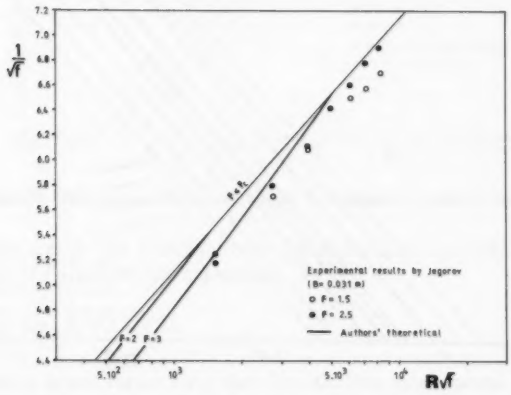

FIG. 6.—Experimental Results Obtained by Jegorov in Comparison with Computed Values

Since the width of the various experimental channels (2,5,8,13,14,15,19,21) varied between 0.03 m (1.2 in.) and 1.10 m (3.6 ft), it may be true that the difference in channel width might partly account for the contradictory results on the influence of the Froude number on the friction factor.

Jegorov (8) found an increase in f of 10%–20% for $0.9 < F < 3.5$. For lower

values of F, the obtained values of f were identical to those obtained from the Blasius formula. For $F > 3.5$, f decreases to the Blasius value. The maximum increase was obtained for $F \simeq 2$–2.3. Some measured values by Jegorov at $F = 1.5$ and 2.5 are compared with our computed values. All values at $F = 2.5$ are close to the curves $F = 2$ and 3 (see Fig. 6). The influence of F on f was explained by Jegorov (8) by studying the stability of the interface layer between the laminar boundary layer and the turbulent flow. Powell found (14) experimentally:

$$\frac{1}{\sqrt{f}} = 2.03 \log_{10} R\sqrt{f} - 0.64 \quad F < F_c \simeq 1.7 \quad \ldots\ldots\ldots\ldots\ldots\ldots \quad (46)$$

$$\frac{1}{\sqrt{f}} = 3.74 \log_{10} R\sqrt{f} + 1.87F - 15.4 \quad F > F_c \quad \ldots\ldots\ldots\ldots\ldots \quad (47)$$

Eq. 46 is according to Brock, and is a reworking of Powell's experimental data (2).

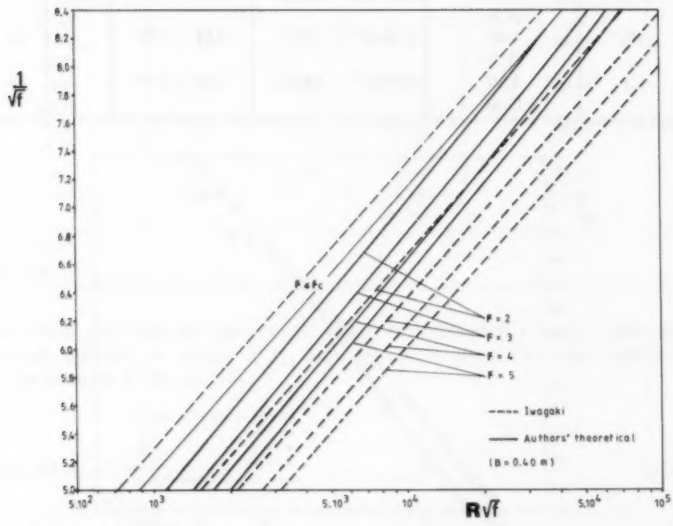

FIG. 7.—Results Obtained by Iwagaki in Comparison with Computed Values

Eq. 47 was obtained from experiments with $F \simeq 3$ (see Table 5). An increase of f up to 66% was obtained. Although Eq. 47 is similar to Eq. 44 it indicates a decreasing value of f with increasing F, which is at variance with Eq. 44. It may be that the narrow interval of F values did not allow the extrapolation of Eq. 47 to values of F much different from 3.

Iwagaki (5) found $F_c = 0.89$ and

$$F < F_c = \frac{1}{\sqrt{f}} = 2.03 \log_{10} R \sqrt{f} - 0.80 \quad \ldots \quad (48)$$

$$F > F_c = \frac{1}{\sqrt{f}} = 2.03 \log_{10} R \sqrt{f} - 2.03 \log_{10} F - 0.89 + 0.426 (\log_{10} F)^2 \quad (49)$$

the last term being small, as compared with the others. As shown in Fig. 7, Eq. 49 yields larger values of f than Eq. 42.

Wakhlu (21) also found an increase of f with F. He, too, obtained larger values of f than the theoretical ones obtained by means of Eq. 42.

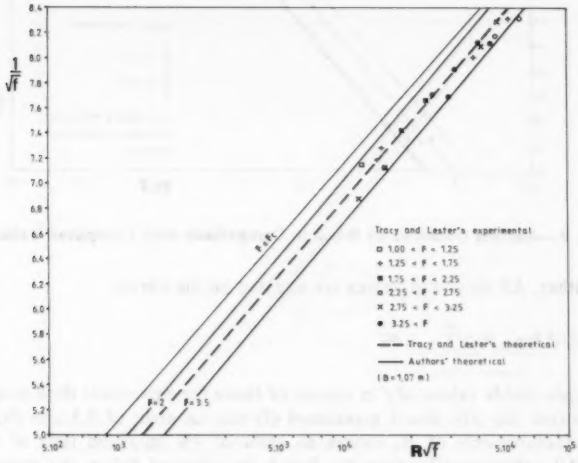

FIG. 8.—Results Obtained by Tracy and Lester in Comparison with Computed Values

Tracy and Lester (19) found for both subcritical and supercritical values of F all values of f satisfying the expression:

$$\frac{1}{\sqrt{f}} = 2.03 \log_{10} R \sqrt{f} - 1.30 \quad \ldots \quad (50)$$

Eq. 50 yields larger values for f than Eq. 32. The experimental values ($1.25 < F < 4.0$) all are situated between our theoretical curves $F = 2$ and 3.5, and thus, are below the curve $F \leq F_c$ (see Fig. 8). It looks as if Eq. 50 yields a mean value of all measurements both for stable and unstable flow conditions. Since almost all experimental values ($F > 1$) yield larger values for f than those given by Eq. 50 one would question Tracy and Lester's conclusion that there is no increase of f with increasing F. From Fig. 8 it is seen, on the contrary, that the measured values are reasonably good in accordance with the computed values.

Brock (2) did not find any influence of the Froude number on the friction

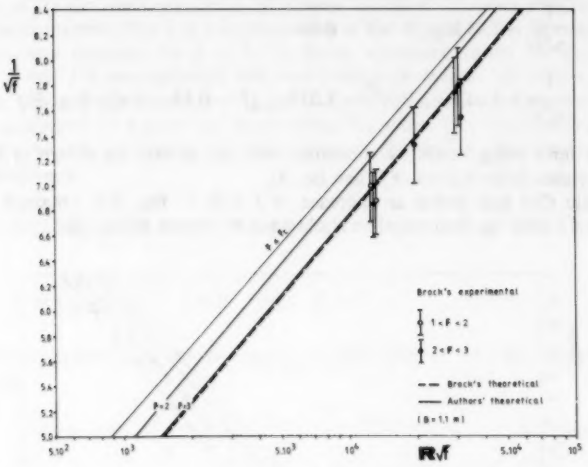

FIG. 9.—Results Obtained by Brock in Comparison with Computed Values

factor either. All measured values are situated on the curve:

$$\frac{1}{\sqrt{f}} = 2.03 \log_{10} R \sqrt{f} - 1.40 \quad \ldots \ldots \ldots \ldots \ldots \ldots \ldots \ldots \quad (51)$$

which again yields values of f in excess of those for subcritical flow in smooth channels (see Eq. 32). Brock mentioned (2) that an error of 0.5 mm (0.02 in.) on the measurements of H_0 causes an error of 8% on f and thus of 4% on $1/\sqrt{f}$. All experimental values by Brock are situated below the curve $F \leq F_c$ (see Fig. 9), and taking into account the error of ±4%, it is seen that they are in good agreement with the values obtained from Eq. 42. The fact that Brock had only seven experimental results in a small interval of Froude numbers ($1.19 < F < 2.88$) did not allow the construction of curves for different values of F. Moreover, it is seen from Fig. 9 that the values of f for the two largest values of F (2.88 and 2.65) are distinctly larger than the values obtained from Eq. 51, which may not be fortuitous. For the measurements at $F = 1.32$ and 1.50 ($R = 2.2\ 10^5$ and $8.4\ 10^5$, respectively) it follows from Fig. 2 that $F < F_c$. These two values are on the curve $F \leq F_c$ within 5%.

At the Hydraulics Laboratory of the Ghent State University, in Ghent, Belgium, some measurements (20) were carried out in a flume made of acrylic sheet 12 m (40 ft) in length and 0.24 m (0.94 in.) in width (1). The waterdepth was measured with a point gage (three measurements in each of three cross sections). The discharge was measured by means of an electromagnetic flowmeter. The relative error on f was:

$$\frac{\Delta f}{f} = 3\frac{\Delta H}{H} + \frac{\Delta S}{S} + \frac{\Delta Q}{Q} + \frac{2\,\Delta H}{240 + 2\,H}$$

in which S = the channel slope ($8\ 10^{-4} < S < 2\ 10^{-2}$); and H = the mean waterdepth (10 mm < H < 40 mm). With $\Delta H = 0.2$ mm, $\Delta S = 0.00005$, and $\Delta Q/Q = 0.01$, one obtains $\Delta f/f = 0.04$–0.08, from which results an error of 2%–4% on $1/\sqrt{f}$.

Measurements of stable flow situations ($F < F_c$) agreed very well with Eq. 32 (1). Some results in unstable flow conditions are shown in Figs. 10 and 11. These results are qualitatively in good agreement with the theoretical results as far as the increase of f with F is concerned. Quantitatively, the measured values of $1/\sqrt{f}$ are approx 3%–4% smaller than the computed values, which difference is of the order of the error on the experimental result.

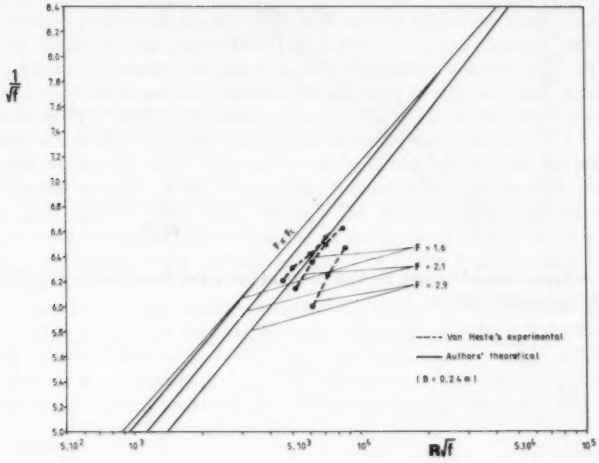

FIG. 10.—Experimental Results by Van Heste at Constant Froude Number, F, in Comparison with Computed Values

In Fig. 12, the relative increase $(f - f_0)/f_0$ is shown as a function of R and θ, in which f is computed by Eq. 42 and f_0 by Eq. 32. It is seen from Fig. 12 that especially for large channels, the curves are very flat over a large interval of R numbers. This might explain the fact that some experimenters working in a rather wide channel and in a restricted interval of Reynolds numbers (2,19) could not recognize the effect of the Froude number on the friction factor, which was, in the conditions of their experiments, of the order of the error on the measurements.

Both Tracy and Lester (19) and Brock (2) worked with a rather large channel (see Table 5) and in an interval of Reynolds numbers in which $\Delta f/f_0$ is almost independent of R (see Fig. 12). This might explain why they could not recognize the influence of the Froude number on the value of f but instead reported larger values for f_0 than given by the Blasius or Thijsse formula. For example, for $R = 10^5$ Brock found $f_0 = 0.0202$, and Tracy and Lester found $f_0 = 0.0197$,

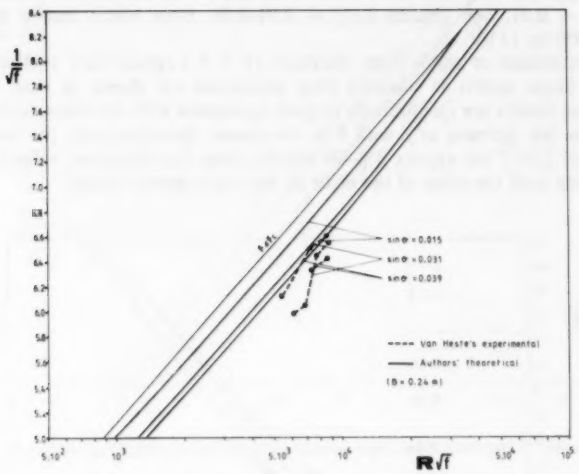

FIG. 11.—Experimental Results by Van Heste at Constant Slope Angle, θ, in Comparison with Computed Values

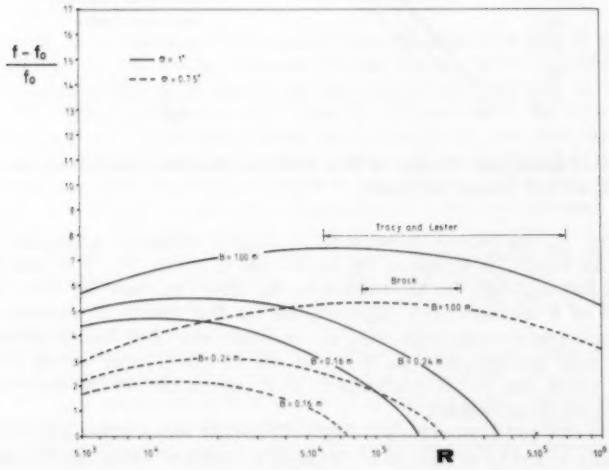

FIG. 12.—Relative Increase, $(f - f_0)/f_0$, as Function of Reynolds Number, R, Channel Width, B, and Slope Angle θ

while Eq. 32 yields $f_0 = 0.0182$, which means an increase of 11% and 8%, respectively. These figures are in good agreement with the results presented in Fig. 12 since reported channel slopes were less than 1°. Wakhlu, although working in a large channel as well, did find an influence of F on f, because he worked in a very large interval of R numbers (see Table 5). All other authors, on the other hand, working in narrower channels, found an influence of F on f.

Conclusions

Using the White-Colebrook friction formula, the critical Froude number for a turbulent flow becoming unstable can be found to be a function of the shape of the velocity profile, the Reynolds number and the relative channel roughness, the wave length of the initial disturbance wave, and the channel width. For a given Reynolds number (discharge), flow instability is more likely to occur in wide rather than in narrow channels. When scale models are built at constant F of channels for unstable turbulent flow, it might occur that the flow in the prototype is unstable while the flow in the model remains stable.

Introducing the critical Froude number in the formula by Rouse, the influence of the Froude number on the value of the friction factor for unstable turbulent flow in both smooth and rough channels can be calculated. The value of f increases with increasing Froude number (channel slope). Moreover, it is found that the coefficients in the formula relating f to R and F are functions of the channel width.

For large channels, the relative increase of f with respect to results obtained with the White-Colebrook formula, becomes almost independent of the Reynolds number, provided that $R > 4\ 10^4$. This fact explains why some authors did not appreciate the influence of F on f although other authors, working in narrow channels and for low R numbers, did indeed report an increase of f with F.

Acknowledgment

Part of this investigation was performed at the Laboratory of Hydraulics of the Ghent State University, Ghent, Belgium. The writers wish to express their sincere thanks to G. Tison and his staff.

Appendix I.—References

1. Berlamont, J., "Roll Waves," thesis presented to the Ghent State University, at Ghent, Belgium, in 1975, in partial fulfillment of the requirements for the degree of Doctor of Philosophy.
2. Farell, C., Chen, C.-L., and Brock, R., discussions of "Critical Analysis of Open-Channel Resistance," by Hunter Rouse, *Journal of the Hydraulics Division*, ASCE, Vol. 92, No. HY2, Proc. Paper 4708, Mar., 1966, pp. 395–409.
3. Homma, M., "Fluid Resistance in Water Flow of High Froude Number," *Proceedings of the Second Japanese National Congress for Applied Mechanics*, 1952, pp. 251–254.
4. Ishihara, T., et al., "On the Roll-Wave Trains Appearing in the Water Flow on a Steep Slope Surface," *Memoirs*, Vol. 14, No. 2, Faculty of Engineering, Kyoto University, Japan, Apr., 1952, p. 83.
5. Iwagaki, Y., "On the Laws of Resistance to Turbulent Flow in Open Smooth Channels," *Proceedings*, Second Japanese National Congress for Applied Mechanics; also *Applied Mechanics Review*, 2749, 1952, pp. 245–250.

6. Iwasa, Y., "The Criterion for Unstability of Steady Uniform Flows in Open Channels," *Memoirs*, Vol. 16, No. 4, Faculty of Engineering, Kyoto University, Japan, Oct., 1954, pp. 264–275.
7. Jeffreys, H., "The Flow of Water in an Inclined Channel of Rectangular Section," *Philosophical Magazine and Journal of Science*, London, England, 1949, p. 793.
8. Jegorov, S. A., "Turbulente Überwellenströmung," *Wasserkraft und Wasserwirtschaft*, Stuttgart, Germany, Vol. 35, 1940, pp. 55–57.
9. Keulegan, G. H., "Laws of Turbulent Flow in Open Channels," *Research Paper 1151, Journal of the National Bureau of Standards*, Vol. 21, Dec., 1938, pp. 707–741.
10. Keulegan, G. H., and Patterson, G. W., "A Criterion for Instability of Flow in Steep Channels," *Transactions*, American Geophysical Union, Part II, 1940, p. 594.
11. Keulegan, G. H., and Patterson, G. W., "Effect of Turbulence and Channel Slope on Translation Waves," *Journal of Research*, National Bureau of Standards, Vol. 30, June, 1943, p. 461.
12. Montuori, C., discussion of "Stability Aspects of Flow in Open Channels," by Francis F. Escoffier and Marden B. Boyd, *Journal of the Hydraulics Division*, ASCE, Vol. 89, No. HY4, July, 1963, pp. 264–273.
13. Powell, R. W., "Flow in a Channel of Definite Roughness," *Transactions*, ASCE, Vol. 3, Paper No. 2276, 1946, pp. 531–554.
14. Powell, R. W., "Resistance to Flow in Smooth Channels," *Transactions*, American Geophysical Union, Vol. 30, Dec., 1949, p. 875.
15. Rouse, H., Koloseus, H. J., and Davidian, J., "The Role of the Froude Number in Open Channel Resistance," *Journal of Hydraulic Research*, Vol. 1, No. 1, 1963, pp. 14–19.
16. Rouse, H., "Critical Analysis of Open-Channel Resistance," *Journal of the Hydraulics Division*, ASCE, Vol. 91, No. HY4, Proc. Paper 4387, July, 1965, pp. 1–15.
17. Straub, L. C., "Studies of the Transition Region between Laminar and Turbulent Flow in Open Channels," *Transactions*, American Geophysical Union, Aug., 1939, pp. 649–653.
18. "Friction Factors in Open Channels (Progress Report)," by the Task Force on Friction Factors in Open Channels of the Committee on Hydromechanics of the Hydraulics Division of the ASCE, E. Silberman, Chmn., *Journal of the Hydraulics Division*, ASCE, Vol. 89, No. HY2, Proc. Paper 3464, Mar., 1963, pp. 97–143.
19. Tracy, H. J., and Lester, C. M., "Resistance Coefficients and Velocity Distribution in Smooth Rectangular Channels," *Water Supply Paper No. 1952-A*, Department of the Interior, United States Geological Survey, Washington, D.C., 1961, pp. 1–17.
20. Vanheste, J. M., "Experimenteel Onderzoek naar de Invloed van het Froude Getal op de Weerstandscoëfficiënt f in Open Rechthoekige Kanalen," (Experimental Determination of the Influence of the Froude Number on the Friction Factor f in Open Rectangular Channels), thesis presented to the Ghent State University, at Ghent, Belgium, in 1975.
21. Wakhlu, O. N., "An Experimental Study of Thin-Sheet Flow over Inclined Surfaces," *Mitteilungen heft 158*, Versuchanstalt für Wasserbau und Kulturtechnik, Universität Fredericiana, Karlsruhe, Germany, 1970, pp. 39–121.
22. Yih, C. S., "Stability of Liquid Flow down an Inclined Plane," *Physics of Fluids*, Vol. 6, No. 3, Mar., 1963, p. 321.

Appendix II.—Notation

The following symbols are used in this paper:

A = cross-sectional area;
B = channel width;
B = dimensionless wave number ($= \beta H_o$);
C = Chézy roughness factor;
C_r = dimensionless wave celerity;
$C_{r,c}$ = critical dimensionless wave celerity;

C_1, C_2, C_3 = constants, the value of which depends upon $F(z)$;
c_r = wave celerity;
F = Froude number;
F_c = critical Froude number;
$F(z)$ = shape function of the velocity profile;
f = Darcy-Weissback friction factor;
f_0 = friction factor in uniform flow, according to White-Colebrook;
g = acceleration of gravity;
H = waterdepth;
i = $\sqrt{-1}$;
k_s/R = equivalent relative channel roughness;
M = $1 - R_0(\partial P/\partial A)_0$;
n = Manning roughness factor;
P = wetted perimeter;
p = pressure at point (x,y), at time t;
Q = discharge;
R = hydraulic radius;
R = Reynolds number;
S = channel slope;
t = time;
U = mean velocity over a cross section;
u, v = velocity components in the x direction and y direction;
x, y = rectangular Cartesian coordinates;
z = y/H;
α = velocity distribution coefficient;
β = wave number;
δ = roughness concentration;
η = infinitesimal small amplitude of the disturbance wave;
θ = slope angle of the channel;
Λ = dimensionless wave length ($= \lambda/H_0$);
λ = wave length;
ν = kinematic viscosity of the liquid;
ρ = mass density of the fluid;
τ = bottom shear stress;
$\tau_{xx}, \tau_{xy}, \tau_{yx}, \tau_{yy}$ = Reynolds stresses; and
ϕ = $(2.671/\{[(K_s/R)/12.20] + (3.03/\mathsf{R}\sqrt{f_o})\}\mathsf{R})$.

JOURNAL OF THE HYDRAULICS DIVISION

SEPARATED FLOW THROUGH LARGE SUDDEN EXPANSIONS

By Prabhulal R. Mehta[1]

INTRODUCTION

Most flows through sudden expansions in closed conduits are turbulent with flow separation and recirculation. If the expansions are axisymmetric (circular pipes), then recirculating regions and flow patterns through the expansions are symmetric. This has been observed and reported by Kalinske (6), Chaturvedi (2), and Hue and Hebrard (5). When the expansions are in rectangular ducts, depending upon whether the expansion ratio is less than or greater than 1.5, the flow patterns and recirculating regions have been found to be symmetric and steady, or unsymmetric and unsteady, respectively. This has been reported by Abbott and Kline (1), Filletti and Kays (4), and Durst, et al. (3). Using analytical and experimental findings, the writer (7) has also reported that the flow patterns through rectangular ducts with an expansion ratio of 1.25 are symmetric and steady, whereas those with an expansion ratio of 2.5 are unsymmetric and unsteady. In this paper, experimental findings for rectangular ducts with expansion ratios of 2.0 and 3.0 are presented. These results will be useful for predicting more accurately the behavior of flows through large, sudden rectangular expansions.

FLOW CONFIGURATION AND INSTRUMENTATION

Problem Defined.—Fig. 1 shows a sudden rectangular conduit expansion of ratio B/b, in which b and B = widths of the rectangular conduit before and after the expansion, respectively; and $T = B - b$. The flow, after leaving the plane of the expansion, develops two unequal cavities (stall regions) on either side of the axis of symmetry, as shown by means of full and dotted

[1]Prof., Dept. of Civ. Engrg., Faculty of Tech., Kalabhavan, P.B. No. 41, Baroda, 380 001, Gujarat State, India; formerly Prof. and Head, Dept. of Civ. Engrg., S.V. Regional Engrg. Coll., Surat, India.

Note.—Discussion open until September 1, 1981. To extend the closing date one month, a written request must be filed with the Manager of Technical and Professional Publications, ASCE. Manuscript was submitted for review for possible publication on June 3, 1980. This paper is part of the Journal of the Hydraulics Division, Proceedings of the American Society of Civil Engineers, ©ASCE, Vol. 107, No. HY4, April, 1981. ISSN 0044-796X/81/0004-0451/$01.00.

lines in Fig. 1. The flow patterns in which the reattachment point on the lower boundary is nearer (at 6 T) to the plane of expansion shall be referred to as flow type I, and that in which the point of reattachment on the lower boundary is away (at 12 T) shall be referred as flow type II. Flow types I and II may get interchanged, giving rise to an unsteady behavior of the flow. Between the primary flow in the axial direction, and the secondary recirculating flow in the stall regions, there exists a free turbulent shear layer which is highly sensitive to disturbances, and causes these alternate types of flow patterns.

Experimental Setup.—A schematic representation of the experimental arrangement is shown in Fig. 2. A 5-hp air blower was used to supply air to the

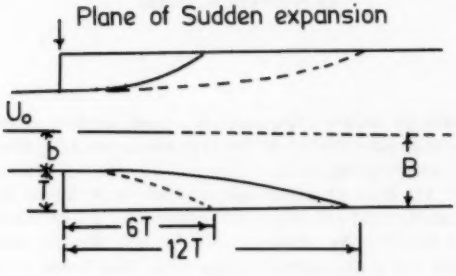

FIG. 1.—Definition Sketch

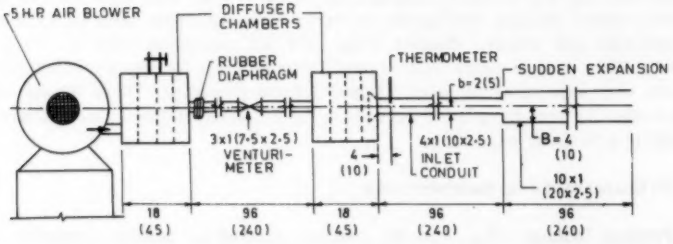

FIG. 2.—Schematic Diagram for Experimental Setup; Expansion Ratio 2.0; All Dimensions in inches (centimeters)

inlet conduit with a 2.5 cm × 10 cm cross section and 2.4-m length. Care was taken to see that the air supplied was dust free and the test assembly free of any mechanical vibrations. Flow in the inlet conduit was fully developed, and the level of initial turbulence was kept between 1%–2% of the mean axial flow velocity, U_o, in the inlet conduit. The inlet conduit was made to join the expansion piece by means of a detachable male-female joint, and the width of the inlet and expansion conduit were the same (namely, 2.5 cm). This arrangement facilitated changes in the expansion ratio to any desired value.

Four different expansion ratios (B/b = 1.25, 2.0, 2.5, and 3.0) were used, and flow patterns were obtained for the Reynolds number range of 0.5×10^5–1.0

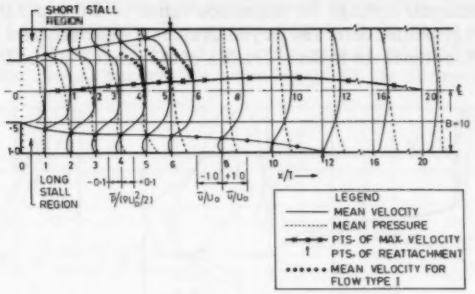

FIG. 3.—Measured Values of Mean Pressure and Mean Velocity; Expansion Ratio 2.0; R1 = 10^5 (Flow Type I and II)

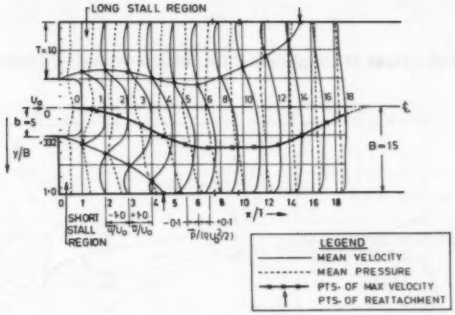

FIG. 4.—Measured Values of Mean Pressure and Mean Velocity; Expansion Ratio 3.0; R1 = 10^5 (Flow Type I)

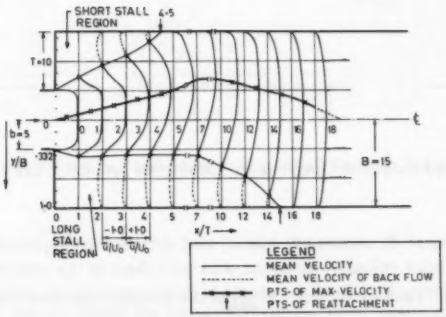

FIG. 5.—Measured Values of Mean Pressure and Mean Velocity; Expansion Ratio 3.0; R1 = 10^5 (Flow Type II)

$\times 10^5$. Experimental findings for expansion ratios of 2.0 and 3.0 at Reynolds number 10^5 are presented here. The Reynolds number was calculated by $\rho U_o D/\mu$, in which D = four times the hydraulic radius of the conduit before the expansion.

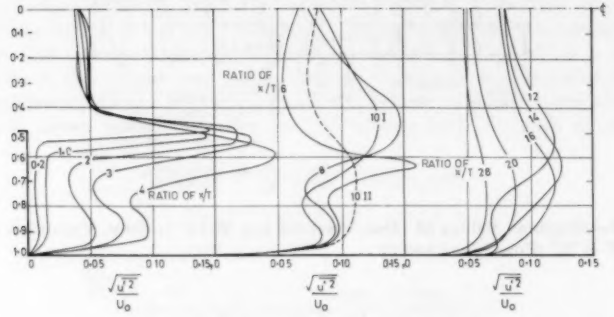

FIG. 6.—Measured Values of Longitudinal Turbulence Intensity; Expansion Ratio 2.0; R1 = 10^5

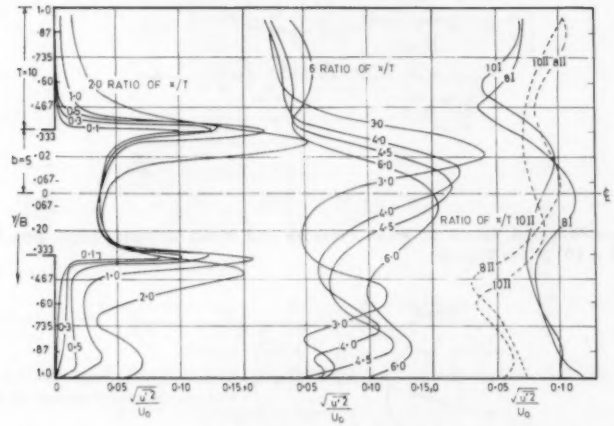

FIG. 7.—Measured Values of Longitudinal Turbulence Intensity; Expansion Ratio 3.0; R1 = 10^5

Instrumentation.—A combined, static, and dynamic-type pitot tube was used to measure the mean velocity, pressure, and wall shear in the conduit downstream of the expansion. Turbulence intensities in the longitudinal direction, $\sqrt{\overline{u'^2}}/U_o$, and in the transverse direction, $\sqrt{\overline{v'^2}}/U_o$, and the Reynolds shear stress, $-\overline{u'v'}/U_o$, were measured by a Dansk Industri Syndikat Associates (of Denmark) hot wire anemometer of constant temperature type. The hot wire probe and

the bridge circuit to measure cold resistance of probe were developed in the laboratory of I.I.T., Bombay. The sensing element of the probe was a copper-coated tungsten filament of 5-μ diam, and was soft soldered to the needle supports of the probe. The central 1-mm length of the filament was etched

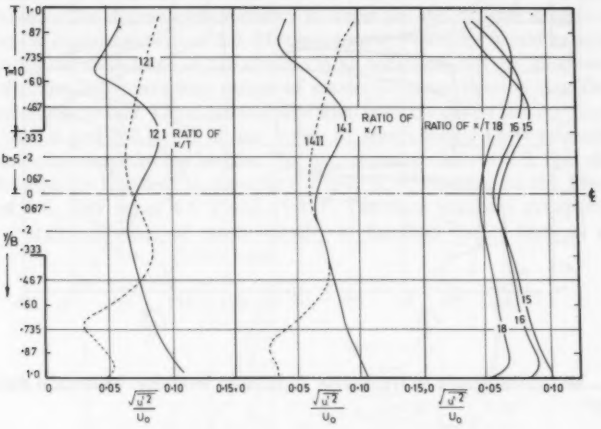

FIG. 7.—*Continued*

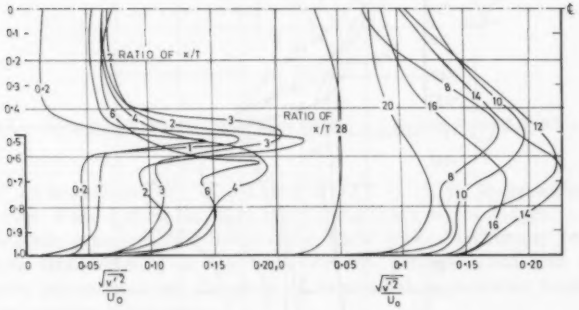

FIG. 8.—Measured Values of Transverse Turbulence Intensity; Expansion Ratio 2.0; R1 = 10^6

out, making use of nitric acid, to give a cold resistance of the sensing element around 5 ohms.

A straight wire probe was used to measure $\sqrt{\overline{u'^2}}/U_o$, and a single, 45° inclined wire, which could be rotated through 180°, was used to measure $\sqrt{\overline{v'^2}}/U_o$. The Reynolds shear stress, $-\overline{u'v'}/U_o$, was calculated from the instantaneous readings of u' and v'.

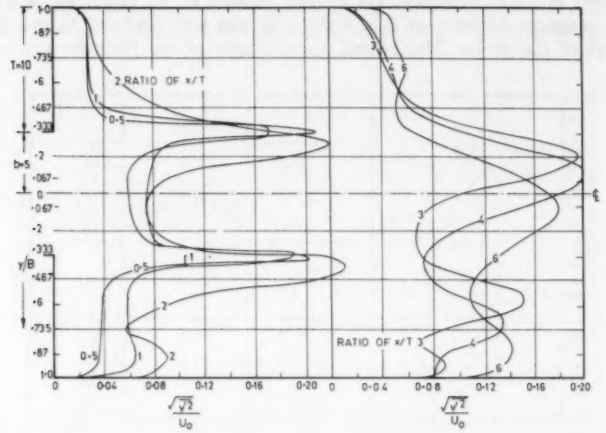

FIG. 9.—Measured Values of Transverse Turbulence Intensity; Expansion Ratio 3.0; R1 = 10^5

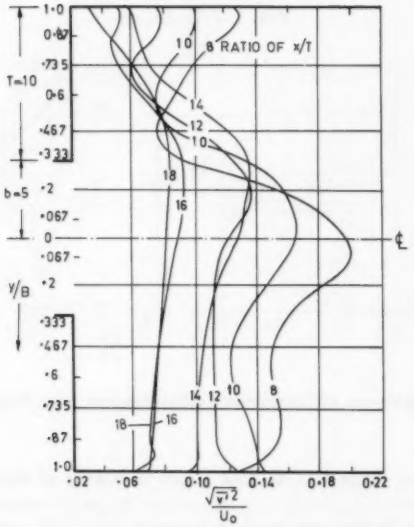

FIG. 9.—*Continued*

Experimental Findings

Mean Velocities and Pressures.—Figs. 3, 4, and 5 show measurements of the mean velocity profile and static pressure distributions at various locations downstream of the plane of expansion for expansion ratios of 2.0 and 3.0, respectively. The degree of asymmetry is larger for the expansion ratio of 3.0 than for the expansion ratio of 2.0. Maximum mean velocities would be expected to occur at the center line of the conduit at all locations, but the measurements show that the line connecting points of maximum mean velocity deviate from the conduit center line. The maximum deviation from the center line for expansion ratios of 2.0 and 3.0 is 0.2 B and 0.466 B, respectively. Flow patterns also show unequal reattachment lengths. For an expansion ratio of 2.0, the reattachment lengths are found to be equal to 6 T and 12 T, whereas for the expansion ratio of 3.0, they equal 4.5 T and 15.0 T. The flow becomes symmetric and stable (maximum value of mean velocity at the duct center line) at $x/T =$

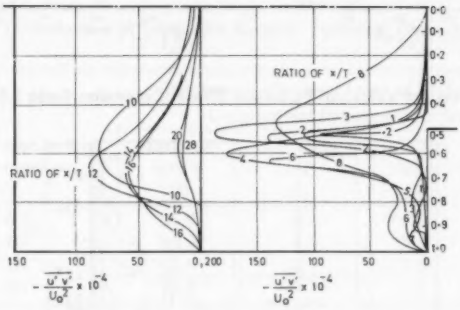

FIG. 10.—Measured Values of Turbulent Shear; Expansion Ratio 2.0; R1 = 10^5

20.0 for an expansion ratio of 2.0, and at $x/T = 16$ for an expansion ratio of 3.0. Figs. 4 and 5 show that flow types I and II are mirror images.

Mean static pressures distributions also show greater asymmetry for larger expansion ratios (similar to the mean velocity patterns), and also become symmetric (downstream of the plane of expansion) at the same locations as the mean velocity distributions.

Turbulent Characteristics.—Figs. 6 and 7 display the results of the turbulence intensity in the longitudinal direction, and Figs. 8 and 9 show the results of the turbulence intensity in the transverse direction. Measured values of the turbulent shear stress are given in Figs. 10 and 11.

Turbulence intensities and shear stress show a higher degree of nonuniformity for the expansion ratio of 3.0 than for the expansion ratio of 2.0. Peak values develop along the free turbulent shear layer. Secondary peaks also occur in the mideddy pocket region nearer to the boundary. The turbulence grows more rapidly and decays more quickly for an expansion ratio of 3.0 than for an expansion ratio of 2.0. Fig. 7 shows that flow types I and II are mirror images.

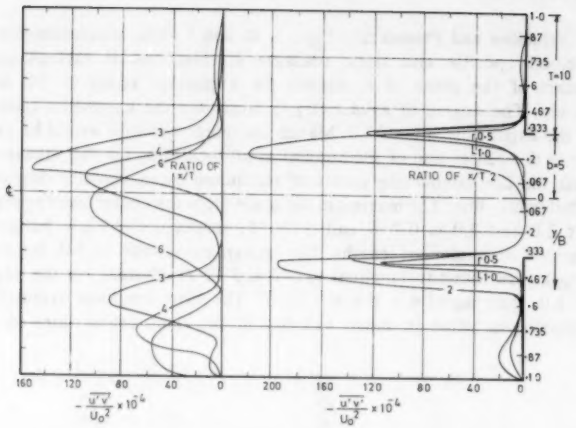

FIG. 11.—Measured Values of Turbulent Shear; Expansion Ratio 3.0; R1 = 10^5

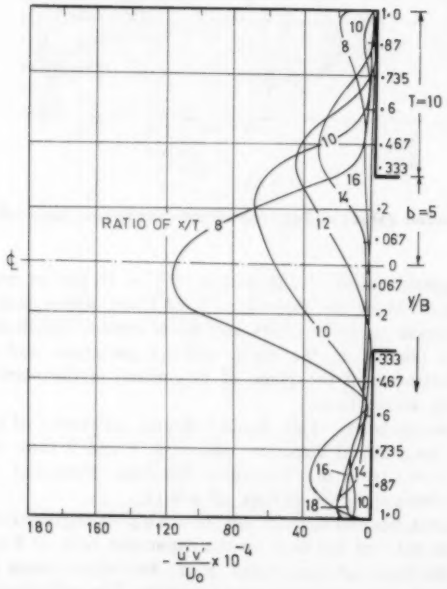

FIG. 11.—*Continued*

Conclusions

The experimental data given in this paper provides useful information regarding the behavior of the mean flow pattern and the turbulent characteristics for two-dimensional flows through large, sudden expansions. These results complement and extend the previous results (7), and show that the expansion ratio affects all the important parameters of the flow field. More specifically, with an increase in the expansion ratio, the reattachment lengths are found to decrease for the short stall region and to increase for the long stall region. For larger expansion ratios, the flow patterns and flow characteristics of the two types of flow (types I and II) are found to be mirror images of each other. The rate of development of the peak values of turbulence and the rate of its decay are found to be higher for larger expansion ratios. The Reynolds number does not influence the flow patterns for the range studied (0.5×10^5–1×10^5). The flow pattern becomes symmetric and stable sooner, and the rate of mixing is higher for larger expansion ratios.

TABLE 1.—Influence of Expansion Ratio on Turbulent Characteristics

Expansion ratio and Reynolds number (1)	Percentage Values of Level of Turbulence in Longitudinal Direction ($\sqrt{u'^2}/U_o$)			
	Maximum value (2)	x/T (3)	Uniform value (4)	x/T (5)
1.25; R2	15.0	6	7.0	28
2.0; R1	20.0	4	9.5	20
2.5; R1	20.0	2	9.0	16
3.0; R1	20.0	2	9.0	16

With an increase in the expansion ratio, mean flow patterns become more unsymmetric and unsteady (see Table 2 in Ref. 7), whereas the degree of level of turbulence remains almost unaltered except that the peak values develop earlier and decay faster than those with low expansion ratios (see Table 1).

The results of experimental findings for large expansion ratios will be useful in designing those engineering devices in which high rates of natural mixing are desired, e.g., chlorine and alum injecting plants of water works, color mixing plants of chemical processes, etc. Present experimental findings will also be useful in constructing a suitable mathematical model for predicting the behavior of large sudden expansions.

Acknowledgments

The experimental findings presented here form a part of writer's doctoral thesis submitted to the Indian Institute of Technology in Bombay, India, under the guidance of S. Narasimhan. The doctoral project was sponsored by the authorities of the S. V. Regional Engineering College, in Surat, India, under the Quality Improvement Programme of the Government of India, between 1975–1977.

Appendix I.—References

1. Abbott, D. E., and Kline, S. J., "Experimental Investigation of Subsonic Turbulent Flow Over Single and Double Backward Facing Steps," *Journal of Basic Engineering*, ASME, Series D, Vol. 84, Paper No. 61-Hyd. 15, Sept., 1962, pp. 317–325.
2. Chaturvedi, M. C., "Flow Characteristics of Axisymmetric Expansions," *Journal of the Hydraulics Division*, ASCE, Vol. 89, No. HY3, Proc. Paper 3515, May, 1963, pp. 61–92.
3. Durst, F., Melling, A., and Whitelaw, J. H., "Low Reynolds Number Flow Over a Plane Symmetrical Sudden Expansion," *Journal of Fluid Mechanics*, London, England, Vol. 64, 1974, p. 111.
4. Filetti, E. G., and Kays, W. M., "Heat Transfer in Separated, Reattached, and Redevelopment Regions Behind a Double Step at Entrance to a Flat Duct," *Journal of Heat Transfer*, ASME, Series C, Vol. 89, Paper No. 66-WA/HT-18, May, 1967, pp. 163–168.
5. Hieu, H. M., and Hebrard, P., "Theoretical and Experimental Study of Flow Separation After a Sudden Increase in Cross-Section of a Circular Pipe," *Journal of Hydraulic Research*, Vol. 15, International Association of Hydraulic Research, 1977, pp. 1–18.
6. Kalinkske, A. A., "Conversion of Kinetic to Potential Energy in Flow Expansions," *Transactions*, ASCE, Vol. 3, Paper No. 2273, 1946, pp. 335–390.
7. Mehta, P. R., "Flow Characteristics in Two-Dimensional Expansions," *Journal of the Hydraulics Division*, ASCE, Vol. 105, No. HY5, Proc. Paper 14579, May, 1979, pp. 501–516.

Appendix II.—Notation

The following symbols are used in this paper:

B, b = half conduit width before and after expansion, respectively;
p = static pressure;
R = Reynolds number (given by $\rho U_o D/\mu$; in which D = four times the hydraulic mean depth at the inlet);
T = step height given by $(B - b)$;
U_o = mean axial velocity at the inlet;
$\overline{u'v'}$ = turbulent shear stress;
$\sqrt{\overline{u'^2}}, \sqrt{\overline{v'^2}}$ = root mean square values of u' and v', respectively;
μ = coefficient of dynamic viscosity;
ρ = mass density;
$\bar{(\ )}$ = denotes temporal mean; and
$'$ = denotes instantaneous deviation from the temporal mean.

JOURNAL OF THE HYDRAULICS DIVISION

SIMULATING MASS TRANSPORT IN UNCONFINED AQUIFERS

By Varuttamadhira Guvanasen[1] and Raymond E. Volker,[2] M. ASCE

INTRODUCTION

As more water is extracted from surface and underground sources to satisfy increasing water demands, more polluted water is returned which may contaminate those sources. Shallow unconfined aquifers are particularly susceptible to pollution from conservative contaminants when little or no natural treatment is afforded by overlying strata. Problems of both steady and transient flow in unconfined aquifers are often solved by considering only the saturated domain below the water table (4,17). Alternatively, the unsaturated zone may also be included (13,16). Mass transport in unconfined aquifers has also been treated by both methods (14,18,19,20,21,22). The approach, using only the saturated region, is usually less expensive because the problems of nonlinearity of the governing equations are less formidable even though the solution domain may be nonstationary.

This paper presents a solution to the mass transport problem for unconfined aquifers. The numerical scheme employed is the conventional weighted residual finite element method (24) with special provisions to allow for the moving water table. The finite element mesh is changed iteratively to locate the new water table in each time step when solving the flow equation. Thus, in the solution of the mass transport equation, the nodes of the mesh may have new positions in successive time intervals. The solution technique presented eliminates the need for interpolation of solute concentration values to accomodate this movement of the mesh.

[1]Staff Scientist, Earth Sciences Div., Lawrence Berkeley Lab., Univ. of California, Berkeley, Calif.; formerly Post Grad. Student, Dept. of Civ. and Systems Engrg., James Cook Univ. of North Queensland, QLD. 4811, Australia.

[2]Sr. Lect., Dept. of Civ. and Systems Engrg., James Cook Univ. of North Queensland, QLD. 4811, Australia.

Note.—Discussion open until September 1, 1981. To extend the closing date one month, a written request must be filed with the Manager of Technical and Professional Publications, ASCE. Manuscript was submitted for review for possible publication on July 22, 1980. This paper is part of the Journal of the Hydraulics Division, Proceedings of the American Society of Civil Engineers, ©ASCE, Vol. 107, No. HY4, April, 1981. ISSN 0044-796X/81/0004-0461/$01.00.

Theoretical Background

The continuity condition in ground-water flow can be tensorially expressed as (3):

$$\frac{\partial q_i}{\partial x_i} = 0 \quad \ldots \ldots \ldots

$$h = x_3 \quad \text{for} \quad x_1 = B, \quad x_3 \in (a_0, H) \quad \ldots\ldots\ldots\ldots\ldots\ldots\ldots\ldots (8)$$

$$\left(R - \theta_e \frac{\partial H}{\partial t}\right) l_3 = K_{ij} \frac{\partial h}{\partial x_j} l_i \quad \text{on the free surface (17),}$$

$$\text{with} \quad R = P_0 \quad \text{for} \quad x_1 \in (0, L) \quad \text{and} \quad R = 0 \quad \text{for} \quad x_1 \in (L, B) \quad \ldots\ldots (9)$$

in which a_0 = initial saturated depth; B = aquifer half width; L = basin half width; θ_e = effective porosity (fillable if $\partial H/\partial t > 0$; drainable if $\partial H/\partial t < 0$); l_i = direction cosine of outward unit vector normal to the free surface; t = time; R = infiltration rate; and P_0 = infiltration rate from the basin.

The hydrodynamic dispersion equation for incompressible flow is given by Bear (3) as:

$$\frac{\partial C}{\partial t} + u_i \frac{\partial C}{\partial x_i} = \frac{\partial}{\partial x_i}\left(D_{ij} \frac{\partial C}{\partial x_j}\right) \quad \ldots\ldots\ldots\ldots\ldots\ldots\ldots\ldots (10)$$

in which C = concentration; u_i = pore velocity = q_i/θ_T; θ_T = Darcy porosity (see Ref. 7); and D_{ij} = hydrodynamic dispersion coefficient tensor.

Eq. 10 is subjected to the following conditions:

$$C = 0 \quad \text{for} \quad t = 0, \quad x_1 \in (0, B), \quad x_3 \in (0, a_0) \quad \ldots\ldots\ldots\ldots\ldots (11)$$

$$\frac{\partial C}{\partial x_1} = 0 \quad \text{for} \quad x_1 = 0, \quad \text{and} \quad x_1 = B, \quad x_3 \in (0, H) \quad \ldots\ldots\ldots\ldots (12)$$

$$\frac{\partial C}{\partial x_3} = 0 \quad \text{for} \quad x_1 \in (0, B), \quad x_3 = 0 \quad \ldots\ldots\ldots\ldots\ldots\ldots\ldots (13)$$

$$\left(R + \theta_{\text{init}} \frac{\partial H}{\partial t}\right) \frac{l_3}{\theta_T} (C - C_0) = -D_{ij} \frac{\partial C}{\partial x_j} l_i$$

$$\text{for} \quad x_1 \in (0, L), \quad x_3 = H \quad \text{and} \quad \frac{\partial H}{\partial t} \geq 0 \quad \ldots\ldots\ldots\ldots\ldots\ldots (14)$$

$$\frac{\theta_{\text{init}}}{\theta_T} \frac{\partial H}{\partial t} l_3 (C - C_{\text{ext}}) = -D_{ij} \frac{\partial C}{\partial x_j} l_i$$

$$\text{for} \quad x_1 \in (L, B), \quad x_3 = H \quad \text{and} \quad \frac{\partial H}{\partial t} \geq 0 \quad \ldots\ldots\ldots\ldots\ldots\ldots (15)$$

$$-D_{ij} \frac{\partial C}{\partial x_j} l_i = 0 \quad \text{for} \quad x_1 \in (L, B), \quad x_3 = H \quad \text{and} \quad \frac{\partial H}{\partial t} < 0 \quad \ldots\ldots\ldots (16)$$

in which θ_{init} = initial moisture content in the saturated zone; and C_{ext} = concentration of pollutant in the unsaturated zone. Eq. 12, which has been found to work well in previous studies (21,22), allows convection of solute across the boundary at $x_1 = B$, while precluding such movement at $x_1 = 0$, where there is no velocity normal to the boundary. The derivations of Eqs. 14 and 15 are presented in Appendix I. It should be stressed that the formulation presented in Appendix I is based on the assumption of a sharp free surface. Furthermore, Eq. 15 can only macroscopically describe the mixing at the free

surface, because of the assumption that the mass influx is instantaneously mixed with the mass already in the saturated zone. Although this assumption contradicts the experimental findings of Warrick, et al. (23), which indicate that the advance of the saturated front into the unsaturated zone precedes that of the solute front, the results obtained with the present analysis give reasonable agreement with the experiment.

Finite Element Formulation

Flow Equation.—Assuming that the solution can be represented by:

$$h \simeq \hat{h} = \sum_{I=1}^{NN} h_I(t)\, N_I(x_1, x_3) \quad \ldots\ldots\ldots\

in which Σ_e represents the sum of elemental contributions.

Approximating the temporal derivative by a simple finite-difference approach, Eq. 21 is recast in the form

$$\left(\lambda [ST]^{t+\Delta t} + \left[\frac{M}{\Delta t}\right]^{t+\Delta t}\right)\{h\}^{t+\Delta t} = \lambda \{F\}^{t+\Delta t} + (1-\lambda)\{F\}^{t}$$

$$+ \left(\left[\frac{M}{\Delta t}\right]^{t} - (1-\lambda)[ST]^{t}\right)\{h\}^{t} \quad \ldots\ldots\ldots\ldots\ldots\ldots\ldots\ldots\ldots\ldots (23)$$

in which λ = time-stepping factor ranging from 0.5–1. The writers (11) recommend a value of $\lambda = 1$ for good accuracy and stability.

The system of simultaneous equations is solved iteratively until convergence is reached, i.e., for all nodes on the free surface, the maximum difference between the piezometric head and the x_3 coordinate of the node must be less than some stipulated tolerance.

Hydrodynamic Dispersion Equation.—In order to accommodate the expansion or contraction of the saturated domain, the solution is sought through the finite element method with a moving mesh. In using such a mesh it is necessary to modify the transport equation to take account of the mesh movement.

Let the equations of transformation from a curvilinear coordinate system to a rectangular cartesian coordinate system (where the coordinates of a point, P, are x_1, x_2, x_3) be

$$x_i = x_i(\xi_j, t), \quad j = 1, 2, 3 \quad \ldots\ldots\ldots\ldots\ldots\ldots\ldots\ldots\ldots\ldots\ldots\ldots (24)$$

in which ξ_j = curvilinear coordinates in the system moving relative to the rectangular system. Eq. 24 can be inverted to give

$$\xi_i = \xi_i(x_j, t), \quad j = 1, 2, 3 \quad \ldots\ldots\ldots\ldots\ldots\ldots\ldots\ldots\ldots\ldots\ldots\ldots (25)$$

which is valid provided that the Jacobian, J, does not vanish (2) where J is defined as

$$J = \frac{\partial(x_1, x_2, x_3)}{\partial(\xi_1, \xi_2, \xi_3)} \quad \ldots\ldots\ldots\ldots\ldots\ldots\ldots\ldots\ldots\ldots\ldots\ldots\ldots\ldots (26)$$

Mollowney (15) has shown that the transport equation for a compressible fluid in the x frame of reference

$$\frac{\partial C}{\partial t} + \frac{\partial u_i C}{\partial x_i} = \frac{\partial}{\partial x_i}\left(D_{ij}\frac{\partial C}{\partial x_j}\right) \quad \ldots\ldots\ldots\ldots\ldots\ldots\ldots\ldots\ldots\ldots\ldots\ldots (27)$$

can be written in the ξ frame of reference as

$$\frac{\partial}{\partial t}(JC^*) + \frac{\partial}{\partial \xi_i}(\Omega_i^* JC^*) = \frac{\partial}{\partial \xi_i}\left(D_{ij}^* J \frac{\partial C^*}{\partial \xi_j}\right) \quad \ldots\ldots\ldots\ldots\ldots\ldots\ldots (28)$$

in which terms with asterisks are equivalent to their counterparts in the x frame. Relationships between variables in these two reference frames are

$$C^*(\xi_i, t) = C(x_i, t) \quad \ldots\ldots\ldots\ldots\ldots\ldots\ldots\ldots\ldots\ldots\ldots\ldots\ldots\ldots\ldots (29)$$

$$D_{ij}^{*} = D_{lm}\frac{\partial \xi_i}{\partial x_l}\frac{\partial \xi_j}{\partial x_m} \quad \ldots \quad (30)$$

and $$\Omega^{*} = u_i^{*} - w_i^{*} \quad \ldots \quad (31)$$

in which $$u_i^{*} = u_j\frac{\partial \xi_i}{\partial x_j} \quad \ldots \quad (32)$$

$$w_i^{*} = w_j\frac{\partial \xi_i}{\partial x_j} \quad \ldots \quad (33)$$

in which $$w_i = \frac{\partial x_i}{\partial t} \quad \ldots \quad (34)$$

Therefore, from Eq. 34, w_i = the velocity of the moving ξ frame relative to the stationary x frame observed in the x frame.

The Jacobian is neither spatially nor temporally invariant and this gives rise to difficulties in accurately evaluating it in the ξ frame of reference. To overcome this problem, it is assumed that each element is geometrically time invariant in each time step of Δt with a geometry which is the average of those at time t and $t + \Delta t$. This is equivalent to an assumption of a unit Jacobian for each element which implies that the motion is isochoric.

The preceding is true if the following transformation is employed between t and $t + \Delta t$

$$\xi_i = x_i - w_i\delta t \quad \ldots \quad (35)$$

in which δt = time elapsed from t; and w_i is assumed to be constant over the subdomain between t and $t + \Delta t$.

From Eq. 35 one can verify that in each subdomain

$$\frac{\partial \xi_i}{\partial x_j} = \delta_{ij} \quad \text{or conversely} \quad \frac{\partial x_i}{\partial \xi_j} = \delta_{ij} \quad \ldots \quad (36)$$

in which δ_{ij} = Kronecker delta.

From the assumption that w_i is constant in each subdomain, and from the condition of incompressible flow it can be established using Eq. 36 that

$$\frac{\partial \Omega_i^{*}}{\partial \xi_i} = \frac{\partial}{\partial x_j}\left(\Omega_j\frac{\partial \xi_i}{\partial x_j}\right)\frac{\partial x_j}{\partial \xi_i} = \frac{\partial \Omega_i}{\partial x_i} = \frac{\partial u_i}{\partial x_i} - \frac{\partial w_i}{\partial x_i} = 0 \quad \ldots \quad (37)$$

Using Eq. 37 and the condition of isochoric motion ($J = 1$), Eq. 28 can be further reduced to

$$\frac{\partial C^{*}}{\partial t} + \Omega_i^{*}\frac{\partial C^{*}}{\partial \xi_i} = \frac{\partial}{\partial \xi_i}\left(D_{ij}^{*}\frac{\partial C^{*}}{\partial \xi_j}\right) \quad \ldots \quad (38)$$

For the present problem, the solution is sought in the ξ_1, ξ_3 plane, and is approximated in the form:

$$C^{*} \simeq \hat{C} = \sum_{I=1}^{NN} C_I^{*}(t)N_I(\xi_1, \xi_3)^{t+(\Delta t/2)} \quad \ldots \quad (39)$$

Applying the weighted residual method to Eq. 38 one obtains

$$\int_A W_I(\xi_1,\xi_3)^{t+(\Delta t/2)}\left[\frac{\partial C^*}{\partial t}+\Omega_i^*\frac{\partial C^*}{\partial \xi_i}-\frac{\partial}{\partial \xi_i}\left(D_{ij}^*\frac{\partial C^*}{\partial \xi_j}\right)\right]^{t+(\Delta t/2)} dA = 0 \quad (40)$$

Using Green's theorem and Eq. 39, Eq. 40 becomes

$$\int_A W_I N_J dA\left\{\frac{dC_J^*}{dt}\right\}+\int_A \Omega_i^* W_I\frac{\partial N_J}{\partial \xi_i}dA\{C_J^*\}$$

$$+\int_A D_{ij}^*\frac{\partial W_I}{\partial \xi_i}\frac{\partial N_J}{\partial \xi_j}dA\{C_J^*\}-\int_S W_I D_{ij}^*\frac{\partial \hat{C}}{\partial \xi_j}l_i dS=0 \quad \ldots\ldots\ldots (41)$$

which yields a system of simultaneous equations written in matrix form as:

$$[MM]^{t+(\Delta t/2)}\left\{\frac{dC^*}{dt}\right\}+[\mathrm{STT}]^{t+(\Delta t/2)}\{C^*\}+\{FF\}^{t+(\Delta t/2)}=0 \ldots\ldots (42)$$

in which $$MM_{IJ}=\sum_e\int_A W_I N_J dA \quad \ldots\ldots\ldots\ldots\ldots\ldots (43a)$$

$$STT_{IJ}=\sum_e\int_A\left(W_I\Omega_i^*\frac{\partial N_J}{\partial \xi_i}+D_{ij}^*\frac{\partial W_I}{\partial \xi_i}\frac{\partial N_J}{\partial \xi_j}\right)dA \quad \ldots\ldots\ldots\ldots (43b)$$

$$FF_I=-\sum_e\int_S W_I D_{ij}^*\frac{\partial \hat{C}}{\partial \xi_j}l_i dS \quad \ldots\ldots\ldots\ldots\ldots\ldots (43c)$$

Using Eqs. 30, 31, 32, 33, 34, and 36, it can be stated that in each element

$$D_{ij}^*=D_{ij} \quad \ldots\ldots\ldots\ldots\ldots\ldots\ldots\ldots\ldots\ldots (44a)$$

and $$\Omega^*=\Omega_i=u_i-w_i \quad \ldots\ldots\ldots\ldots\ldots\ldots\ldots\ldots (44b)$$

From the preceding relationships one can see that Ω_i^* coincides with Ω_i, and D_{ij}^* coincides with D_{ij}. Their values calculated from the x frame can therefore be conveniently utilized in the foregoing finite element formulation.

The velocity, w_i, of each element is approximated by $\Delta x_i/\Delta t$, in which Δx_i = the movement of the centroid of the element between time t and $t+\Delta t$ obtained in the solution of the flow equation and resulting from the free-surface movement.

Replacing the dC^*/dt and C^* terms by

$$\left.\frac{dC^*}{dt}\right|^{t+(\Delta t/2)}=\frac{\{C(x_i^t+\Delta x_i,t+\Delta t)-C(x_i^t,t)\}}{\Delta t} \quad \ldots\ldots\ldots\ldots (45a)$$

and $$C^{*t+(\Delta t/2)}=\frac{1}{2}\{C(x_i^t+\Delta x_i,t+\Delta t)+C(x_i^t,t)\} \quad \ldots\ldots\ldots\ldots (45b)$$

In Eq. 42 one obtains

$$\left(\frac{[MM]}{\Delta t}+\frac{1}{2}[STT]\right)^{t+(\Delta t/2)}\{C\}^{t+\Delta t}$$

$$+\left(\frac{1}{2}[STT]-\frac{[MM]}{\Delta t}\right)^{t+(\Delta t/2)}\{C\}^t+\{FF\}^{t+(\Delta t/2)}=0 \ldots\ldots\ldots (46)$$

This equation uses a time-stepping factor of 0.5 which, for the case of Galerkin's method ($N_I = W_I$), in the stationary domain, has been shown by Gray and Pinder (9) to minimize smearing at the front at the expense of numerical dispersion.

Experiments

Experiments for a situation similar to that shown in Fig. 1 were conducted in a sand box model to verify the mathematical models. Because of symmetry only one half is considered here.

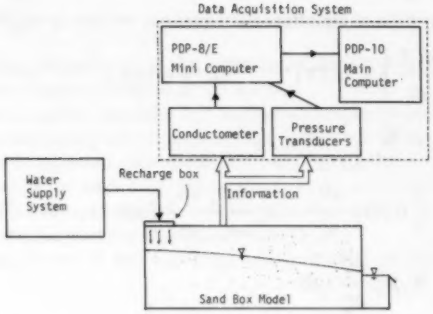

FIG. 2.—Layout of Experimental Facilities

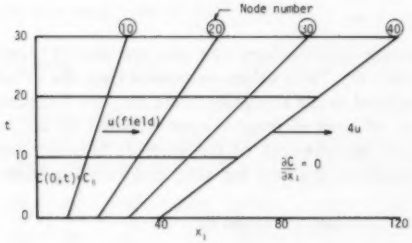

FIG. 3.—Mesh Layout (Nonstationary Element)

A matrix of conductivity probes was embedded in the sand box at various locations to monitor the movement of the contaminated front. These probes were connected to a conductometer which was in turn linked with a minicomputer. Piezometric heads at various locations along the sand box were recorded manually in piezometric tubes and automatically, using pressure transducers which were also connected to the minicomputer. This data acquisition system is diagrammatically shown in Fig. 2.

In each experiment, an NaCl solution was employed to represent a conservative pollutant and was introduced at the upstream end of the sand box ($0 \leq x$

$\leq L$). The concentration of the solution was in the order of 0.1% by weight, so that the change in density and viscosity due to the presence of the salt solution was negligible. For more details, readers are referred to the first writer (10).

Results

The accuracy of the nonstationary element scheme was first tested using a one-dimensional model in a hypothetical situation in which the domain expands with time. As shown in Fig. 3, there is a constant concentration source at $x_1 = 0$ in a uniform flow of water with constant velocity, u, in the x_1 direction. The right-hand edge of the flow domain is arbitrarily assumed to move with a velocity, $4u$, and this in turn causes the discretization inside the domain to expand to accommodate the new domain. The left-hand side of the domain remains stationary at all times, and the boundary condition at that point is $C(o,t) = C_0$. An analytical solution to this particular problem is

$$\frac{C(x,t)}{C_0} = \frac{1}{2}\,\text{erfc}\left[\frac{(x-ut)}{(4\,Dt)^{1/2}}\right] + \frac{1}{2}\exp\left(\frac{ux}{D}\right)\text{erfc}\left[\frac{(x+ut)}{(4\,Dt)^{1/2}}\right] \quad \ldots . \quad (47)$$

in which erfc (x) = complimentary error function of argument, x.

A comparison between the analytical and numerical solutions is made in Fig. 4 from which it is evident that the numerical solution agrees well with the analytical solution.

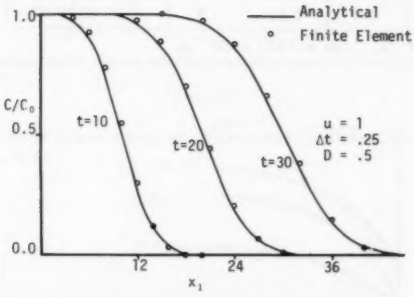

FIG. 4.—Concentration Profiles

A typical discretization of the nonstationary two-dimensional domain used 287 nodes (7 rows × 41 columns) and 480 linear triangular elements with the horizontal node spacing increasing with distance from the recharge basin. Since the horizontal length of aquifer is fixed, the water table movement can be simulated by using horizontally-constrained elements with the nodes moving only vertically.

Data from two experiments were selected to verify the two-dimensional numerical models. As shown in Table 1, the original saturated depth in experiment B is larger than that in experiment A, while the reverse is true for infiltration rates. As a consequence, the rise of the free surface in relation to the original saturated depth is larger in experiment A.

The coefficients of advective dispersion for the homogeneous sand medium were calculated by first estimating longitudinal and lateral coefficients of advective dispersion, D_L and D_T, respectively along the principal axes using the following expressions which were obtained from laboratory experiments (10):

$$D_L = 1.75\,\nu \mathrm{R}^{1.22} \quad \ldots\ldots\ldots\

Verification of the transport model was made by comparing the experimental and calculated breakthrough curves as shown in Figs. 6 and 7. In Fig. 6, results are drawn from two cases incorporating two different boundary conditions at the free surface outside the recharge basin; namely:

$$\text{case 1:}\quad D_{ij}\frac{\partial C}{\partial x_j}l_i = 0 \qquad (50)$$

$$\text{case 2:}\quad D_{ij}\frac{\partial C}{\partial x_j}l_i = \frac{\partial H}{\partial t}l_3\frac{\theta_{\text{init}}}{\theta_T}(C_{\text{ext}} - C) \qquad (51)$$

In case 2, C_{ext} is equated to zero since the moisture in the unsaturated zone is that of freshwater. Thus, application of the boundary condition in case 2

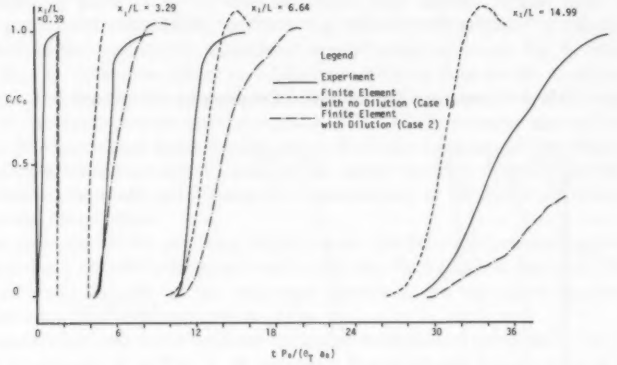

FIG. 6.—Comparison of Experimental and Calculated Breakthrough Curves for Experiment A at $x_3/a_0 = 1.70$

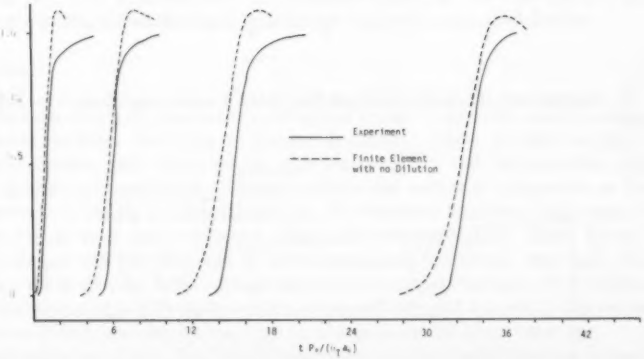

FIG. 7.—Comparison of Experimental and Calculated Breakthrough Curves for Experiment A at $x_3/a_0 = 0.79$

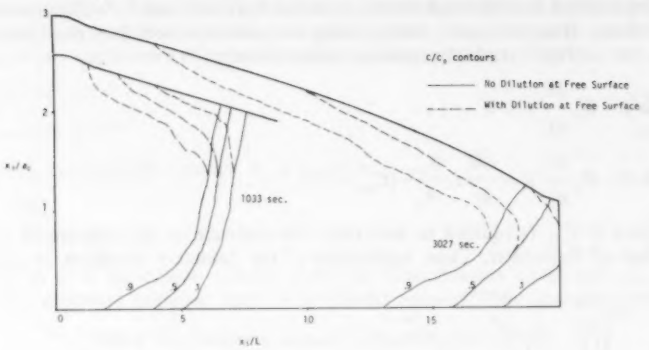

FIG. 8.—Calculated Concentration Contours for Experiment A

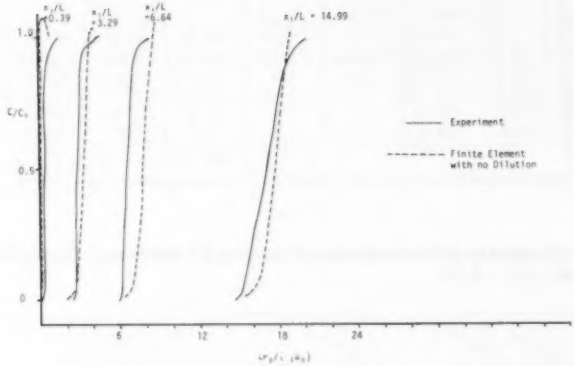

FIG. 9.—Comparison of Experimental and Calculated Breakthrough Curves for Experiment B

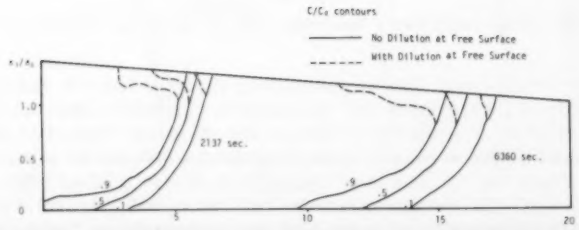

FIG. 10.—Calculated Concentration Contours for Experiment B

implies that dilution of the pollutant in the saturated zone takes place in the vicinity of the free surface. Concentration contours from the preceding two cases are exhibited in Fig. 8, in which one can see that the inclusion of the moisture in the unsaturated zone results in the retardation of the front in the vicinity of the free surface.

Figs. 5, 6, and 7 show results from experiment A. An inspection of Fig. 6 which shows breakthrough curves at locations close to the free surface reveals that the use of the boundary condition in Eq. 51 causes the breakthrough curves to lag behind those employing the boundary condition in Eq. 50. In Fig. 6, at $x_1/L = 14.99$, dilution of the front due to the inclusion of moisture from the unsaturated zone can be observed in the experimental result, although not to the extent predicted in case 2. In Fig. 5, the predicted piezometric heads are somewhat lower than those experimentally measured. This implies that outside the recharge basin ($x_1 > L$), the calculated free surface is also lower than its experimental counterpart, because the pressure distribution is almost hydrostatic in that region (10). Calculated breakthrough curves in Fig. 6, resulting from Eq. 51, therefore appear to suffer more dilution than do the experimental curves. Also in Fig. 6, the calculated breakthrough curves do not correspond well to the experimental ones at $x_1/L = 0.39$, which is under the infiltration basin. The calculated breakthrough curve is abrupt because of the abrupt rise of the calculated free surface passing the probe location; however during the experiment, the probe did register the concentration of the NaCl infiltrate while above the free surface.

The inclusion of the moisture influx across the free surface does not affect breakthrough curves at locations well inside the flow domain, and only results derived using Eq. 50 as the boundary condition are compared against the experimental breakthrough curves in Fig. 7.

Results from the finite element transport models are compared with those from experiment B in Fig. 9. In this case, breakthrough curves derived using either Eq. 50 or Eq. 51 as boundary condition are almost identical. Only those using Eq. 50 are displayed in Fig. 9. From the concentration contours shown in Fig. 10, it is apparent that the moisture influx at the free surface does not appreciably affect the mass distribution inside the saturated domain.

Analysis

Crank and Gupta (6) proposed a moving grid system to solve the one-dimensional diffusion problem involving a moving boundary. Their method employs a finite-difference grid which moves with the boundary and utilizes cubic spline or Lagrangian interpolation schemes to determine values of concentration from the previous timestep at the new locations. Al-Niami and Rushton (1) also proposed a similar moving grid technique using linear interpolation. Such forms of interpolation are not practical in multidimensional problems, especially those using a finite element mesh with geometrically irregular elements. The numerical scheme proposed in this study surpasses the moving grid system in this respect, because it does not require any kind of interpolation between timesteps.

An inspection of Figs, 5, 6, 7, and 9 indicates that there exist some discrepancies between the models and experimental results. There are several possible explanations for this, including experimental errors such as pockets of nonhomogeneity

in the sand, possible fingering instability at the salt front, and inherent numerical errors of the numerical models. The differences between the numerical and experimental results are relatively small, and could be accounted for by the aforementioned factors. It may therefore be inferred that the flow and transport models are accurate in simulating the movement of mass in the saturated zone.

From Figs. 8 and 10, it is evident that the magnitude of the area in which the mass distribution is affected by the moisture flux across the free-surface boundary is dependent upon the rate of rise of the free surface ($\partial H/\partial t$) which, in turn, is governed by the infiltration rate. Thus, for a large rise in the free surface, lack of knowledge of the mass in the unsaturated zone may result in an appreciable error in predicting the mass movement in the neighborhood of the free surface.

Conclusions

In this study, the weighted residual technique, in conjunction with the finite element method, was utilized to formulate numerical models of flow and transport in a nonstationary saturated ground-water zone. Through the formulation presented, elements are allowed to expand and contract as required to accommodate the nonstationary saturated domain without the necessity for interpolation of solute concentration values when proceeding from one timestep to the next.

Comparisons between the numerical results and those from a limited number of experiments indicate that the models can accurately simulate the flow of water and the movement of pollutants in the saturated zone of a homogeneous isotropic aquifer. Even though the models are primarily intended for the saturated zone, they can also approximate the mass transfer as a result of the movement of the saturated-unsaturated interface (free surface). The models can thus be linked with independent unsaturated flow and transport models in areas where the flow in the unsaturated zone is significant. This should provide a more economical alternative to the conventional saturated-unsaturated scheme.

Appendix I.—Derivation of Free-Surface Boundary Conditions

Considering an elemental volume at the free surface depicted in Fig. 11(*a*) during time t to $t + \Delta t$, the principle of conservation of mass is written: mass retained = net contribution of mass from which

$$\theta_T \frac{\partial H}{\partial t} \Delta t\, l_3\, C = R\, C_0 l_3 \Delta t + \theta_T \left(-D_{ij} \frac{\partial C}{\partial x_j} - \frac{K_{ij}}{\theta_T} \frac{\partial h}{\partial x_j} C \right) l_i \Delta t$$

$$+ \theta_{\text{init}} \frac{\partial H}{\partial t} \Delta t\, l_3\, C_0 \quad \ldots \ldots \ldots

The preceding equation implies that the invading fluid is instantaneously mixed with the resident fluid at the free surface. The basic concept of pore space division is shown in Fig. 11(*b*) from which it follows that

$$\theta_T = \theta_e + \theta_{\text{init}} \quad \ldots \ldots \ldots \ldots \ldots \ldots \ldots \ldots \ldots \ldots \ldots \ldots \ldots \quad (53)$$

This assumes that the stagnant or dead-end portion where fluid is usually considered to be immobile (5,8) is negligible, so that the Darcy porosity (or interconnected porosity) is approximately equal to the total porosity.

The first term on the right-hand side of Eq. 52 denotes the influx due to infiltration, the second term the flux from the saturated domain, and the last the contribution of mass already occupying the pore space.

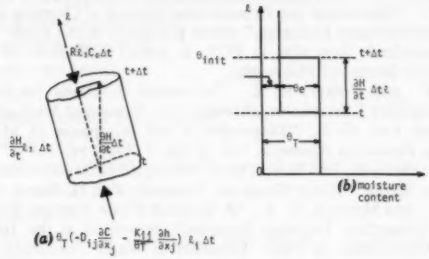

FIG. 11.—Free-Surface Definition: (*a*) Elementary Volume; (*b*) Hypothetical Moisture Profile at Free Surface

It is assumed that the moisture in the θ_{init} portion has been replaced with tracer of concentration C_0.

Dividing Eq. 52 through by Δt, and using Eq. 9, Eq. 52 becomes

$$-D_{ij}\frac{\partial C}{\partial x_j}l_i = \left(R + \theta_{\text{init}}\frac{\partial H}{\partial t}\right)\frac{l_3}{\theta_T}(C - C_0) \quad \ldots \ldots \ldots \ldots \ldots \quad (54)$$

which is Eq. 14.

Similarly, where $R = 0$, and a tracer of concentration C_{ext} occupies the water in the unsaturated zone which has a moisture content of θ_{init}, one can easily verify that Eq. 15 results.

For the case of a receding free surface ($\partial H/\partial t < 0$) outside the basin, Eq. 16 is employed because the concentration immediately inside the free surface is equal to that immediately outside.

Appendix II.—References

1. Al-Niami, A. N. S., and Rushton, K. R., "Finite-Difference Solutions for One-Dimensional Dispersion Using an Improved Mesh Design," *Journal of Hydrology*, Amsterdam, The Netherlands, Vol. 39, 1978, pp. 301–310.
2. Aris, R., *Vector, Tensors, and the Basic Equations of Fluid Mechanics*, Prentice-Hall, Inc., London, England, 1962.
3. Bear, J., *Dynamics of Fluid sin Porous Media*, American Elsevier Publishing Co., Inc., New York, N.Y., 1972.

4. Cheng, R. T.-S., and Li, C.-Y., "On the Solution of Transient Free Surface Flow Problems in Porous Media by the Finite Element Method," *Journal of Hydrology*, Amsterdam, The Netherlands, Vol. 20, 1973, pp. 49–63.
5. Coats, K. H., and Smith, B. D., "Dead-End Pore Volume and Dispersion in Porous Media," *Society of Petroleum Engineers Journal*, Vol. 4, No. 1, 1964, pp. 73–84.
6. Crank, J., and Gupta, R. S., "A Method for Solving Moving Boundary Problems in Heat Flow Using Cubic Spline or Polynomials," *Journal of Institute of Mathematics and Applications*, Vol. 10, 1972, pp. 296–304.
7. Fried, J. J. *Groundwater Pollution*, Elsevier Publishing Co., Inc., Amsterdam, The Netherlands, 1975.
8. Gaudet, J.-P., Jegat, H., and Vachaud, G., "Etude du Mécanisme des Transferts d'Eau et de Soluté en Zone Non-Saturée avec Prise en Compte d'une Fraction Liquide Immobile," *La Houille Blanche*, Grenoble, France, No. 3/4, 1976, pp. 243–251.
9. Gray, W. G., and Pinder, G. F., "An Analysis of the Numerical Solution of the Transport Equation," *Water Resources Research*, Vol. 10, No. 4, 1976, pp. 821–828.
10. Guvanasen, V., "Theoretical and Experimental Studies of Clogging and Contamination in Artificial Groundwater Recharge," thesis presented to the James Cook University, at North Queensland, Australia, in 1979, in partial fulfillment of the requirements for the degree of Doctor of Philosophy.
11. Guvanasen, V., and Volker, R. E., "Numerical Solutions for Unsteady Flow in Unconfined Aquifers," *International Journal for Numerical Methods in Engineering*.
12. Li, W.-H., and Yeh, G.-T., "Dispersion at the Interphase of Miscible Liquids in a Soil," *Water Resources Research*, Vol. 4, No. 2, 1968, pp. 369–377.
13. Luthin, J. N., Orhun, A., and Taylor, G. S., "Coupled Saturated-Unsaturated Transient Flow in Porous Media," *Water Resources Research*, Vol. 11, No. 6, 1975, pp. 973–978.
14. Marino, M. A., and Matanga, G. B., "A Galerkin-Finite Element Simulation of Solute Transport in Subsurface Drainage Systems," presented at the July, 1978, Second International Conference on Finite Elements in Water Resources, held at Imperial College, London.
15. Mollowney, B. M., "Solution of the Advective-Diffusion Equation by the Method of Moving Coordinate Systems with Particular Reference to the Modelling of Estuarine Pollution," *Mathematical Models for Environmental Problems*, C. A. Brebbia, ed., Pentech Press, London, England, 1976, pp. 313–327.
16. Neuman, S. P., "Saturated-Unsaturated Seepage by Finite Elements," *Journal of the Hydraulics Division*, ASCE, Vol. 99, No. HY12, Proc. Paper 10201, Dec., 1973, pp. 2233–2250.
17. Neuman, S. P., and Witherspoon, P. A., "Variational Principles for Confined and Unconfined Flow in Groundwater," *Water Resources Research*, Vol. 6, No. 5, 1970, pp. 1376–1382.
18. Pickens, J. F., and Lennox, W. C., "Numerical Simulation of Waste Movement in Steady Groundwater Flow Systems," *Water Resources Research*, Vol. 12, No. 2, 1976, pp. 171–190.
19. Pickens, J. F., Gillham, R. W., and Cameron, D. R., "Finite-Element Analysis of the Transport of Water and Solutes in Tile-Drained Soils," *Journal of Hydrology*, Amsterdam, The Netherlands, Vol. 40, 1979, pp. 243–264.
20. Segol, G., "A Three-Dimensional Galerkin Finite-Element Model for the Analysis of Contaminant Transport in Saturated-Unsaturated Porous Media," *Finite Elements in Water Resources*, W. G. Gray, G. F. Pinder, and C. A. Brebbia, eds., Pentech Press, London, England, 1977, pp. 2.123–2.144.
21. Taylor, C., and Huyakorn, P. S., "Finite-Element Analysis of Three-Dimensional Groundwater Flow with Convective Dispersion," presented at the June 14–18, 1976, Second International Symposium on Flow Problems, held at Rapallo, Italy.
22. Volker, R. E., and Guvanasen, V., "Finite Element Solutions for Pollutant Movement in Aquifers," presented at the July, 1979, Third International Conference in Australia on Finite Element Methods, held at Sydney, Australia.
23. Warrick, A. W., Biggar, J. W., and Nielsen, D. R., "Simultaneous Solute and Water Transport for an Unsaturated Soil," *Water Resources Research*, Vol. 7, No. 5, 1971, pp. 1216–1225.
24. Zienkiewicz, O. C., *The Finite Element Method*, 3rd ed., McGraw-Hill Book. Co., Inc., London, England, 1977.

Appendix III.—Notation

The following symbols are used in this paper:

a_0 = initial saturated depth;
B = half width of aquifer;
C = concentration;
C_{ext} = concentration in the unsaturated zone;
C_0 = concentration at the inflow boundary;
D_{ij} = hydrodynamic dispersion coefficient tensor;
D_L = longitudinal convective dispersion coefficient;
D_T = lateral convective dispersion coefficient;
d_{50} = mean grain-size diameter;
H = free-surface elevation;
h = piezometric head;
J = Jacobian;
K_{ij} = hydraulic conductivity tensor;
L = half width of basin;
l_i = i component of unit outward normal to the boundary;
N_I = basis function at node I;
P_0 = infiltration rate;
q_i = ith component of superficial velocity = $-K_{ij}(\partial h/\partial x_j)$;
R = recharge rate;
R = Reynold's number = Ud_{50}/ν;
t = time;
U = absolute pore velocity;
u_i = ith component of pore velocity;
W_I = weighting function at node I;
w_i = velocity of the moving frame relative to the stationary frame observed in the stationary frame;
x_i = cartesian coordinate of the stationary frame;
Δt = time increment;
Δx_i = movement of centroid of element from t to $t + \Delta t$;
δ_{ij} = Kronecker delta;
θ_e = effective porosity;
θ_{init} = initial moisture content;
θ_T = Darcy porosity;
ν = kinematic viscosity;
ξ_i = moving coordinates; and
Ω_i = $u_i - w_i$.

JOURNAL OF THE HYDRAULICS DIVISION

MATHEMATICAL MODEL OF SHALLOW WATER FLOW OVER POROUS MEDIA

By Ali Osman Akan[1] and Ben Chie Yen,[2] F. ASCE

INTRODUCTION

Modeling of unsteady shallow water flow on porous media has many engineering applications, including the investigation of overland flow, infiltration, surface irrigation, and seepage from channels. Theoretically, the process is described by a conjunctive surface-subsurface flow system. The subsurface flow region may contain both saturated and unsaturated zones. The surface and subsurface flow components are in dynamic equilibrium and they interact through the process of infiltration.

Surface flow was studied as a separate component in the past. A number of researchers including Wooding (30), Chen and Chow (4), and Chow and Ben-Zvi (5) proposed various methods to simulate surface runoff in which infiltration was either disregarded or treated somewhat casually. Also, in mathematical models developed for surface irrigation including those by Chen (3), Hart et al. (10), and Sakkas and Strelkoff (20), infiltration rates were approximately estimated. Meanwhile, most subsurface flow studies were restricted either to unsaturated zone or to saturated ground-water flow. Whisler and Klute (29), Staple (24), Remson et al. (18), and Rubin (19) studied vertical moisture flow in an unsaturated soil column.

Verma and Brutsaert (28), Prickett and Lonnquist (16), and Singh (22) examined saturated ground-water flow disregarding the zone of aeration. Saturated and unsaturated zones were combined by Freeze (7), Hornberger and Remson (11), Abbott et al. (1), and Vauclin et al. (27). Reeder et al. (17) examined the effect

[1]Asst. Prof., Dept. of Civ. Engrg., Middle East Technical Univ., Ankara, Turkey.
[2]Prof. of Civ. Engrg., Univ. of Illinois at Urbana-Champaign, Urbana, Ill. 61801.

Note.—Discussion open until September 1, 1981. To extend the closing date one month, a written request must be filed with the Manager of Technical and Professional Publications, ASCE. Manuscript was submitted for review for possible publication on July 23, 1980. This paper is part of the Journal of the Hydraulics Division, Proceedings of the American Society of Civil Engineers, ©ASCE, Vol. 107, No. HY4, April, 1981. ISSN 0044-796X/81/0004-0479/$01.00.

of variation in water depth on infiltration by treating the surface water depth as a prescribed function of time. A conjunctive surface-subsurface flow model was first developed by Smith and Woolhiser (23) in a remarkable study of overland flow on pervious surfaces. However, they simplified the problem by using a kinematic wave approximation to represent the surface flow and by considering the subsurface flow with only vertical movement of water through an unsaturated soil column bounded by a fixed water table at the bottom.

A more sophisticated conjunctive surface-subsurface flow model is developed in the present study. Surface flow is described by a set of one-dimensional dynamic wave equations. Subsurface flow is assumed to be two-dimensional with potential gradients in the vertical as well as the surface flow direction. Both saturated and unsaturated zones are considered. All components of the system are in dynamic equilibrium, satisfying the principles of continuity and momentum. A brief description of this model is given in this paper. Further details can be found in Ref. 2.

Surface Runoff

In the present study, surface runoff is represented by the Saint-Venant equations simplified for wide channels

$$\frac{\partial (vy)}{\partial x} + \frac{\partial y}{\partial t} - r + f = 0 \quad \ldots \quad (1)$$

$$\frac{\partial (vy)}{\partial x} + \frac{\partial (v^2 y)}{\partial x} - gy\left(S_o - \frac{\partial y}{\partial x} - S_f\right) = 0 \quad \ldots \quad (2)$$

in which v = cross-sectional average velocity; x = horizontal distance; y = flow depth normal to x; t = time; r = time rate of lateral inflow; f = time rate of infiltration; g = gravitational acceleration; S_o = bottom slope; and S_f = friction slope. The assumptions and the rigorous derivations of the Saint-Venant equations were reported by Strelkoff (25) and Yen (32) and will not be repeated here.

The friction slope S_f is computed by using the Darcy-Weisbach formula

$$S_f = f_d \frac{v^2}{8gy} \quad \ldots \quad (3)$$

The frictional resistance coefficient f_d is evaluated from an approximate Moody diagram utilized in a watershed model proposed by Kareliotis and Chow (13). Depending upon the instantaneous state of the flow, f_d is evaluated using Eqs. 4–6 respectively, for laminar, transitional, and fully turbulent flow as

$$f_d = \frac{C_L}{\mathrm{R}} \quad \ldots \quad (4)$$

$$f_d = \frac{0.223}{\mathrm{R}^{0.25}} \quad \ldots \quad (5)$$

$$f_d = \left(2 \log \frac{2y}{k} + 1.74\right)^{-2} \quad \ldots\ldots\ldots\ldots\ldots\ldots\ldots\ldots\ldots\ldots\ldots\ldots\ldots\ldots (6)$$

In Eqs. 4–6, R = the Reynolds number, equal to the product vy divided by the kinematic viscosity; k = a length measure of surface roughness; and C_L = a coefficient. As proposed by Shen and Li (21), C_L is evaluated by using the equation

$$C_L = 24 + 27.162\, r^{0.407} \quad \ldots\ldots\ldots\ldots\ldots\ldots\ldots\ldots\ldots\ldots\ldots\ldots\ldots\ldots (7)$$

in which r = rainfall intensity in in./h. The effect of the pervious ground surface as a leaking boundary on f_d is negligible for the range of infiltration velocity to surface velocity ratio investigated in the present study (31).

A four-point implicit finite difference scheme is employed for the solution of the surface runoff equations. As shown in Fig. 1, the flow domain is divided into a number of flow reaches. Similarly, the time variable is also discretized

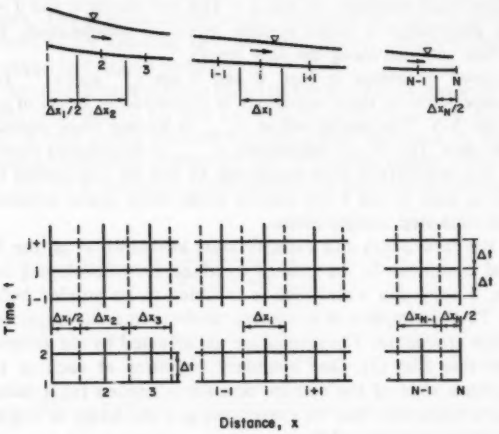

FIG. 1.—Schematic Diagram of Surface Flow and Computational Grid

and solutions at discrete time intervals are sought. Accordingly, the Saint-Venant equations (Eqs. 1 and 2) are written in finite difference quotients as

$$\frac{2\theta}{\Delta x_i + \Delta x_{i+1}}(y_{i+1}^{n+1}v_{i+1}^{n+1} - y_i^{n+1}v_i^{n+1}) + \frac{2(1-\theta)}{\Delta x_i + \Delta x_{i+1}}(y_{i+1}^{n}v_{i+1}^{n} - y_i^{n}v_i^{n})$$

$$+ \frac{1}{2\Delta t}(y_{i+1}^{n+1} - y_{i+1}^{n} + y_i^{n+1} - y_i^{n}) - \bar{F}_{i+0.5} + \bar{f}_{i+0.5} = 0 \quad \ldots\ldots\ldots\ldots (8)$$

$$\frac{1}{2\Delta t}(y_{i+1}^{n+1}v_{i+1}^{n+1} - y_{i+1}^{n}v_{i+1}^{n} + y_i^{n+1}v_i^{n+1} - y_i^{n}v_i^{n})$$

$$+\frac{2\theta}{\Delta x_i+\Delta x_{i+1}}\left[y_{i+1}^{n+1}(v_{i+1}^{n+1})^2-y_i^{n+1}(v_i^{n+1})^2\right]+\frac{2(1-\theta)}{\Delta x_i+\Delta x_{i+1}}\left[y_{i+1}^{n}(v_{i+1}^{n})^2\right.$$

$$\left.-y_i^{n}(v_i^{n})^2\right]+\theta\frac{g(y_{i+1}^{n+1}+y_i^{n+1})}{2}\left[\frac{2(y_{i+1}^{n+1}-y_i^{n+1})}{\Delta x_i+\Delta x_{i+1}}-\frac{S_{o_i}+S_{o_{i+1}}}{2}\right.$$

$$\left.+\frac{S_{f_i}^{n+1}+S_{f_{i+1}}^{n+1}}{2}\right]+(1-\theta)\frac{g(y_{i+1}^{n}+y_i^{n})}{2}\left[\frac{2(y_{i+1}^{n}-y_i^{n})}{\Delta x_i+\Delta x_{i+1}}\right.$$

$$\left.-\frac{S_{o_i}+S_{o_{i+1}}}{2}+\frac{S_{f_i}^{n}+S_{f_{i+1}}^{n}}{2}\right] \quad \ldots\ldots\ldots\ldots\ldots\ldots\ldots\ldots\ldots\ldots (9)$$

in which Δt = fixed computation time interval; Δx = the projection on a horizontal plane of the length of the flow reach which is centered at the ith grid station; $\bar{r}_{i+0.5}$ and $\bar{f}_{i+0.5}$ = the average time rates of rainfall and infiltration, respectively, along the flow reach between ith and $(i+1)$th grid stations; and θ = a weighting factor. The superscript n refers to time levels of computation. The subscript i refers to flow sections along the flow length.

The unknown quantities in Eqs. 8 and 9 are y_i^{n+1} and v_i^{n+1} for $i = 1, 2, \ldots, N$. Friction slope in these equations is expressed in terms of y_i^{n+1} and v_i^{n+1} by using Eqs. 3–5. The lateral inflow $\bar{r}_{i+0.5}$ is known from rainfall or surface water supply data. The rate of infiltration, $\bar{f}_{i+0.5}$, is determined from the coupling of surface and subsurface flow equations as will be considered later. All the other terms in Eqs. 8 and 9 are known either from initial conditions or from the previous time-step computations.

Initially, the flow depth and velocity must be known at all the flow sections as the initial condition. In the case of overland flow developing on an initially dry surface, a very thin water film is assumed to be ponded before the flow is initiated. This assumption is necessary to overcome the numerical singularity in the solution procedure. The results are not affected by the assumed thickness of this very thin film (2). One boundary condition at each of the upstream and downstream ends of the surface domain is needed for a subcritical flow. The boundary conditions may be prescribed as a discharge or stage hydrograph or a discharge-stage relationship.

By applying Eqs. 8 and 9 to each of the $(N-1)$ rectangular grids along the surface flow length and combining these with two equations representing the boundary conditions, a set of $(2N)$ simultaneous nonlinear algebraic equations in $(2N)$ unknowns is obtained. The unknown quantities are y_i^{n+1} and v_i^{n+1} for $i = 1, 2, \ldots, N$. A solution to this set of nonlinear equations is obtained by a generalized Newton iteration technique. The coefficient matrix obtained in the iteration process has a banded structure, and this property is used to great advantage in devising a fast solution technique (2).

Subsurface Flow

Subsurface flow is modeled as two-dimensional motion of a single-phase incompressible fluid in a nondeformable porous medium and it is represented

by the equation

$$\frac{\partial}{\partial x}\left(K_{sx}K_r\frac{\partial H}{\partial x}\right)+\frac{\partial}{\partial z}\left(K_{sz}K_r\frac{\partial H}{\partial z}\right)=\tilde{n}\frac{\partial S}{\partial P}\frac{\partial H}{\partial t} \quad \ldots\ldots\ldots\ldots (10)$$

in which K_{sx} and K_{sz} = saturated permeabilities in x and z directions, respectively; K_r = relative permeability; H = piezometric head; P = capillary pressure head; $\tilde{n}$ = soil porosity; S = degree of saturation; and t = time. The derivation and physical interpretation of Eq. 10 was given elsewhere, e.g., Ref. 6, and is not repeated here.

Eq. 10 is applied to saturated groundwater flow as well as unsaturated soil water flow. In the zone of saturation P is the positive pressure head and K_r is unity. By neglecting the entrapped gases in the soil, for saturated flow S is also set equal to unity and $\partial S/\partial P = 0$.

Hydraulic relationships among P, S, and K_r are needed in order to employ Eq. 10 in the zone of aeration. Unfortunately, unique P-S-K_r relationships cannot be obtained since soils exhibit different behavior during wetting and drying processes. The present model partly accounts for this property of soils known as hysteresis by allowing two different P-S-K_r relationships: one for each of the wetting and drying processes.

An implicit finite difference scheme based on the successive line over-relaxation method (SLOR) is employed for the solution of subsurface flow equation. As shown in Fig. 2, the entire porous medium being analyzed is divided into rectangular volume elements. Assuming soil properties remain constant within each element, Eq. 10 is written in finite difference form for an interior element (i, j) as

$$\begin{aligned}
&(K_{sz}K_r)^{n+1}_{i,j-0.5}(H^{n+1}_{i,j-1}-H^{n+1}_{i,j})\frac{\Delta x_{i,j-1}+\Delta x_{i,j}}{\Delta z_{i,j-1}+\Delta z_{i,j}}\\
&+(K_{sz}K_r)^{n+1}_{i,j+0.5}(H^{n+1}_{i,j+1}-H^{n+1}_{i,j})\frac{\Delta x_{i,j+1}+\Delta x_{i,j}}{\Delta z_{i,j+1}+\Delta z_{i,j}}\\
&+(K_{sx}K_r)^{n+1}_{i-0.5,j}(H^{n+1}_{i-1,j}-H^{n+1}_{i,j})\frac{\Delta z_{i-1,j}+\Delta z_{i,j}}{\Delta x_{i-1,j}+\Delta x_{i,j}}\\
&+(K_{sx}K_r)^{n+1}_{i+0.5,j}(H^{n+1}_{i+1,j}-H^{n+1}_{i,j})\frac{\Delta z_{i+1,j}+\Delta z_{i,j}}{\Delta x_{i+1,j}+\Delta x_{i,j}}\\
&=\frac{V_{i,j}n_{i,j}}{\Delta t}\left(\frac{\partial S}{\partial P}\right)^{n+0.5}_{i,j}(H^{n+1}_{i,j}-H^{n}_{i,j}) \quad \ldots\ldots\ldots\ldots\ldots\ldots (11)
\end{aligned}$$

in which V_{ij} = volume of the rectangular element enclosing the node (i, j) which is the centroid of the element; Δx and Δz = the side lengths of the element; n = time stage of computation; and Δt = computational time increment.

The unknown quantities in Eq. 11 are $H^{n+1}_{i,j}$ for i = 1, 2, ..., N and j = 1, 2, ..., M in which N = the number of elements in a horizontal strip, and M = the number of elements in a vertical strip as shown in Fig. 2. The coefficients K_{sx}, K_{sz}, K_r, and $\partial S/\partial P$ are prescribed functions of $H^{n+1}_{i,j}$. All other terms are known either from specified initial condition or from previous time-step

computations. Any antecedent moisture distribution can be adopted as the initial condition of the subsurface flow.

On all external boundaries, Eq. 11 is modified to incorporate the boundary conditions. Specified-flux or specified-head conditions, which may be time varying, constitute the boundary conditions at the bottom and end boundaries of the flow domain. The top boundary condition is determined from the surface flow depth. In the case of an initially dry surface, a specified mass-flux boundary is employed prior to surface saturation. After a thin layer of soil becomes saturated at the land surface, ponding or overland flow is initiated, and the top boundary condition is changed from the specified mass-flux to specified head condition. The pressure head at each boundary element is determined by the surface water depth above it.

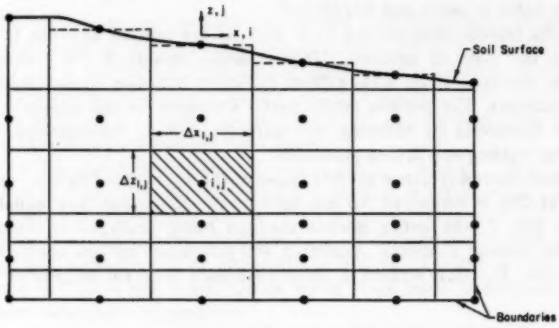

FIG. 2.—Computation Mesh for Subsurface Flow Solution

Equation 11 written for each of the $(M \times N - 2M - 2N + 4)$ interior nodes together with $(2M + 2N - 4)$ boundary equations form a set of $(M \times N)$ simultaneous nonlinear algebraic equations with $(M \times N)$ unknowns, $H_{i,j}^{n+1}$ for $i = 1, 2, 3, \ldots, N$, and $j = 1, 2, 3, \ldots, M$. Solution to this set of nonlinear equations is obtained by using a successive line over-relaxation (SLOR) technique oriented in the z direction. Details of the solution procedure was given by Akan (2).

Coupling of Surface and Subsurface Flow Components

Surface and subsurface flow components are interrelated by a common pressure head and an exchange of water at the ground surface as shown schematically in Fig. 3. The inter-relation between the two components depends upon the instantaneous flow conditions, and for transient flow it changes with time. In the mathematical sense, the top boundary condition for the subsurface flow domain is determined by the surface flow conditions. Conversely, infiltration, a lateral outflow term in Eq. 8, is controlled by the soil water conditions. Therefore, solution can be obtained only if the finite difference equations representing the two components are coupled at each time step. A quasi-implicit coupling procedure is adopted and described as follows:

1. Using the subsurface flow solutions obtained or specified at the previous time stage, the rate of infiltration f_i at each one of the subsurface volume element on the ground surface is computed from

$$f_i = \frac{V_{i,1}}{\Delta t}\tilde{n}\left(\frac{\partial S}{\partial P}\right)^{n+0.5}_{i,1}(H^{n+1}_{i,1} - H^{n}_{i,1}),$$

$$- (K_{sx}K_r)^{n+1}_{i,1+0.5}(H^{n+1}_{i,2} - H^{n+1}_{i,1})\frac{\Delta x_{i,2} + \Delta x_{i,1}}{\Delta z_{i,2} + \Delta z_{i,1}}$$

$$- (K_{sx}K_r)^{n+1}_{i-0.5,1}(H^{n+1}_{i-1,2} - H^{n+1}_{i,1})\frac{\Delta z_{i-1,1} + \Delta z_{i,1}}{\Delta x_{i-1,1} + \Delta x_{i,1}}$$

$$- (K_{sx}K_r)^{n+1}_{i+0.5,1}(H^{n+1}_{i+1,1} - H^{n+1}_{i,1})\frac{\Delta z_{i+1,1} + \Delta z_{i,1}}{\Delta x_{i+1,1} + \Delta x_{i,1}} \quad \ldots\ldots\ldots\ldots (12)$$

2. Knowing the rate of infiltration at each surface flow cross section, the surface flow equations are solved.

3. Using the surface flow solutions, the piezometric head at each computational node lying on the upper boundary of the subsurface domain is determined from the surface flow depth as shown in Fig. 3. Employing these values as the top boundary condition at the current time step, the subsurface flow is computed.

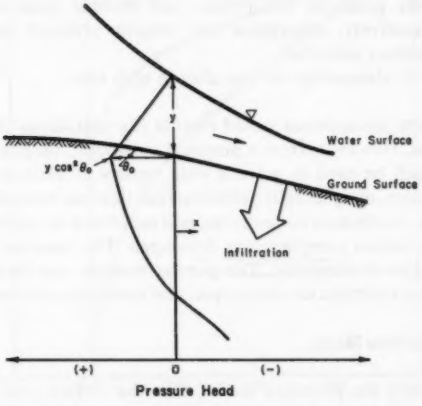

FIG. 3.—Schematic Diagram of Pressure Head for Surface and Subsurface Flow

4. With the moisture distribution computed in step 3, the rate of infiltration is re-estimated from Eq. 12, and the surface flow is recomputed using the new estimates for infiltration.

Steps 2–4 are repeated until the surface and subsurface flow solutions change within a specified acceptable error for two consecutive iterations. However, usually one cycle of iteration is sufficient since the response of the subsurface

flow to the variation in surface flow depth is much slower than the response of the surface flow to changes in the rate of infiltration.

Important Assumptions

The important assumptions involved in the development of the proposed model are listed below.

For the surface flow, the flow is gradually varied with respect to space, accordingly:

1. The piezometric pressure is distributed uniformly over a flow cross section.
2. The velocity is distributed uniformly over a flow cross section.
3. The effects of boundary friction and turbulence on surface flow can be described by Eqs. 3–6.

For the subsurface flow:

1. Darcy's Law is applicable to transient subsurface flow.
2. The flow of air phase in the zone of aeration is negligible, and there is no effect of air compression on the liquid flow.
3. The porous medium is nondeformable, and the fluid is incompressible and homogeneous.
4. The osmotic pressure, adsorption, and thermal potential gradients are negligible. Alternatively, adsorption and osmotic pressure can be treated as a part of the capillary potential.
5. The P-K_r-S relationships do not change with time.

Naturally, these assumptions would restrict the usefulness of the conjunctive model developed. However, from a practical viewpoint, despite the assumptions the model can still be used to solve a wide variety of surface-subsurface flow problems. The unsteady, gradually varied surface flow can be laminar, transitional, or fully turbulent, uniform or nonuniform, and subcritical or supercritical provided no roll waves or similar complications developed. The transient subsurface flow can be one- or two-dimensional. The porous medium can be homogeneous or nonhomogeneous, isotropic or anisotropic, and saturated or unsaturated, or both.

Verification of Proposed Model

In order to verify the proposed model, first the surface and subsurface flow components are tested separately with available experimental data and analytical solutions. Then, by using a set of published experimental data, the model is verified as applied to a conjunctive surface-subsurface flow.

Izzard's (12) experimental results are adopted to verify the surface flow component. In Run 138 of his experiment, the runoff from a simulated uniform rainfall over the entire area of a plot was recorded. The plot was 6 ft (1.8 m) wide and 72 ft (21.9 m) long and had a bottom slope of 0.001. The surface of the plot was covered with crushed slate roofing paper which is represented by a surface roughness of $k = 0.01$ ft (3 mm) in the numerical solution. The time-variable intensity of the simulated rainfall, the observed runoff, and the

computed runoff are shown in Fig. 4. The sudden jump in the runoff hydrograph when the rainfall terminates is apparently due to a sudden decrease in the flow resistance. As can be inspected visually in Fig. 4, the agreement between numerical and experimental results is good.

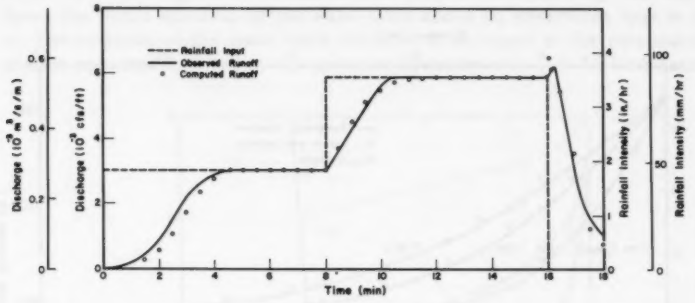

FIG. 4.—Verification of Surface Flow Prediction with Izzard's Experimental Data

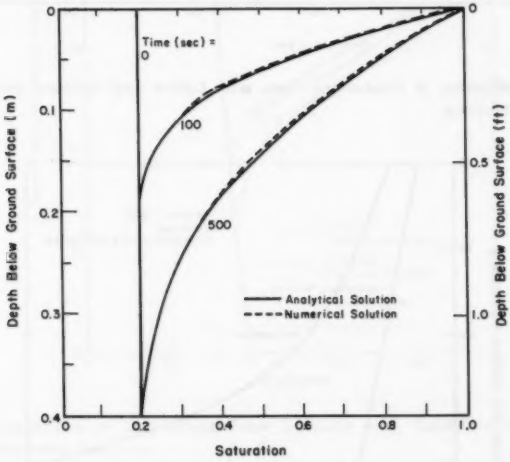

FIG. 5.—Verification of Subsurface Flow with Philip's Analytical Solution

In order to verify the subsurface flow component of the proposed model, Philip's (15) analytical solution for vertical flow of water in an initially unsaturated soil, Luthin and Holmes' (14) and Hantush's (9) analytical solutions for horizontal saturated flow, and a set of experimental data reported by Vachaud and Thony (26) are adopted.

In the idealized case of vertical percolation of water through a deep homoge-

neous soil column, the initial saturation of the soil is assumed uniform and equal to 0.20 throughout the entire depth. The surface soil becomes fully saturated at zero time and remains so throughout the entire process. Sufficient amount of water is supplied continuously on the soil surface under zero pressure head. The idealized hydraulic properties of the soil are $K_{zz} = 6.25 \times 10^{-3}$ mm/s,

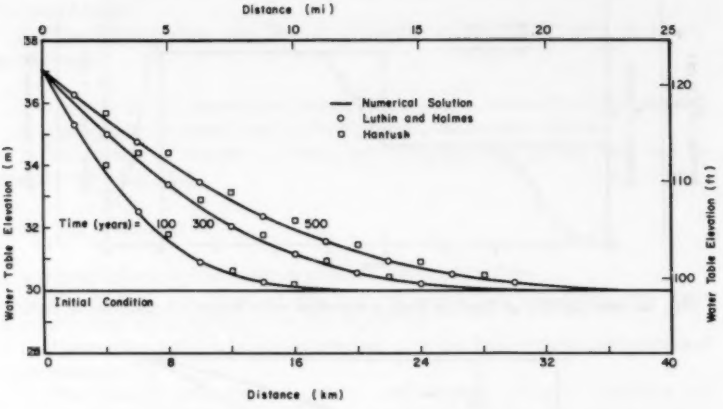

FIG. 6.—Verification of Subsurface Flow with Luthin and Holmes' and Hantush's Analytical Solutions

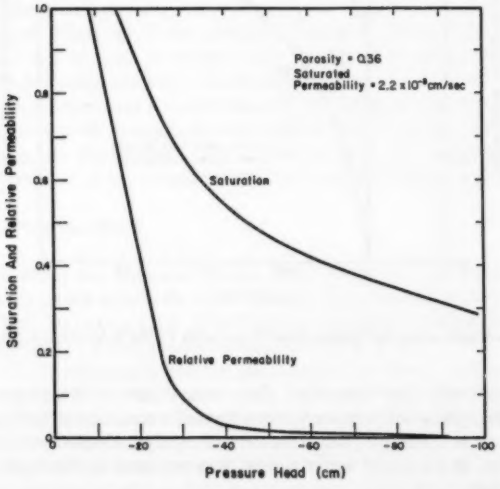

FIG. 7.—Hydraulic Properties of Soil Used in Comparison of Fig. 8

$K_r = 1$, $\partial S/\partial P = 0.2\ \text{mm}^{-1}$, and $\bar{n} = 0.125$. As shown in Fig. 5, the moisture profiles obtained for this idealized situation using the proposed model and Philip's (15) analytical method are in a good agreement.

In another hypothetical situation, the subsurface flow component of the proposed model is applied to the horizontal movement of a saturated ground-water flow. The initial elevation of the water table above an impervious base is 30 m. The variation of the water table elevation is examined as the piezometric head is increased to 37 m at the upstream boundary at $t = 0$. In Luthin and

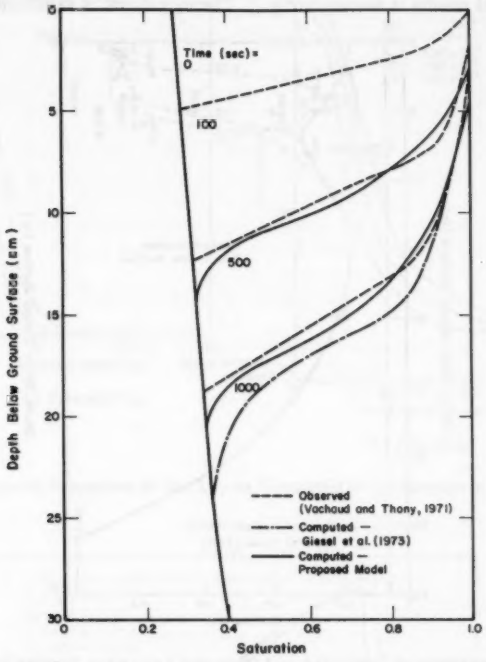

FIG. 8.—Comparison of Subsurface Flow Solution with Experimental Data and Another Numerical Solution

Holmes' (14) and Hantush's (9) analytical solutions, the aquifer is characterized by a storage coefficient of 0.45 and a permeability of 0.36 m/h. The same aquifer is reproduced in the numerical scheme with $K_{zz} = 0.36$ m/h, $K_r = 1$, and the product $\bar{n}\ \partial S/\partial P = 0.05\ \text{m}^{-1}$. As can be inspected in Fig. 6, the numerical solution is a good agreement with the analytical solutions.

In Vachaud and Thony's (26) experimental study of one-dimensional vertical movement of water percolating through a homogeneous unsaturated soil column, the soil moisture was initially in static equilibrium. Throughout the process,

the pressure head at the soil surface was maintained at −0.12 m. No outflow occurred from the bottom of the soil except at the later part of the experiment which is not considered here. The hydraulic properties of the soil measured and used in the numerical simulation are given in Fig. 7. In order to avoid a possible time lag between the initial times of the experimental and the mathematically simulated conditions, the numerical solutions are started at t = 100 sec with the corresponding moisture distribution as determined experimentally. A comparison of the saturation profiles obtained from the proposed model and from another numerical solution method by Giesel et al. (8) with the experimental results is shown in Fig. 8. The agreement is satisfactory.

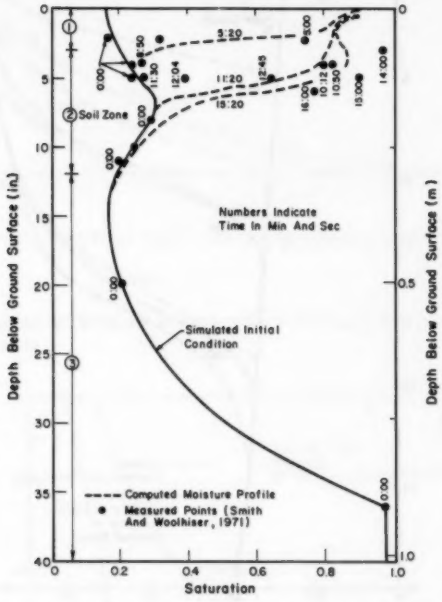

FIG. 9.—Comparison of Computed and Observed Saturation Profiles for Conjunctive Model

As to a conjunctive surface-subsurface flow system, the presently developed model is tested with the experimental data of Smith and Woolhiser (23). A laboratory watershed consisting of a soil flume and a rainfall simulator was employed in the experiment. The soil flume was 2 in. (51 mm) in width, 4 ft (1.22 m) in depth, and 40 ft (12.2 m) in length. The bottom of the flume was impervious, but seepage was allowed at both ends. The thickness of the three zones of soil placed in layers in the flume are shown in Fig. 9. The hydraulic properties of the soil layers are given in Fig. 10. The fluid used was a light oil with a kinematic viscosity of 0.003 sq in./sec (1.94×10^{-6} m^2/s). The intensity of the nozzle generated rainfall was 9.9 in./h (250 mm/h)

over a duration of 15 min. A surface roughness $k = 0.05$ in. (1.3 mm) is used in the numerical simulation. The numerical and experimental results of the soil moisture distributed at a flow section 18.3 ft (5.58 m) from the upstream end of the flume and the surface runoff from the flume are shown in Figs. 9 and 11, respectively. Due to very few and scattering experimental points it is difficult

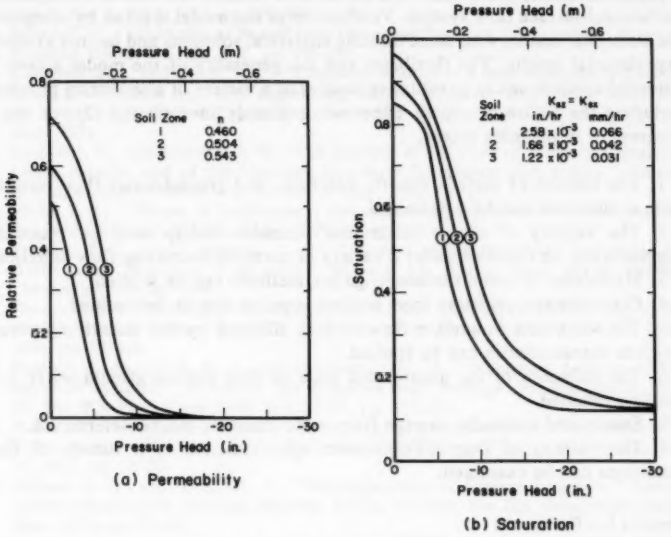

FIG. 10.—Hydraulic Properties of Soil Layers Simulated in Verification of Conjunctive Model

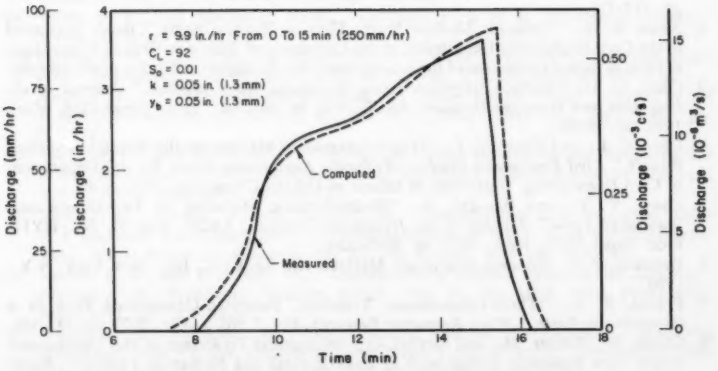

FIG. 11.—Comparison of Observed and Computed Runoff for Conjunctive Model

to make a comparison for the soil moisture profiles. However, the agreement between the observed and computed surface hydrographs is reasonably good.

Concluding Remarks

A physically based mathematical model is developed to simulate a conjunctive surface-subsurface flow system. Verification of the model is given by comparing the numerical results with some existing analytical solutions and limited available experimental results. The flexibility and the generality of the model allows its potential applications to quantitative studies of a variety of engineering problems including the following which either were already investigated (2), or are in progress or in planning stages.

1. The amount of surface runoff, interflow, and ground-water flow resulting from a rainstorm can be determined.
2. The validity of simple infiltration formulas widely used by practicing engineers can be checked under a variety of naturally occurring flow situations.
3. Hydraulics of some surface irrigation methods can be studied.
4. Ground-water recharge from surface supplies can be determined.
5. The variations in surface flow as it is affected by the underlying porous medium characteristics can be studied.
6. The influence of the unsaturated zone on free surface ground-water flow can be evaluated.
7. Steady and unsteady seepage from wide channels can be determined.
8. The validity of Dupuit-Forcheimer approximation in a variety of flow conditions can be examined.

Appendix I.—References

1. Abbott, M. B., Warren, I. R., Jensen, K. H., Jønch-Clausen, T., and Havnø, K., "Coupling of Unsaturated Zone and Saturated Zone Models," *Proceedings*, 18th Congress of the International Association for Hydraulic Research, Vol. 5, Sept., 1979, pp. 119–125.
2. Akan, A. O., "Unsteady Shallow Water Flow on Porous Media," thesis presented to the Civil Engineering Department at the University of Illinois at Urbana-Champaign, in 1976, in partial fulfillment of the requirements for the degree of Doctor of Philosophy.
3. Chen, C. L., "Surface Irrigation Using Kinematic-Wave Method," *Journal of the Irrigation and Drainage Division*, ASCE, Vol. 96, No. IR1, Proc. Paper 7134, Mar., 1970, pp. 39–46.
4. Chen, C. L., and Chow, V. T., "Hydrodynamics of Mathematically Simulated Surface Runoff," *Civil Engineering Studies, Hydraulic Engineering Series No. 18*, Department of Civil Engineering, University of Illinois at Urbana-Champaign, Aug., 1968.
5. Chow, V. T., and Ben-Zvi, A., "Hydrodynamic Modeling of Two-Dimensional Watershed Flow," *Journal of the Hydraulics Division*, ASCE, Vol. 99, No. HY11, Proc. Paper 10172, Nov., 1973, pp. 2023–2040.
6. Eagleson, P. S., *Dynamic Hydrology*, McGraw-Hill Book Co., Inc., New York, N.Y., 1970.
7. Freeze, R. A., "Three-Dimensional, Transient, Saturated-Unsaturated Flow in a Groundwater Basin," *Water Resources Research*, Vol. 7, No. 2, Apr., 1971, pp. 347–366.
8. Giesel, W., Renger, M., and Strebel, O., "Numerical Treatment of the Unsaturated Water Flow Equation: Comparison of Experimental and Numerical Results," *Water Resources Research*, Vol. 9, No. 1, Feb., 1973, pp. 174–177.
9. Hantush, M. S., discussion of "An Analysis of the Flow of Water in a Shallow,

Linear Aquifer and of the Approach to a New Equilibrium after Intake," by J. N. Luthin, and J. W. Holmes, *Journal of Geophysical Research*, Vol. 65, No. 11, Nov., 1960, pp. 3847–3848.

10. Hart, W. E., Bassett, D. L., and Strelkoff, T., "Surface Irrigation Hydraulics-Kinematics," *Journal of the Irrigation and Drainage Division*, ASCE, Vol. 94, No. IR4, Proc. Paper 6284, Dec., 1968, pp. 419–440.
11. Hornberger, G. M., and Remson, I., "A Moving Boundary Model of One-Dimensional Saturated-Unsaturated, Transient Porous Flow Systems," *Water Resources Research*, Vol. 6, No. 3, June, 1970, pp. 898–905.
12. Izzard, C. F., "Hydraulics of Runoff from Developed Surfaces," *Proceedings*, Highway Research Board, Vol. 26, 1946, pp. 129–146.
13. Kareliotis, S. J., and Chow, V. T., "Computer Solution of a Hydrodynamic Watershed Model (IHW Model II)," *Civil Engineering Studies, Hydraulic Engineering Series No. 25*, Department of Civil Engineering, University of Illinois at Urbana-Champaign, Mar., 1971.
14. Luthin, J. N., and Holmes, J. W., "An Analysis of the Flow of Water in a Shallow, Linear Aquifer, and of the Approach to a New Equilibrium after Intake," *Journal of Geophysical Research*, Vol. 65, No. 5, May, 1960, pp. 1573–1576.
15. Philip, J. R., "Theory of Infiltration," *Advances in Hydroscience*, V. T. Chow, ed., Academic Press, New York, N.Y., 1969, pp. 215–296.
16. Prickett, T. A., and Lonnquist, C. G., "Selected Digital Computer Techniques for Groundwater Resource Evaluation," *Bulletin 55*, Illinois State Water Survey, Champaign, Illinois, 1971.
17. Reeder, J. W., Freyberg, D. L., Franzini, J. B., and Remson, I., "Infiltration Under Rapidly Varying Surface Depths," *Water Resources Research*, Vol. 16, No. 1, Feb., 1980, pp. 97–104.
18. Remson, I., Fungaroli, A. A., and Hornberger, G. M., "Numerical Analysis of Soil Moisture Systems," *Journal of the Irrigation and Drainage Division*, ASCE, Vol. 93, No. IR3, Proc. Paper 5429, Sept., 1967, pp. 153–166.
19. Rubin, J., "Numerical Method for Analyzing Hysteresis-Affected, Post Infiltration Redistribution of Soil Moisture," *Proceedings*, Soil Science Society of America, Vol. 31, 1967, pp. 13–20.
20. Sakkas, J. G., and Strelkoff, T., "Hydrodynamics of Surface Irrigation," *Journal of the Irrigation and Drainage Division*, ASCE, Vol. 100, No. IR1, Proc. Paper 10422, Mar., 1974, pp. 31–48.
21. Shen, H. W., and Li, R. M., "Rainfall Effect on Sheet Flow Over Smooth Surface," *Journal of the Hydraulics Division*, ASCE, Vol. 99, No. HY5, Proc. Paper 9733, May, 1973, pp. 771–792.
22. Singh, R., "Prediction of Mound Geometry Under Recharge Basin," *Water Resources Research*, Vol. 12, No. 4, Aug., 1976, pp. 775–780.
23. Smith, R. E., and Woolhiser, D. A., "Overland Flow on an Infiltrating Surface," *Water Resources Research*, Vol. 7, No. 3, June, 1971, pp. 899–913.
24. Staple, W. J., "Infiltration and Redistribution of Water in Vertical Columns of Loam Soil," *Proceedings*, Soil Science Society of America, Vol. 30, 1966, pp. 553–558.
25. Stelkoff, T., "One-Dimensional Equations of Open-Channel Flow," *Journal of the Hydraulics Division*, ASCE, Vol. 95, No. HY3, Proc. Paper 6557, May, 1969, pp. 861–876.
26. Vachaud, G., and Thony, J. L., "Hysteresis During Infiltration and Redistribution in a Soil Column on Different Initial Water Contents," *Water Resources Research*, Vol. 7, No. 1, Feb., 1971, pp. 111–127.
27. Vauclin, M., Khanji, D., and Vachaud, G., "Experimental and Numerical Study of a Transient Two-Dimensional Unsaturated-Saturated Water Table Recharge Problem," *Water Resources Research*, Vol. 15, No. 5, Oct., 1979, pp. 1089–1101.
28. Verma, R. D., and Brutsaert, W., "Unsteady Free Surface Groundwater Seepage," *Journal of the Hydraulics Division*, ASCE, Vol. 97, No. HY8, Proc. Paper 8337, Aug., 1971, pp. 1213–1229.
29. Whisler, F. D., and Klute, A., "The Numerical Analysis of Infiltration, Considering Hysteresis, Into Vertical Column at Equilibrium Under Gravity," *Proceedings*, Soil Science Society of America, Vol. 29, 1965, pp. 489–494.
30. Wooding, R. A., "A Hydraulic Model for the Catchment-Stream Problem II. Numerical

Solutions," *Journal of Hydrology*, Vol. 3, Nos. 3/4, 1965, pp. 268–282.
31. Yen, B. C., "Spatially Varied Open-Channel Flow Equations," *Research Report No. 51*, Water Resources Center, University of Illinois at Urbana-Champaign, Dec., 1971.
32. Yen, B. C., "Open-Channel Flow Equations Revisited," *Journal of the Engineering Mechanics Division*, ASCE, Vol. 99, No. EM5, Proc. Paper 10073, Oct., 1973, pp. 979–1009.

Appendix II.—Notation

The following symbols are used in this paper:

C_L = coefficient;
f = time rate of infiltration;
f_d = Darcy-Weisbach resistance coefficient;
g = gravitational acceleration;
H = piezometric head;
i = index for surface flow sections, also, index for subsurface flow element;
j = index for subsurface flow element;
K_r = relative permeability;
K_{sx} = saturated permeability in x direction;
K_{sz} = saturated permeability in z direction;
k = ground surface hydraulic roughness measure;
n = time stage;
$\bar{n}$ = porosity;
P = capillary pressure head;
R = Reynolds number = vy/kinematic viscosity;
r = time rate of lateral inflow;
S = degree of saturation;
S_f = friction slope;
S_o = bottom slope;
t = time;
V = volume of subsurface flow element;
v = cross-sectional average velocity;
x = horizontal distance;
y = surface flow depth;
z = vertical distance;
Δt = time increment;
Δx = surface flow reach length, also, length of subsurface flow domain element;
Δz = height of subsurface flow domain element; and
θ = weighting factor.

JOURNAL OF THE
HYDRAULICS DIVISION

TECHNICAL NOTES

Note.—Discussion open until September 1, 1981. To extend the closing date one month, a written request must be filed with the Manager of Technical and Professional Publications, ASCE. This paper is part of the Journal of the Hydraulics Division, Proceedings of the American Society of Civil Engineers, ©ASCE, Vol. 107, No. HY4, April, 1981.

Technical Notes

To provide a place within ASCE for publication of technical ideas that have not advanced, as yet, to the point where they warrant publication as a Proceedings paper in a *Journal*, the publication of Technical Notes was authorized by the Board of Direction on October 16–18, 1967, under the following guidelines:

1. An original manuscript and two copies are to be submitted to the Manager of Technical and Professional Publications, ASCE, 345 East 47th Street, New York, N.Y., 10017, along with a request by the author that it be considered as a Technical Note.
2. The two copies will be sent to an appropriate Technical Division or Council for review.
3. If the Division or Council approves the contribution for publication, it shall be returned to Society Headquarters with appropriate comments.
4. The technical publications staff will prepare the material for use in the earliest possible issue of the *Journal*, after proper coordination with the author.
5. Each Technical Note is not to exceed 4 pages in the *Journal*. As an approximation, each full manuscript page of text, tables, or figures is the equivalent of one-half a *Journal* page.
6. The Technical Notes will be grouped in a special section of each *Journal*.
7. Information retrieval abstracts and key words will be unnecessary for Technical Notes.
8. The final date on which a Discussion should reach the Society is given as a footnote with each Technical Note.
9. Technical Notes will not be included in *Transactions*.
10. Technical Notes will be included in ASCE's annual and cumulative subject and author indexes.

The manuscripts for Technical Notes must meet the following requirements:

1. Titles must have a length not exceeding 50 characters and spaces.
2. The author's full name, Society membership grade, and a footnote reference stating present employment must appear on the first page of the manuscript. Authors need not be Society members.
3. The manuscript is to be submitted as an original copy (with two duplicates) that is typed double-spaced on one side of 8-1/2-in. (220-mm) by 11-in. (280-mm) white bond paper.
4. All mathematics must be typewritten and special symbols must be properly identified. The letter symbols used must be defined where they first appear, in figures or text, and arranged alphabetically in an Appendix.—Notation.
5. Standard definitions and symbols must be used. Reference must be made to the lists published by the American National Standards Institute and to the *Authors' Guide to the Publications of ASCE*.
6. Tables must be typed double-spaced (an original ribbon copy and two duplicate copies) on one side of 8-1/2-in. (220-mm) by 11-in. (280-mm) paper. An explanation of each table must appear in the text.
7. Figures must be drawn in black ink on one side of 8-1/2-in. (220-mm) by 11-in. (280-mm) paper. Because figures will be reproduced with a width of between 3 in. (76 mm) to 4-1/2 in. (110 mm), the lettering must be large enough to be legible at this width. Photographs must be submitted as glossy prints. Explanations and descriptions must be made within the text for each figure.
8. References cited in text must be typed at the end of the Technical Note in alphabetical order in an Appendix.—References.
9. Dual units, i.e., U.S. Customary followed by SI (International System) units in parentheses, should be used throughout the paper.

SCALES FOR CIRCULAR JETS IN CROSS-FLOW

By Nallamuthu Rajaratnam,[1] M. ASCE and Thimmaiah Gangadharaiah[2]

INTRODUCTION

Circular jets injected into cross-flows have been studied because of their application to the disposal of effluents into rivers and the atmosphere, and also because the resulting flow is a rather complex form of turbulent shear flow. Consider a circular jet of diameter, d, issuing with a uniform velocity of U_0 into a free-stream of large extent, which has a uniform velocity of U_1, as shown in Fig. 1. Experimental observations show that close to the jet nozzle, due to the pressure field imposed by the free-stream or cross-flow, the jet gets deflected. Since the outer layers of the jet lose a part of their momentum to the entrained fluid due to the turbulent mixing, they are more easily deflected than the central region, and the jet acquires a characteristic kidney shape within a short distance from the jet nozzle (1). This deformed cross section of the jet houses on its sides a pair of attached vortices (3,5,8,10). Entrainment of the free-stream fluid (and thus, momentum) causes further deflection of the jet, and increases the circulation in its cross section, which is reflected in the growth of the counter-rotating vortex pair. After some more distance along the jet, the jet is moving only at a small differential angle from the free-stream, and the cross section of the jet is almost completely occupied by the vortex pair. In addition to this bound vortex system, the cross-flow creates another vortex system which is shed from the deformed jet (7,8).

Considering the deflected jet in the fully-developed flow region (i.e., after the end of the potential core), in the ζ-η plane (Fig. 1), the distribution of the velocity component, u (normal to the ζ-η plane) has been found to be similar in the η direction by Keffer and Baines (6) for $\alpha = 4$, 6, and 8, in which α = the ratio of the jet to free-stream velocity. The velocity scale was taken as $(u_m - U_1)$ in which u_m = the velocity on the axis in the ξ direction, and the length scale was taken as η_b in which $u - U_1 = (1/2)(u_m - U_1)$. This length scale was found to increase linearly with ξ measured from the virtual origin, located about 1.3 d behind the nozzle, with the coefficient of proportionality equal to 0.215. The velocity scale $(u_m - U_1)$ was found to decay much faster than in a simple circular jet. Based on the results of an

[1]Prof., Dept. of Civ. Engrg., Univ. of Alberta, Edmonton, Alberta, Canada T6G 2G7.
[2]Asst. Prof., Dept. of Civ. Engrg., I.I.T., Kanpur, U.P. India; formerly Post-Doctoral Fellow, Dept. of Civ. Engrg., Univ. of Alberta, Edmonton, Canada T6G 2G7.

Note.—Discussion open until September 1, 1981. To extend the closing date one month, a written request must be filed with the Manager of Technical and Professional Publications, ASCE. Manuscript was submitted for review for possible publication on August 22, 1980. This paper is part of the Journal of the Hydraulics Division, Proceedings of the American Society of Civil Engineers, ©ASCE, Vol. 107, No. HY4, April, 1981. ISSN 0044-796X/81/0004-0497/$01.00.

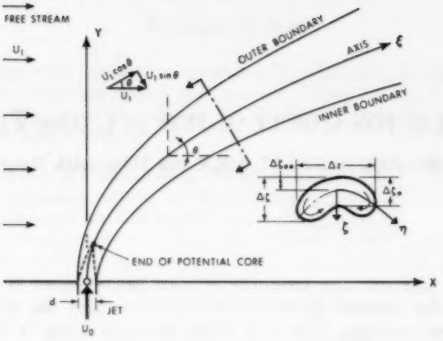

FIG. 1.—Definition Sketch: Circular Jet in Cross-Flow

experimental study on circular jets in cross-flows for α from 2.7 to about 23, this note presents practically useful correlations for the velocity and length scales.

Experimental Results and Analysis

The experiments were performed in a rectangular open channel with the jets issuing from a plate fixed parallel to and slightly above the bed. For the first three experiments with $\alpha = 2.73$, 4.52, and 7.05, the diameter of the jet was 0.5 in. (12.7 mm), and the width of the flume was 9 in. (22.9 cm), whereas for the fourth experiment with $\alpha = 23.4$, d was equal to 1/8 in. (3.2 mm), and the width of the flume was increased to 18 in. (45.7 cm). The depth of flow was maintained at 10 in. (25.4 cm) for all four experiments.

The axial velocity, u, in the deflected jet was measured with a 3-mm external diameter Prandtl-type pitot-static tube alined with the ξ-axis. The velocity field was measured for $\bar{\xi}/d$ up to about seven for the first experiment; for the other three experiments, the corresponding values of $\bar{\xi}/d$ were approx 11, 17, and 58, wherein $\bar{\xi}$ is measured from the nozzle. More details regarding these experiments are available in a report by the writers (12).

In the region of developed flow, in the ζ-η plane, the velocity profiles were tested for similarity by plotting $(u - U_1)/(u_m - U_1)$ versus η/η_b, in which u_m = the maximum value of u occurring on the axis of the jet; and $\eta_b = \eta$, where $u - U_1 = 1/2\ (u_m - U_1)$. It was found that these profiles are similar for the $\bar{\xi}/d$ values tested. It was also found that the velocity profiles are similar in the ζ direction for the $\eta = 0$ and $\eta \neq 0$ planes in which ζ_b = the corresponding length scale (12). These similarity profiles are described well by the familiar exponential relation (11).

For these similarity plots, the velocity scale is $(u_m - U_1)$, and the length scales are η_b and ζ_b. Considering the maximum velocity, u_m, the results of the writers and several others, when plotted with $(u_m - U_1)/(U_0 - U_1)$ against $\bar{\xi}/d$, showed that the dimensionless excess velocity in the deflected jet decays more rapidly as α becomes smaller. Fig. 2 shows one successful correlation

developed for the dimensionless excess velocity, in which $\bar{\xi}_*$ = the intercept of the straight lines on the $(u_m - U_1)/(U_0 - U_1)$ versus $\bar{\xi}/d$ (double log) plot on the $(u_m - U_1)/(U_0 - U_1) = 1.0$ line. As shown in Fig. 3, $\bar{\xi}_*/d$ increases linearly with α on a log-log plot. Thus, using Figs. 2 and 3, $(u_m$

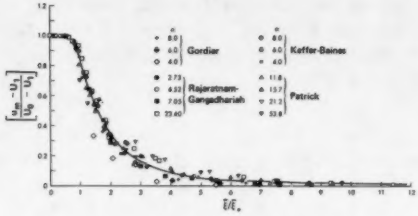

FIG. 2.—Correlation for Velocity Scale

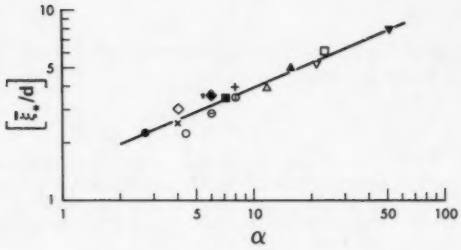

FIG. 3.—Variation of $\bar{\xi}_*/d$ with α

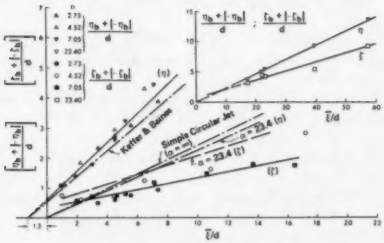

FIG. 4.—Length Scales

$- U_1$) can be found for any value of $\bar{\xi}/d$ within the range studied. It has also been found in Ref. 12 that a similar analysis can be performed for $(u_m - U_1 \cos \theta)/(U_0 - U_1)$, in which θ = the angle of the jet at any $\bar{\xi}$ with the cross-flow, and an empirical correlation for predicting θ at any $\bar{\xi}$ has been developed in Ref. 12.

Regarding the length scales, as shown in Fig. 4, both the η and ζ scales appear to increase linearly with $\bar{\xi}/d$ (the scales with the minus sign refer to the negative side). For the three smaller values of α tested, the η scale is much larger than the ζ scale, whereas for $\alpha = 23.4$, the η scale is only slightly larger than the ζ scale. Of course, for the simple jet (into a stagnant ambient) for which $\alpha = \infty$, both the scales will be the same. Fig. 4 also shows the growth rate of the length scale for the simple jet for comparison, which is slower than the η scale and faster than the ζ scale of the jets in cross-flow for the three smaller α values.

Conclusions

Based on an experimental study on circular jets in cross-flow for $\alpha = 2.73$, 4.52, 7.05, and 23.4, in which the u velocity profiles with respect to the cross-flow have been found to be similar in the η and ζ directions in the fully-developed flow region, the length scales have been found to grow linearly. An empirical correlation has also been developed for the dimensionless velocity scale.

Acknowledgment

The first writer is thankful to the National Research Council of Canada for the financial assistance provided.

Appendix.—References

1. Abramovitch, G. N., *The Theory of Turbulent Jets*, Massachusetts Institute of Technology Press, Cambridge, Mass., 1963, 671 p. (English translation).
2. Chassaing, P., George, J., Claria, A., and Sananes, F., "Physical Characteristics of Subsonic Jets in a Cross-Stream," *Journal of Fluid Mechanics*, London, England, Vol. 62, Part, 1, 1974, pp. 41–64.
3. Fearn, R. L., and Weston, R. P., "Induced Velocity Field of a Jet in a Cross-Flow," *Technical Paper 1087*, National Aeronautics and Space Administration, May, 1978.
4. Gordier, R. L., "Studies on Fluid Jets Discharging Normally into Moving Fluid," *Technical Paper 28*, Series B, St. Anthony Falls Hydraulics Laboratory, University of Minnesota, Minneapolis, Minn., 1959.
5. Kamotani, Y., and Greber, I., "Experiments on a Turbulent Jet in a Cross-Flow," American Institute of Aeronautics and Astronautics, 10th Aerospace Sciences Meeting, San Diego, Calif., 1972, 9 p.
6. Keffer, J. F., and Baines, W. D., "The Round Jet in a Cross-Wind," *Journal of Fluid Mechanics*, London, England, Vol. 8, 1963, pp. 481–496.
7. McMahon, H. M., Hester, D. D., and Palfrey, J. G., "Vortex Shedding from a Turbulent Jet in a Crosswind," *Journal of Fluid Mechanics*, London, England, Vol. 48, 1971, pp. 73–80.
8. Moussa, Z. M., Trischka, J. W., and Eskinazi, S., "The Near Field in the Mixing of a Round Jet With a Cross-Stream," *Journal of Fluid Mechanics*, London, England, Vol. 80, Part 1, 1977, pp. 49–80.
9. Patrick, M. A., "Experimental Investigation of the Mixing and Penetration of a Round Turbulent Jet Injected Perpendicularly into a Transverse Stream," *Transactions*, Institute of Chemical Engineers, Vol. 45, 1967, pp. T16–T31.
10. Pratte, B. D., and Baines, W. D., "Profiles of the Round Turbulent Jet in a Cross-Flow," *Journal of the Hydraulic Division*, ASCE, Vol. 92, No. HY6, Proc. Paper 5556, Nov., 1967, pp. 53–64.
11. Rajaratnam, N., *Turbulent Jets*, Elsevier Scientific Publishing Co., 1976, 304 p.
12. Rajaratnam, N., and Gangadhariah, T., "Circular Jets in Cross-Flow," *Technical Report*, Department of Civil Engineering, University of Alberta, Edmonton, Canada, 1980.

A Sand-Water Slurry Experiment

By M. R. Carstens,[1] F. ASCE and Graeme Addie[2]

Introduction

Experimentally-determined results of the flow of a sand-water slurry in an 8-in. diam (200-mm) polished steel pipe are reported herein.

Experiments

Experimental results of two tests in the 8-in. (200-mm) slurry test loop at the Georgia Iron Works (GIW) Hydraulic Laboratory are presented (one is a test with water, Test 102-79; the other is a test with a sand-water slurry, Test 97-79). Because of the modern instruments used in these tests and because of the data-acquisition system, the data are sufficiently precise to warrant physical interpretation of the small difference revealed between the flow of water and the flow of a sand-water slurry.

The principal reason for accuracy of the experiments is the 32-channel data-acquisition and the data-processing system installed at the GIW Hydraulic Laboratory. All of the measuring instruments transduce the sensed physical quantities into 4 ma–20 ma electrical signals which are then processed through analog-to-digital converters for further processing through a minicomputer. By means of this system, the output of all temperature, pressure, and discharge measuring instruments are recorded during the same time period. Mean values of all measured flow variables are displayed on a cathode ray tube (CRT) for the test engineer. The period during which mean values are calculated in the computer can be selected by the test engineer. In addition, one column of the CRT display is devoted to a three-digit coded display indicating the change in value from the previous mean so that the test engineer can avoid transients in the recorded data. When the test engineer is satisfied that the flow is tolerably steady, a run is taken with the digital data being recorded.

A second method of insuring accuracy is the use of redundant instrumentation, as demonstrated in Table 1. Values of the discharge, Q, in the column labeled CH3 were determined by means of an 8-in. Fischer and Porter magnetic flowmeter.

[1]Prof. Emeritus, Georgia Inst. of Tech.; and Consultant, Georgia Iron Works Co., P.O. Box 626, Grovetown, Ga. 30813.

[2]Vice Pres. of Engrg., Research & Development, Georgia Iron Works Co., P.O. Box 626, Grovetown, Ga. 30813.

Note.—Discussion open until September 1, 1981. To extend the closing date one month, a written request must be filed with the Manager of Technical and Professional Publications, ASCE. Manuscript was submitted for review for possible publication on April 8, 1980. This paper is part of the Journal of the Hydraulics Division, Proceedings of the American Society of Civil Engineers, ©ASCE, Vol. 107, No. HY4, April, 1981. ISSN 0044-796X/81/0004-xxxx/$01.00.

The Q values listed in the CH6 column were determined by means of an *in-situ* calibrated bend meter. Values of the friction-pressure gradient were determined from two completely independent sensing and measuring systems for determining

TABLE 1.—Measured Values of Q and i_m

Run (1)	Q, in gallons per minute		i_m, in feet of water per foot of pipe[a]		s_m (6)
	CH 3 (2)	CH 6 (3)	CH 11 (4)	CH 13 (5)	
			(*a*) Test 102-79		
1	280	235	0.000	0.0011	1.00
2	482	451	0.002	0.0034	1.00
3	715	694	0.006	0.0072	1.00
4	877	868	0.010	0.0106	1.00
5	1,040	1,013	0.015	0.0150	1.00
6	1,219	1,195	0.020	0.0206	1.00
7	1,552	1,535	0.030	0.0306	1.00
8	1,781	1,755	0.039	0.0397	1.00
9	1,991	1,974	0.048	0.0489	1.00
10	2,237	2,226	0.060	0.0606	1.00
11	2,483	2,478	0.073	0.0735	1.00
12	2,713	2,709	0.086	0.0869	1.00
13	2,949	2,941	0.101	0.1018	1.00
14	3,173	3,164	0.116	0.1163	1.00
15	3,406	3,400	0.132	0.1319	1.00
			(*b*) Test 97-79		
1	436	470	0.003	0.0042	1.00
2	631	601	0.007	0.0083	1.00
3	843	819	0.011	0.0121	1.00
4	1,000	977	0.019	0.0198	1.00
5	1,253	1,197	0.026	0.0269	1.02
6	1,413	1,365	0.030	0.0305	1.04
7	1,598	1,542	0.036	0.0366	1.04
8	1,788	1,726	0.042	0.0425	1.05
9	2,061	1,930	0.050	0.0507	1.05
10	2,197	2,101	0.057	0.0578	1.05
11	2,468	2,384	0.071	0.0714	1.06
12	2,746	2,604	0.082	0.0831	1.06
13	2,877	2,770	0.092	0.0927	1.06
14	3,076	2,967	0.104	0.1052	1.06
15	3,470	3,355	0.131	0.1319	1.06

[a] i_m is unitless but not dimensionless.
Note: 1 gal/min = 6.31 (10^{-5}) m^3/s.

the pressure drop in the 50.0-ft (15.24-m) long horizontal, 7.98-in. (203-mm) diam, steel pipe test section.

Sand.—The results of a sieve analysis of the foundry sand, $s_s = 2.65$, are listed in Table 2.

The sieve-size data were plotted on log probability paper, and a straight line passed through the 15.9% and 84.1% points from which d_g (geometric mean diameter) = 270 μm; and σ_g (geometric standard deviation) = 1.6 were determined.

Test Section.—The 50.0-ft (15.24-m) long horizontal test section of 8-in. (200-mm) diam steel pipe is fitted with two 1/8-in. (3-mm) diam piezometers in the cross sections at the ends of the straight test section. The piezometers are positioned at 45° on either side top dead center. The test section is preceded by a 60.9-ft (18.6-m) length of straight horizontal pipe. Each piezometer is connected by means of plastic tubing to an enclosed sediment trap which, in turn, is connected to one side of a Rosemount pressure transducer, thereby forming two independent pressure-measuring systems; see CH 11 and CH 13, in Table 1.

Pressure-transducer calibration is checked at intervals by means of an open-column manometer and a water-mercury differential manometer. All pressure transducers are calibrated in feet of water having the specific weight of 62.4 lb/cu ft (9802 N/m^3).

Discharge.—The discharge, Q, is metered by means of an 8-in. Fischer and Porter magnetic flowmeter and a bend meter. Calibration of both meters is checked at intervals by means of water flow through a standard square-edged orifice and a volumetric tank. The bend meter is utilized as a backup meter because the pressure differences across the bend become very small at low flows, and because the bend meter is a questionable instrument when a slurry containing settling solid is forced through the bend.

TABLE 2.—Size Determination

Sieve number (1)	Amount finer than, as a percentage (2)
30	96.5
40	83.1
50	51.4
70	25.8
100	10.3
140	4.5

Temperature.—Slurry temperature is measured by means of a temperature transducer cemented to the exterior of the steel pipe downstream from the pump and upstream from the test section.

Concentration.—Solids concentration is determined by means of pressure measurements in the upward and downward flowing legs of an inverted U tube. The 20.7-ft (6.3-m) high inverted U tube is instrumented with piezometers with an 8.00-ft (2.44-m) axial spacing in both legs. Since measurements are made in vertical sections of pipe, all of the solid particles are suspended with the result that concentration is delivered concentration or transport concentration. The accuracy of the instrument has been checked with the flow of water, by means of the Marcy meter with the flow of nonsettling slurries and by a total diversion sampler. Based upon the basic theory and the numerous confirmations, the values of slurry specific gravity, s_m, listed in the sixth column of Table 1 are believed to be accurate to the listed significant figures.

Analysis

The concept of a pseudofluid is employed in the following. As applied to a water-sand slurry, the fluid density, ρ_m, is the mixture density based upon the delivered concentration and the fluid viscosity, μ, is that of the fluid carrier, water.

The flow characteristic of greatest interest to engineers is resistance to flow. For flow of a fluid (or pseudofluid), resistance to flow is described by the Darcy-Weisbach boundary drag coefficient, f. For the flow of Newtonian fluids in a pipe, the value of f is found to be a function of the Reynolds number, R, and the relative roughness, ϵ/D, as expressed in the Colebrook function

$$\frac{1}{\sqrt{f_w}} = 1.14 - 2\log\left(\frac{\epsilon}{D} + \frac{9.35}{R\sqrt{f_w}}\right) \quad \ldots\ldots\ldots\ldots\ldots\ldots\ldots\ldots\ldots\ldots (1)$$

in which w signifies "theoretical." The value of f_m is determined from experimentally-determined values of the friction-pressure gradient, i_m, and the Darcy-Weisbach equation, as follows

$$f_m = \frac{2\left(\frac{\Delta p_m}{L}\right)D}{\rho_m V^2} \quad \ldots\ldots\ldots\ldots\ldots\ldots\ldots\ldots\ldots\ldots\ldots\ldots\ldots\ldots (2)$$

in which D = pipe diameter; $\Delta p_m/L$ = pressure gradient in a horizontal pipe; V = mean velocity; and ρ_m = density of the mixture.

The friction-pressure gradient is given in Table 1 in terms of i_m, which has the units of foot of water per foot of pipe or meter of water per meter of pipe. Conversions are as follows

$$\frac{\Delta p_m}{L} = 62.4\, i_m \quad \ldots\ldots\ldots\ldots\ldots\ldots\ldots\ldots\ldots\ldots\ldots\ldots\ldots\ldots (3a)$$

for a pressure gradient having the units of pounds per square foot per foot and

$$\frac{\Delta p_m}{L} = 9802\, i_m \quad \ldots\ldots\ldots\ldots\ldots\ldots\ldots\ldots\ldots\ldots\ldots\ldots\ldots\ldots (3b)$$

for a pressure gradient having the units of pascals per meter.

At the GIW Hydraulic Laboratory, characteristics of the flow of settling slurries are compared to the flow characteristics of water through the 50.0-ft (15.24-m) long, 7.98-in. (203-mm) diam test section. The water test, Test 102-79, was performed two days after the slurry test, Test 97-79. The value of the relative roughness, ϵ/D, of the test section is evaluated from the water test by finding the value of ϵ/D to obtain close agreement between the value of f determined from experimental measurements (see Col. 5 of Table 3), and the value of f calculated from the Colebrook function (see Col. 8 of Table 3). By this procedure, the value $\epsilon/D = 6(10^{-5})$, was found to represent the relative roughness of the steel pipe in the test section at the time of Tests 102-79 and 97-79.

In Test 97-79 enough foundry sand was placed in the slurry loop to produce a slurry specific gravity, $s_m = 1.06$, during Runs 11–15, (see Table 1), when all of the sand was carried as suspended load and none as bed load. With lesser values of Q and V, more of the sand was transported as slower-moving

TABLE 3.—Boundary Drag Coefficients

Run (1)	Temperature, in degrees Fahrenheit (2)	V, in foot per second (CH 3) (3)	f_m (CH 13) (4)	ϵ/D (5)	$R \times 10^{-5}$ (6)	f_w (7)
			(*a*) Test 102-79			
1	84.2	1.79	0.0147	$6(10^{-5})$	1.4	0.0172
2	84.1	3.09	0.0152	$6(10^{-5})$	2.4	0.0157
3	84.1	4.59	0.0147	$6(10^{-5})$	3.5	0.0147
4	84.1	5.62	0.0144	$6(10^{-5})$	4.3	0.0143
5	84.3	6.67	0.0144	$6(10^{-5})$	5.1	0.0139
6	84.3	7.82	0.0144	$6(10^{-5})$	6.0	0.0136
7	84.6	9.95	0.0132	$6(10^{-5})$	7.6	0.0132
8	84.6	11.42	0.0130	$6(10^{-5})$	8.8	0.0130
9	84.9	12.77	0.0128	$6(10^{-5})$	9.8	0.0128
10	85.5	14.35	0.0126	$6(10^{-5})$	11.0	0.0127
11	85.6	15.93	0.0124	$6(10^{-5})$	12.3	0.0125
12	85.9	17.41	0.0123	$6(10^{-5})$	13.5	0.0124
13	86.2	18.92	0.0122	$6(10^{-5})$	14.7	0.0123
14	86.7	20.35	0.0121	$6(10^{-5})$	15.9	0.0123
15	86.9	21.85	0.0119	$6(10^{-5})$	17.1	0.0122
			(*b*) Test 97-79			
1	83.8	2.80	0.0228	$6(10^{-5})$	2.1	0.0160
2	84.0	4.05	0.0216	$6(10^{-5})$	3.1	0.0150
3	85.2	5.41	0.0175	$6(10^{-5})$	4.2	0.0143
4	85.6	6.41	0.0204	$6(10^{-5})$	5.0	0.0140
5	86.1	8.03	0.0174	$6(10^{-5})$	6.3	0.0136
6	86.9	9.07	0.0153	$6(10^{-5})$	7.1	0.0133
7	87.3	10.25	0.0143	$6(10^{-5})$	8.1	0.0131
8	88.2	11.47	0.0132	$6(10^{-5})$	9.2	0.0129
9	88.9	13.22	0.0118	$6(10^{-5})$	10.6	0.0127
10	89.5	14.09	0.0118	$6(10^{-5})$	11.4	0.0126
11	90.0	15.83	0.0115	$6(10^{-5})$	12.9	0.0125
12	90.0	17.61	0.0108	$6(10^{-5})$	14.3	0.0124
13	90.1	18.46	0.0110	$6(10^{-5})$	15.0	0.0123
14	91.7	19.73	0.0109	$6(10^{-5})$	16.3	0.0122
15	92.3	22.26	0.0109	$6(10^{-5})$	18.6	0.0121

Note: 1 fps = 0.305 m/s; Col. 5 is from Eq. 2; Col. 8 is from Eq. 1.

bed load, as evidenced by the lower values of s_m. During Runs 1 and 2 (see Table 1), the value of $s_m = 1.0$ means that no sand was being transported either as bed load or suspended load, i.e., all of the sand was deposited in a stationary bed throughout the system. Thus, Test 97-79 encompassed the

range of flow regimes, i.e., stationary bed, heterogeneous suspension, and homogeneous suspension. Inasmuch as the volume concentration of the sand was small, i.e., 4%, calculation of the boundary drag coefficient, f_m, from Eq. 2, using the total cross-sectional area, A, of the pipe for calculating velocity, V, is reasonable regardless of the flow regime prevailing during any run of Test 97-79. Values of f_m calculated from experimental measurements are listed in Col. 5 of Table 3.

In order to display the effects of the sand upon the flow as compared to flow of a Newtonian fluid, values of $f_m - f_w = \phi(V)$ are plotted in Fig. 1. In the writers' opinion, the results of Test 102-79 shown in Fig. 1 are indicative of the veracity of the Colebrook function, (see Eq. 1), and of the experiment in that, except for Runs 1 and 6, experimentally-determined values, f_m, are within two significant-figure agreement with the Colebrook values of f in Eq.

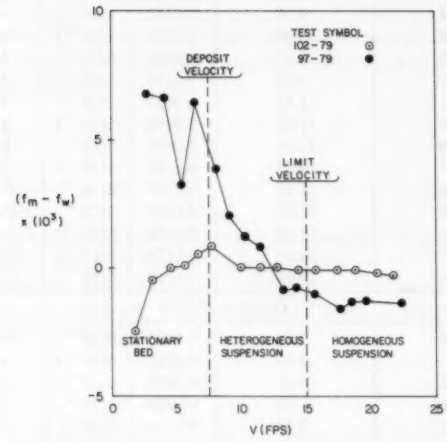

FIG. 1.—$f_m - f_w = \phi(V)$

1. The experimentally-determined results of Test 97-79 are shown as solid circles in Fig. 1. The three flow regimes are labeled in the lower portion of Fig. 1 with the regimes being delineated by the *deposit velocity* and the *limit velocity*.

The deposit velocity of 8.5 fps (2.6 m/s) was established by observing the beginning of a stationary bed in the glass section of the pipe located downstream from the resistance test section.

The limit velocity of 15 fps (4.6 m/s) was established from the values of the slurry specific gravity, s_m, listed in Table 1. During Runs 11–15, Test 97-79, $s_m = 1.06$. The constant value of s_m when $V > 15$ fps (4.6 m/s) is indicative that almost all of the sand was carried as suspended load with a negligible portion or none being carried as slower-moving bed load.

The anomalous point, Run 3 of Test 97-79 in the stationary-bed regime, probably results from dunes migrating slowly past the piezometers in the test section.

ACKNOWLEDGMENTS

Thomas W. Hagler, Jr., President of GIW, encourages the staff of the Hydraulic Laboratory to pursue and to report in-house noncommercial studies like the one reported herein. John Maffett was the test engineer during Tests 102-79 and 97-79.

NEW DESIGN EQUATIONS FOR SCOUR AROUND BRIDGE PIERS

By Christopher James Baker[1]

INTRODUCTION

Breusers, et al. (2), after an extensive study of the experimental data of scour depth around bridge piers in sand beds, arrived at the following design formula

$$\frac{d_s}{b} = \left[2 \tanh\left(\frac{d_o}{b}\right)\right]\left[f_1\left(\frac{\bar{U}}{\bar{U}_c}\right)\right][f_2 f_3] \quad \ldots\ldots\ldots\ldots\ldots\ldots (1)$$

in which d_s = the maximum scour depth measured from the mean bed surface; b = the pier diameter; d_o = the water depth; $\bar{U}$ = the channel mean velocity; $\bar{U}_c$ = the value of $\bar{U}$ at which general sediment motion begins; and

$$f_1 = 0, \quad \text{for} \quad 0.0 < \frac{\bar{U}}{\bar{U}_c} < 0.5; \quad f_1 = 2\left(\frac{\bar{U}}{\bar{U}_c}\right) - 1,$$

$$\text{for} \quad 0.5 < \frac{\bar{U}}{\bar{U}_c} < 1.0, \quad \text{(clear water scour)}; \quad f_1 = 1.0,$$

$$\text{for} \quad 1.0 < \frac{\bar{U}}{\bar{U}_c} \quad \text{(scour with continuous sediment motion)} \quad \ldots\ldots\ldots\ldots (2)$$

Functions f_2 and f_3 = functions of the pier shape, incidence to the flow, etc., which are described in (2). Fig. 1 shows the scour depths measured by Chabert

[1]Engr., Aerodynamics Section, Railway Technical Centre, British Rail, London Road, Derby, England.

Note.—Discussion open until September 1, 1981. To extend the closing date one month, a written request must be filed with the Manager of Technical and Professional Publications, ASCE. Manuscript was submitted for review for possible publication on July 14, 1980. This paper is part of the Journal of the Hydraulics Division, Proceedings of the American Society of Civil Engineers, ©ASCE, Vol. 107, No. HY4, April, 1981. ISSN 0044-796X/81/0004-xxxx/$01.00.

and Engeldinger (3) around circular piers in a large variety of flow conditions, and compares them with the scour depth predicted by Eqs. 1 and 2. For these tests, $\bar{U}/\bar{U}_c > 1$; $0.67 < d_o/b < 7.0$; $33.3 < d_o/D < 1{,}346$; and $0.28 \times 10^3 < G < 355 \times 10^3$, in which D = the mean sediment diameter; and $G = (\rho_s - \rho)\, gD^3/\rho\nu^2$ where ρ_s = the sediment density; ρ = the water density; and ν = the kinematic viscosity. It can be seen that the predictions are not entirely adequate, d_s/b being grossly overpredicted in some cases. This note suggests possible improvements to Eqs. 1 and 2.

Baker's Formula (1)

After a study of the mechanics of the vortex in the scour hole for $\bar{U}/\bar{U}_c < 1$, Baker (1) arrived at the following formula for scour depth around a cylinder in a bed of sand

$$\frac{d_s}{b} = (a_1 N - a_2) \tanh\left(a_3 \frac{d_o}{b}\right) \quad \ldots\ldots\ldots\ldots\ldots\ldots\ldots\ldots\ldots\ldots (3)$$

in which $N = \bar{U}/[(\rho_s/\rho - 1)gD]^{1/2}$, and a_1, a_2, and a_3 = functions of G

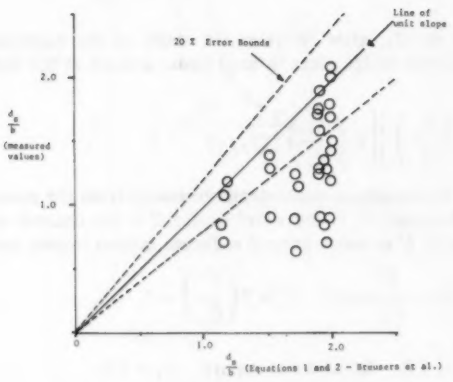

FIG. 1.—Comparison of Experimental Results of Chabert and Engeldinger (3) with Formulas of Breusers, et al. (2) (see Eqs. 1 and 2)

and d_o/D. Eq. 3 can be recast in the form of Eqs. 1 and 2 for $\bar{U}/\bar{U}_c < 1$, by writing

$$a_1 = \frac{a_4}{N_c} \quad \ldots\ldots\ldots\ldots\ldots\ldots\ldots\ldots\ldots\ldots\ldots\ldots\ldots\ldots\ldots\ldots (4)$$

in which N_c = the value of N at which general sediment motion begins (and is easily shown to be a function of d_o/D and G); and a_4 = another function of G and d_o/D. Eq. 3 then becomes

$$\frac{d_s}{b} = \left[a_4\left(\frac{N}{N_c}\right) - a_2\right] \tanh\left(a_3 \frac{d_o}{b}\right) \quad \ldots\ldots\ldots\ldots\ldots\ldots\ldots\ldots (5)$$

The ratio (N/N_c) is of course equal to $(\bar{U}/\bar{U}_c)$ used in Eqs. 1 and 2.

Improved Design Formula

The form of Eq. 5 suggests that Eqs. 1 and 2 might be made to agree more closely with experimental results if they are written

$$\frac{d_s}{b} = \left[g_1\left(\frac{\bar{U}}{\bar{U}_c}\right)\right]\left[k_1 \tanh\left(k_2 \frac{d_o}{b}\right)\right][g_2 g_3] \quad \ldots\ldots\ldots\ldots\ldots\ldots\ldots\ldots (6)$$

in which k_1 and k_2 = functions of G and d_o/b; g_1 = a function of $(\bar{U}/\bar{U}_c)$

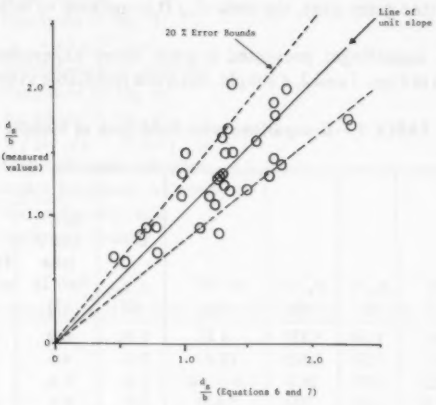

FIG. 2.—Comparison of Experimental Results of Chabert and Engeldinger (3) with Modified Formulas (Eqs. 6 and 7)

or (N/N_c); and g_2 and g_3 = functions of shape and incidence to the flow. A "best fit" analysis of the experimental results of Chabert and Engeldinger (3) suggests the following relationships

$$k_1 = 1.625\left[3.55 - \log\left(\frac{G}{10^3}\right)\right]\left[\frac{50}{\left(\frac{d_o}{D}\right)} + 0.35\right] \quad \text{for} \quad G < 355 \times 10^3;$$

$$k_1 = 1.625\left[\frac{50}{\left(\frac{d_o}{D}\right)} + 0.35\right] \quad \text{for} \quad G > 355 \times 10^3;$$

$$k_2 = 0.26 \log\left(\frac{G}{10^3}\right) + 0.32 \quad \text{for} \quad G < 355 \times 10^3;$$

$$k_2 = 1.0 \quad \text{for} \quad G > 355 \times 10^3 \ldots\ldots\ldots\ldots\ldots\ldots\ldots\ldots\ldots\ldots\ldots\ldots (7)$$

Variables g_1, g_2, and g_3 can be adequately taken to be equal to f_1, f_2, and f_3. The scour depths predicted by Eqs. 6 and 7 for the experimental conditions of Chabert and Engeldinger (3) already described, are compared with experimental results of Fig. 2. It can be seen that nearly all experimental results lie within 20% of the predicted values.

Now let us consider the physical meaning of Eq. 7. It can be seen that at high values of G, k, and k_2 (and thus, the scour depth) do not depend on G. This is to be expected, since G is a function of viscosity and thus, indirectly, of grain-size Reynolds number. At high values of the Reynolds number (and thus, of G), viscous effects become unimportant. Similarly, at high values of d_o/D, the scour depth can be seen to be little influenced by variations in d_o/D. This is again to be expected, because when d_o (the water depth) is very much greater than D (the grain size), the ratio d_o/D is unlikely to influence the scour depth.

Chabert and Engeldinger presented a great many experimental results. To avoid confusion in Figs. 1 and 2, a simple, but quite justifiable averaging procedure

TABLE 1.—Comparison with Field Data of Melville

Bridge (1)	N (2)	d_o/b (3)	d_o/D (4)	$G/10^3$ (5)	$f_2 f_3$ (6)	d_s, in meters: Eqs. 1 and 2 (see Ref. 2) (7)	d_s, in meters: Eqs. 6 and 7 (8)	d_s, in meters: Observed (9)
Tuakau	8.7	1.24	3,833	5.82	1.69	6.9	3.6	2.8
Waitangi	3.2	3.59	3,500	13.4	2.5	4.5	3.4	3.8
Wanganui	2.2	2.33	16.5	1.9×10^8	1.0	1.4	4.0	4.9
Matawhero	7.4	2.02	431	5,620	2.4	6.9	2.7	4.0

has been adopted. Many investigators have realized that for $\bar{U} > \bar{U}_c$ (or $N > N_c$), the scour depth does not depend on $\bar{U}$ or N. This is reflected in Eq. 1. Thus, for the results of Chabert and Engeldinger, an average has been taken of the experimental measurements of scour depth for fixed values of d_o/b, d_o/D, and G, in which $\bar{U} > U_c$. This enabled a considerable reduction in the number of data points displayed in Figs. 1 and 2.

It would thus seem that Eqs. 6 and 7 predict the scour depth more accurately than Eqs. 1 and 2. This is to some extent confirmed in Table 1 where the predictions of these formulas are compared with the field data of Melville (4). It can be seen that the improved design formulas predict the measured depth of scour rather better than the original formulas for a wide range of flow conditions.

APPENDIX I.—REFERENCES

1. Baker, C. J., Theoretical Approach to the Prediction of Scour Around Bridge Piers," *Journal of Hydraulics Research*, Vol. 18, No. 1, 1980, pp. 1–12.
2. Breusers, H. N. C., Nicollet, G., and Shen, H. W., "Local Scour Around Cylindrical

Piers," *Journal of Hydraulics Research*, Vol. 15, No. 3, 1977, pp. 211–252.
3. Chabert, J., and Engeldinger, P., "Etude des Affouillements Autour des Piles de Ponts," Laboratoire Nationale d'Hydrolique, Chatou, France, 1956.
4. Melville, B. W., "Local Scour at Bridge Sites," *Report Number 117*, University of Auckland, School of Engineering, Auckland, New Zealand, 1975.

Appendix II.—Notation

The following symbols are used in this paper:

a_1, a_2, a_3 = function in Eq. 3;
b = pier diameter;
D = sediment size;
d_o = water depth;
d_s = scour depth;
f_1, f_2, f_3 = functions in Eq. 1;
G = $(\rho_s - \rho)\, gD^3/\rho\nu^2$;
g = acceleration of gravity;
g_1, g_2, g_3 = functions in Eq. 6;
k_1, k_2 = functions in Eq. 6;
N = $\bar{U}/[(\rho_s/\rho - 1)\, gD]^{1/2}$;
$\bar{U}$ = mean channel velocity;
ν = water kinematic viscosity;
ρ = water density; and
ρ_s = sediment density.

Subscript

c = conditions at start of general sediment motion.

JOURNAL OF THE
HYDRAULICS DIVISION

DISCUSSION

Note.—This paper is part of the Journal of the Hydraulics Division, Proceedings of the American Society of Civil Engineers, ©ASCE, Vol. 107, No. HY4, April, 1981. ISSN 0044-796X/81/0004-0515/$01.00.

Discussions

Discussions may be submitted on any Proceedings paper or technical note published in any *Journal* or on any paper presented at any Specialty Conference or other meeting, the *Proceedings* of which have been published by ASCE. Discussion of a paper/technical note is open to anyone who has significant comments or questions regarding the content of the paper/technical note. Discussions are accepted for a period of 4 months following the date of publication of a paper/technical note and they should be sent to the Manager of Technical and Professional Publications, ASCE, 345 East 47th Street, New York, N.Y. 10017. The discussion period may be extended by a written request from a discusser.

The original and three copies of the Discussion should be submitted on 8-1/2-in. (220-mm) by 11-in. (280-mm) white bond paper, typed double-spaced with wide margins. The length of a Discussion is restricted to two *Journal* pages (about four typewritten double-spaced pages of manuscript including figures and tables); the editors will delete matter extraneous to the subject under discussion. If a Discussion is over two pages long it will be returned for shortening. All Discussions will be reviewed by the editors and the Division's or Council's Publications Committees. In some cases, Discussions will be returned to discussers for rewriting, or they may be encouraged to submit a paper or technical note rather than a Discussion.

Standards for Discussions are the same as those for Proceedings Papers. A Discussion is subject to rejection if it contains matter readily found elsewhere, advocates special interests, is carelessly prepared, controverts established fact, is purely speculative, introduces personalities, or is foreign to the purposes of the Society. All Discussions should be written in the third person, and the discusser should use the term "the writer" when referring to himself. The author of the original paper/technical note is referred to as "the author."

Discussions have a specific format. The title of the original paper/technical note appears at the top of the first page with a superscript that corresponds to a footnote indicating the month, year, author(s), and number of the original paper/technical note. The discusser's full name should be indicated below the title (see Discussions herein as an example) together with his ASCE membership grade (if applicable).

The discusser's title, company affiliation, and business address should appear on the first page of the manuscript, along with the *Proceedings* paper number of the original paper/technical note, the date and name of the *Journal* in which it appeared, and the original author's name.

Note that the discusser's identification footnote should follow consecutively from the original paper/technical note. If the paper/technical note under discussion contained footnote numbers 1 and 2, the first Discussion would begin with footnote 3, and subsequent Discussions would continue in sequence.

Figures supplied by the discusser should be designated by letters, starting with A. This also applies separately to tables and references. In referring to a figure, table, or reference that appeared in the original paper/technical note use the same number used in the original.

It is suggested that potential discussers request a copy of the *ASCE Authors' Guide to the Publications of ASCE* for more detailed information on preparation and submission of manuscripts.

Estimation of Direct Runoff from Urban Watersheds[a]

Errata

The following correction should be made to the discussion by Diskin (August, 1980):

Page 1404, Eq. 19: Should read $Y_n = AH_n + BH_{n-m} + A^2G_{n,n} + B^2G_{n-m,n-m} + 2ABG_{n,n-m}$ instead of $Y_n = AH_n + BH_{n-m} + A^2G_{n,n} + B^2G_{n-m,n-m} + ABG_{n,n-m}$

Estimating Average Velocity in Gravel-Bed Rivers[b]

Closure by Dale I. Bray,[7] A. M. ASCE

The writer appreciates the fact that the tabulated Alberta gravel-bed river data have been used by the discussers, Blaisdell, Thomas, and Agarwal, et al. to test results obtained from laboratory studies and field observations.

Both Blaisdell and Thomas apply the Alberta gravel-bed river data to evaluate the state of activity of the channel bed based on an initiation of motion criterion. Blaisdell adopts the Anderson, et al. (20) approach which is essentially the Shields approach with the critical mobility number taken to be about 0.044. Thomas adopts a value of the critical Shields mobility number of 0.060. Neill (27) has suggested that a value of 0.030 be adopted for the design of stable gravel-bed channels. It is apparent that there is no universal acceptance of the value of the critical mobility number for gravelbed channels.

The writer has adopted the Neill (27) criterion for estimating if the bed of a gravel-bed channel was in motion at a condition characterized by the 2-yr flood flow. The Neill criterion is based on critical average velocity rather than critical boundary shear stress as in the Shields criterion. The Neill criterion is strictly applicable for relatively uniform gravel-sized materials for two-dimensional uniform flow and is stated as:

---

[a]February, 1978, by Aolad Hossain, A. Ramachandra Rao, and Jacques W. Delleur (Proc. Paper 13565).

[b]September, 1979, by Dale I. Bray (Proc. Paper 14810).

[7]Prof. of Civ. Engrg., Dept. of Civ. Engrg, Univ. of New Brunswick, P.O. Box 4400, Fredericton, N.B., Canada E3B 5A3.

$$\frac{\rho V_c^2}{\gamma' D_{50}} = 2.0\left(\frac{d}{D_{50}}\right)^{1/3} \quad \ldots\ldots\ldots\ldots\ldots\ldots\ldots\ldots\ldots\ldots\ldots\ldots (46)$$

in which V_c = the critical average velocity for initiation of motion of the gravel bed. When the Neill criterion was applied to the Alberta data, 16% of the gravel-bed river reaches show indicated movement; whereas, 27% show indicated movement by the Anderson, et al. criterion as tested by Blaisdell.

The difficulty with most of the initiation of motion criteria is that they are generally derived from two-dimensional flow in a straight laboratory channel. The plan form of a natural river is not straight and the cross-sectional shape varies along the study reach; therefore, the direct applicability of any initiation of motion criterion to a natural gravel-bed channel is an estimate at best.

Blaisdell asked about the effect of using data from river reaches for which it has been estimated that the bed material is in motion for relatively high in-bank flows. The writer recognizes that in a few cases, the bed material transport may be appreciable at the 2-yr flood flow. Bray (2) reported that hydrophone data obtained at a few of the river reaches indicated movement of material over a portion or all of the river bed at flows near the 2-yr flood flow. However, the data do not indicate if the bed was in motion or if there was transport of fine material over the armor layer of the gravel bed. The writer considers that, for the generalized analysis, the effects of bed material transport do not significantly influence the results presented in the original paper. On the other hand, the writer recommends that the original equations not be applied to gravel-bed river reaches for conditions which result in known major bed material transport. In summary, if the channels were straight rectangular channels of constant bottom slope, a more definitive answer could be given to the questions raised by Blaisdell.

Thomas asks if the gravel and boulders are exposed at all stages of the flow for the study reaches. As far as the writer knows, none of the river reaches experience a major modification due to a large injection of fines as reported by Simons, et al. (22).

Thomas discusses the variation of Manning's n with stage. The writer stages that the average velocity equations in the paper are for relatively high in-bank flows. The basic Alberta gravel-bed river data (12) do confirm that n is typically higher for low flows. The writer considers that average velocity equations for relatively low flows for gravel-bed rivers are difficult to develop due to the problem of defining average reach properties and due to the fact that the flow sometimes becomes highly three-dimensional for low flows as a result of the jet and wake type of flow. The writer recommends that the original equations not be used if d/D_{90} is less than 3.

Agarwal, et al. state that Lacey's regime type equation for average velocity (Eq. 9) is not expected to apply to gravel-bed channels. The writer would like to point out that Lacey did incorporate some data from gravel-bed and boulder-bed river reaches in the analysis from which Eq. 9 was developed. These data are shown in Fig. 1 of the 1946 paper by Lacey (15). Thus, it does seem reasonable to expect that the Lacey equation (Eq. 9) should apply to gravel-bed river reaches for the case of relatively high in-bank flows.

Agarwal, et al. apply the Alberta gravel-bed river data to test the dimensionless flow relation (Eq. 45) developed by Garde and Ranga Raju (24,25). Since K_1

and K_2 in the relationship presented in Fig. 6 are constant in the gravel range; γ_s, γ, and ρ are essentially constant; and the slope of the line in Fig. 6 is equal to 1/2, then the Ranga Raju relationship presented in Fig. 6 can be rewritten in the more common form as:

$$\frac{1}{\sqrt{f}} = c\left(\frac{d}{D_{50}}\right)^{1/6} \quad \ldots \ldots \ldots

or not they are induced by molecular or turbulent processes. The writer did emphasize lateral turbulent diffusion as opposed to molecular diffusion, for obvious reasons in the context of gravel streams. However, lateral molecular diffusion can be invoked in the laminar case to explain the distribution of Fig. 4.

The second point raised by Thorne, Alonso, and Bathurst is a most important one. It concerns the difficult problem of straight-channel secondary currents. These currents are indeed much weaker than the primary flow. However, the main motivation for neglecting them was the lack of a satisfactory way to include them; the analysis can hardly be said to be complete until this is done. The discussers are correct in emphasizing them.

Recently Ikeda (34) has conducted an experimental study of self-formed, mobile-bed, straight channels in nonsuspendable material, which casts some light on the problem. In certain experiments parallel bed ridges occurred, providing evidence of paired cellular vortices. Measurements of downstream mean flow velocity distributions revealed that the isovels oscillated in the lateral in a manner consistent with the upwelling of slow water and downwelling of fast water that would be produced by such cells. Ikeda's data, however, provide strong support for Eqs. 21, 22, and 26, even though these equations are based on

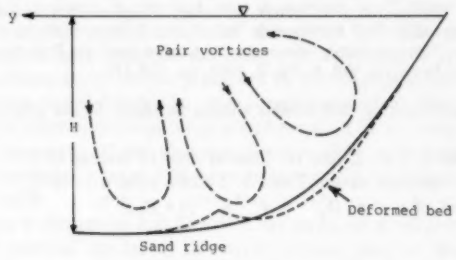

FIG. 10.—Schematic View of Inferred Secondary Vortices and Bank Geometry (Courtesy of S. Ikeda)

an analysis that neglects secondary current. He concludes that the cellular nature of the secondary currents causes their effect to be rather local so that they do not affect significantly the gross balance that maintains stable banks and a mobile bed.

An indication of the secondary flow structure near the bank, and its effect on the toe of the bank, is given in Fig. 10, courtesy of Ikeda. Some steepening of the toe of the bank is apparent.

Kondap and Garde have provided a set of dimensionless hydraulic relations for sand-bed streams that are in the same format as Eqs. 29*a*, 29*b*, and 29*c*, and possess some interesting similarities. A comparison of the width relations of the two sets reveals an oft-noted but remarkable feature. Consider a gravel stream with a rather typical pavement D_{50} of 40 mm and a sand-bed stream with a rather typical D_{50} of 0.35 mm; let B_G and B_S be their respective widths. Eqs. 29*c* and 37 yield

$$\frac{B_S}{B_G} = 0.747\, Q^{0.048} \quad \ldots \ldots \ldots

in which the widths are in meters; and Q is in cubic meters per second. For the range $50\,m^3/s < Q < 500/m^3/s$, B_S/B_G varies from 0.90–1.01. The implication is that sand-bed streams, the mechanics of which differ considerably from gravel-bed streams, nevertheless maintain widths comparable to their gravel counterparts when dominant discharges are also comparable. A mechanistically well-founded explanation of this would be invaluable to the river engineer.

Appendix.—Reference

34. Ikeda, S., "Self-Formed Straight Channels in Non-Cohesive Bed Materials. Part I. Experiments," *Technical Report*, Saitama University, Urawa, Japan, 1980.

Approximate Flood Routing Methods: A Review[a]

Errata

The following corrections should be made to the discussion by Kundzewicz (December, 1980):

Page 2073, paragraph 2, line 2: Should read "to prove that the heuristic condition (Eq. 19) is not generally true." instead of "to prove, that the heuristic condition (25) is not generally true."
Page 2073, paragraph 3, line 6: Should read "the constraint (Eq. 19) is fulfilled." instead of "the constraint (25) is fulfilled."

Log Pearson Type 3 Distribution: A Generalized Evaluation[b]

Discussion by M. Riazul Hasan,[2] M. ASCE

The clear definition and delineation of different forms of Log Pearson type 3 (LP) distribution in Fig. 1 by the author would be welcome by many practicing engineers and hydrologists together with the new methodology he proposes. The writer applied the author's methodology to the ALE data of some six rivers in Africa, Asia and United Kingdom to which he had previously applied

[a]December, 1979, by P. Erwin Weinmann and Eric M. Laurenson (Proc. Paper 15057).
[b]May, 1980, by Donthamsetti Veerabhadra Rao (Proc. Paper 15391).
[2]Sr. Engr.-Hydro., Sir William Halcrow & Partners, Consulting Engrs., Burderop Park, Swindon, Wiltshire SN4 0QD, England.

the United States Water Resources Council (WRC) methodology (2,5) and observed very good agreement between the two results. As an example of this comparative study, the flood magnitudes and return periods for an Ethiopian river with 13 yr of ALE data are given in Table 6. Although both the author's and the WRCs methodologies estimate the parameters of LP by the method of moments, the former, which fits real data to LP, looks much simpler to the writer than the latter, which fits logarithmic data to P (Pearson type 3 distribution). Also, by converting the data into dimensionless variables by $K_i = X_i/\bar{X}$ (p. 869), the author's methodology reduces one of the three LP parameters to unity.

TABLE 6.—Flood Magnitudes and Return Periods for Ethiopian River with 13 yr of ALE Data

Return period, in years (1)	Flood Flow, in cubic meters per second	
	WRC[a] (2)	Author (3)
2	514.3	512.3
5	598.3	588.1
10	661.3	649.7
25	749.0	738.2
50	820.0	812.1
100	895.6	892.3
200	976.5	980.3
500	1,092.7	1,108.8
1,000	1,188.5	1,216.4

[a]From Ref. 5.

Benson (6), who was Chairman of the Work Group on Flow-Frequency Methods, describes how the choice of LP as a "uniform flood-frequency estimating technique" was made after a critical comparison of six methods:

> No single method of testing the computed results against the original data was acceptable to all those on the Work Group, and the Statistical Consultants could not offer a mathematically rigorous method. It appeared, consequently, that if a choice could not be made solely on statistical grounds, a choice on administrative grounds, for which compelling reasons existed, was justified.

It was made clear by the Work Group that the choice of LP was not "final" and "continuing study of flood-frequency analysis and improvement or revisions of methods" was recommended (6). As a result of this, the original guidelines (5) have undergone two revisions in 1976 (2) and 1977 (10). It is surprising that neither Bobee's (1,8) important work with respect to the mathematical properties of LP nor the investigation by Matalas, et al. (12) of the usefulness of the coefficient of skewness on a regional basis have been incorporated in these revisions. Other significant contributions similar to the author's have also been made since the last revision of the WRC guidelines (7,9,11). All this work,

the writer believes, calls for a further review and updating of the WRC guidelines at an early date.

Lastly, in a subsequent paper on the same topic (13), the author presents the method of mixed moments (MXM1). The writer would like to know how this method compares with the computationally more difficult maximum likelihood approach to LP.

Appendix.—References

5. "A Uniform Technique for Determining Flood Flow Frequencies," *Bulletin No. 15*, Water Resources Council, Washington, D.C., Dec., 1967.
6. Benson, M. A., "Uniform Flood-Frequency Estimating Methods for Federal Agencies," *Water Resources Research*, Vol. 4, No. 5, Oct., 1968, pp. 891–908.
7. Bobee, B. B., "Comment on 'The Log Pearson Type 3 Distribution: The T-Year Event and Its Asymptotic Standard Error by Maximum Likelihood Theory,'" *Water Resources Research*, Vol. 15, No. 1, Feb., 1979, pp. 189–190.
8. Bobee, B. B., and Robitaille R., "The Use of the Pearson Type 3 and Log Pearson Type 3 Distributions Revisited," *Water Resources Research*, Vol. 13, No. 2, Apr., 1977, pp. 427–443.
9. Condie, R., "The Log Pearson Type 3 Distribution: The T-Year Event and Its Asymptotic Standard Error by Maximum Likelihood Theory," *Water Resources Research*, Vol. 13, No. 6, Dec., 1977, pp. 987–991.
10. "Guidelines for Determining Flood Flow Frequency," *Bulletin No. 17A*, Water Resources Council, Washington, D.C., June, 1977.
11. Kite, G. W., "Summary and Conclusions," *Frequency and Risk Analysis in Hydrology*, Water Resources Publications, Fort Collins, Colo., 1977, Chap. 15., pp. 214–224.
12. Matalas, N. C., Slack, H. R., and Wallis, J. R., "Regional Skew in Search of a Parent," *Water Resources Research*, Vol. 11, No. 6, Dec., 1976, pp. 815–826.
13. Rao, D. V., "Log Pearson Type 3 Distribution: Method of Mixed Moments," *Journal of the Hydraulics Division*, ASCE, Vol. 106, No. HY6, Proc. Paper 15477, June, 1980, pp. 999–1019.

Heat Loss From Sidearms of Cooling Lakes[a]

Discussion by Subhash C. Jain,[3] M. ASCE, and Nevzat Yildirim[4]

It appears to the writers that the shape of the assumed temperature profile in the authors' numerical experiments was guided by the measured temperature profiles in their laboratory experiments. Though the assumed profile may be a good approximation for a very short sidearm, as it was the case in their laboratory experiments, it is not valid for a long sidearm, particularly in the outflow (bottom) layer where the temperature is assumed constant and equal to the temperature along the bottom. According to the assumed temperature profile, the temperature of the water sinking from the inflow layer to the outflow layer is independent of x and is equal to T_o which is not correct as it is discussed in the following sections.

---

[a]May, 1980, by Terry W. Sturm and John F. Kennedy (Proc. Paper 15398).

[3]Research Engr., Inst. of Hydr. Research, Univ. of Iowa, Iowa City, Iowa 52242.
[4]Grad. Student, Civ. and Environmental Engrg., Univ. of Iowa, Iowa City, Iowa 52242.

In the authors' numerical results it is shown that the velocity and temperature approximately decrease linearly and parabolically, respectively. Based on dimensional reasoning the senior writer predicted the same variations for the velocity and temperature (11). According to his analysis the velocity and the temperature distributions in a long sidearm are given by

$$T - T_e = \frac{A_2^3 k^2}{\alpha g D^3}(L_e - x)^2 \theta(\eta) \quad \ldots \quad (56)$$

and $$u = A_1 A_2 \frac{k}{D}(L_e - x) f'(\eta) \quad \ldots \quad (57)$$

in which A_1 and A_2 = constants; $k = K/\rho_o c_p$; K = surface heat loss coefficient; f = normalized similarity function; prime denotes the differentiation with respect to η; α = coefficient of thermal expansion of water, $\theta = (T - T_o)/(T_s - T_o)$.

Substitution for u from Eq. 57 into Eq. 6 and integration yields

$$v = A_1 A_2 k f(\eta) \quad \ldots \quad (58)$$

The equations of motion (Eqs. 3, 4, and 5) can now be written in terms of the similarity functions θ and f. Eliminating the pressure term from Eqs. 3 and 4 by cross-differentiation, and substituting u and v from Eqs. 57 and 58, it is found that

$$-f'f'' + ff''' = \frac{1}{A_1 A_2 kD}(k_m f'')'' + \frac{2A_2}{A_1^2}\theta \quad \ldots \quad (59)$$

In deriving Eq. 59, the shear stress in Eq. 3 is expressed as $\tau_{xy}/\rho_o = k_m(\partial u/\partial y)$ in which k_m = turbulent momentum diffusivity. The energy equation (5) becomes

$$f\theta' - 2f'\theta = \frac{1}{A_1 A_2 kD}(E_y \theta')' \quad \ldots \quad (60)$$

Eq. 60 on differentiation with respect to η yields

$$f\theta'' - f'\theta' - 2f''\theta = \frac{1}{A_1 A_2 kD}(E_y \theta')'' \quad \ldots \quad (61)$$

Eqs. 59, 60, and 61 may be written for the special case of $\eta = 0$, the condition at the bottom. At $\eta = 0$, both the x and y velocity components u and v are zero and also the temperature gradient $\partial T/\partial y$ is zero as there is no heat flux through the bottom boundary; Eqs. 59, 60, and 61 become

$$\frac{2A_2}{A_1^2}(\theta)_{\eta=0} + \frac{1}{A_1 A_2 kD}(k_m'' f'' + 2k_m' f''' + k_m f'^v)_{\eta=0} = 0 \quad \ldots \quad (62)$$

$$(\theta'')_{\eta=0} = 0 \quad \ldots \quad (63)$$

$$-2(f''\theta)_{\eta=0} = \frac{1}{A_1 A_2 kD}(E_y \theta''')_{\eta=0} \quad \ldots \quad (64)$$

On eliminating $(\theta)_{\eta=0}$ between Eqs. 62 and 64 and solving for $(f'')_{\eta=0}$, one gets

$$(f'')_{\eta=0} = \frac{A_2 D(E_y \theta''')_{\eta=0}}{A_1^2(k''_m f'' + 2k'_m f''' + k_m f'^{v})_{\eta=0}} \quad \ldots\ldots\ldots\ldots\ldots\ldots (65)$$

One can see from Eq. 65 that $(\theta''')_{\eta=0} \neq 0$ since $(f'')_{\eta=0} \neq 0$, and then from Eq. 64 that $(\theta)_{\eta=0} \neq 0$. One would expect that the temperature would be minimum at the bottom where θ is not zero. Therefore θ cannot be zero anywhere.

APPENDIX.—REFERENCE

11. Jain, S. C., "Density Currents in Sidearms of Cooling Ponds," *Journal of the Hydraulics Division*, ASCE, Vol. 106, No. EY1, Proc. Paper 15320, Apr., 1980, pp. 9–21.

CHARACTERISTICS OF LOW FLOWS[a]

Discussion by Michel North[1]

This paper is a most important attempt to summarize the state of the art and the needs in low flow analysis. As far as frequency analysis is concerned, it clearly emphasizes the urgency of developing alternatives to the *M*-day, *T*-year low flow approach. The method proposed by Weisman (36) is promising. Actually, the practical importance of characterizing low flows by the duration of negative daily flow runs has been recognized for many years by some institutions. In France for instance, the "Laboratoire national d'hydraulique" applies the concept of depth-duration-frequency to daily flow series, the depth corresponding then to the threshold flow (40). This partial duration series approach is more convenient than the annual maximum series approach in this sense that the latter can be applied only at high threshold flows or to very periodic streams, or both, ensuring at least one negative run per observed year. On the other hand, the annual maximum series approach may be more practical for the fitting of a theoretical distribution.

Renewal theory teaches that the survivor function $R(x)$ of a duration, that is its probability to reach an "age" larger than x, is uniquely determined by its age-specific failure rate $\phi(x)$ and has the form:

$$R(x) = \exp\left[-\int_o^x \phi(\alpha)\, d\alpha \right] \quad \ldots\ldots\ldots\ldots\ldots\ldots\ldots\ldots\ldots\ldots (1)$$

---

[a]May, 1980, by the Task Committee on Low-Flow Evaluation and Needs of the Committee on Surface-Water Hydrology of the Hydraulics Division (Proc. Paper 15400).

[1]Research Engr., Hydr. Lab., Dept. of Civ. Engrg., Federal Inst. of Tech., CH-1015 Lausanne, Switzerland.

However, the verification of a variable failure rate, that is of a departure from the exponential distribution, may lead to erroneous conclusions and to the use of physically poorly founded models. Actually, Eq. 1 supposes a homogeneous process, whereas the succession of positive and negative daily flow runs is generally a strongly seasonal phenomenon. In the case of small streams, the seasonal effect is often a sufficient explanation for a departure from the exponential distribution; the writer (41) derived the survivor function applicable

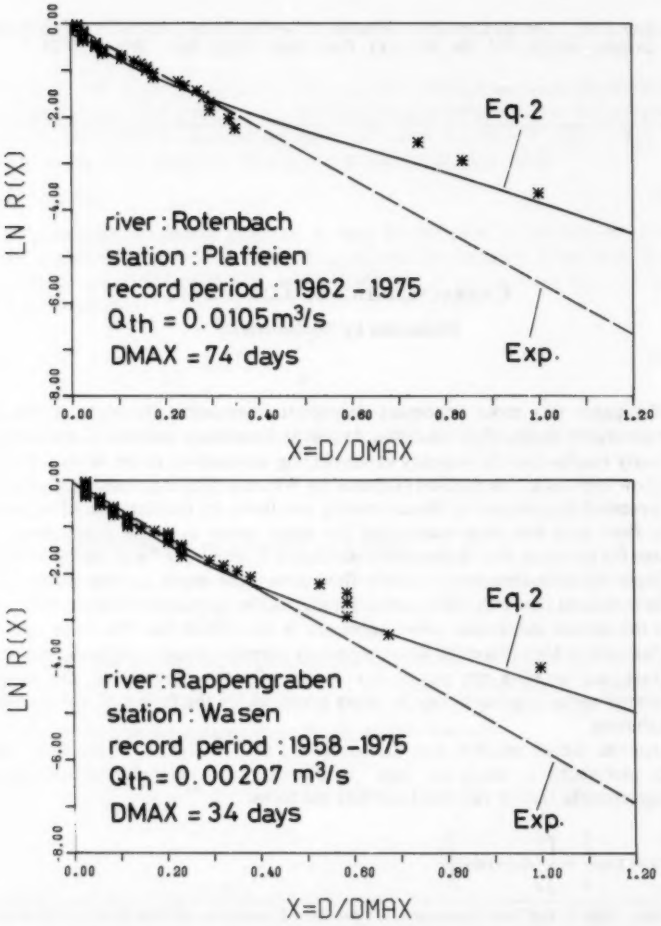

FIG. 4.—Empirical and Theoretical Log Survivor Functions of Negative Runs Duration (*D* = Duration, DMAX = Maximum Duration, *Q*th = Threshold Flow)

to this case:

$$R(x) = \frac{\int_o^P \lambda^*(t) \exp\left[-\int_t^{t+x} \lambda(\alpha)\, d\alpha\right] dt}{\int_o^P \lambda^*(t)\, dt} \quad \ldots\ldots\ldots\ldots\ldots\ldots\ldots\ldots (2)$$

in which $\lambda^*(t)$ = the cyclic occurrence rate of the downcrossings; $\lambda(t)$ = the cyclic failure rate of the negative runs duration; and P = the fundamental period

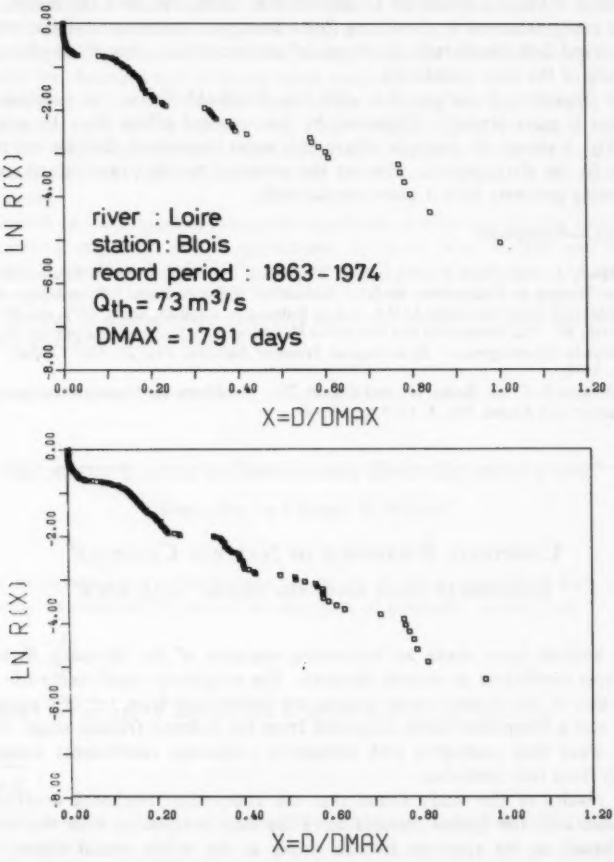

FIG. 5.—Empirical (Left) and Theoretical (Simulated, Right) Log Survivor Functions of Positive Runs Duration

(365 days). Fig. 4 shows two examples of the fit of Eq. 2 to two small streams in Switzerland by the maximum likelihood method.

However, the frequency analysis of the duration of negative runs has also its limitations: as Schröder (42) most pertinently points out, a single negative run of, say, 15 days is then considered as a more severe event than a sequence of, say, 6-days, 9-days, 5-days and 2-day negative runs separated by very short positive runs.

Actually, negative and positive runs should be analyzed simultaneously. The simulation of alternating inhomogeneous renewal processes (41) permits an exhaustive use of the observed sequence of up and downcrossings. For larger streams it is usually necessary to introduce a "memory" into the model. This can be easily achieved by simulating first a homogeneous nonpoissonian renewal process and then transforming it into an inhomogeneous process by an alternating rescaling of the time coordinate.

It is important to notice that with low threshold flows, the positive runs duration is more strongly influenced by the seasonal effect than the negative one. Fig. 5 shows an example where any usual theoretical distribution would fail to fit the data closely, whereas the seasonal model (transformed gamma alternating process) does it quite satisfactorily.

Appendix.—References

40. Miquel, J., and Phien Bou Pha, B., "Evaluation des Ressources en Eau—Définition des Étiages et Estimation de leur Probabilité d'Occurrence," *Proceedings of the Eighteenth Congress of the IAHR*, Vol. 2, Subject A, Cagliari, Sept., 1979, pp. 287–294.
41. North, M., "La Simulation des Processus Hydrologiques Intermittents par des Modèles Alternés Inhomogènes," *Hydrological Sciences Bulletin*, Vol. 25, No. 1, Mar., 1980, pp. 5–12.
42. Schröder, R. C. M., Belke, D., and Brandt, Th., "Probleme der Niedrigwasseranalyse," *Wasser und Boden*, No. 4, 1978, pp. 86–89.

Composite Roughness of Natural Channels[a]

Discussion by James Grant Mac Broom,[3] A. M. ASCE

The authors have made an interesting analysis of the Manning Equation roughness coefficient in natural channels. The roughness coefficients for each subsection of the channel cross section are determined from velocity measurements and a composite value computed from the average friction slope. These values were then compared with composite roughness coefficients computed directly from four formulas.

The results of the study found that the composite roughness coefficients computed with the Lotter formula have the best correlation with the overall value based on the apparent friction slope, as the writer would expect. The

[a]June, 1980, by Asok K. Motayed and Muthusamy Krishamurthy (Proc. Paper 15449).
[3]Asst. Vice Pres., Flaherty Giavara Assocs., P.C., One Columbus Plaza, New Haven, Conn. 06510.

Lotter equation weighs the roughness coefficients of the overall cross section in proportion to the conveyance in each subsection. It is also compatible with the method of computing the total channel conveyance as in the U.S. Army Corp of Engineers HEC-2 computer program.

The Horton equation for estimating the composite roughness coefficient of natural channels would not be expected to match field data because the equation does not represent actual flow conditions. The equation assumes that there are equal flow velocities in all subsection of the channel, which is a condition that seldom occurs in natural rivers with irregular cross sections.

The equation by Einstein and Banks is also a simplified expression that does not mathematically model actual field conditions. It assumes that the hydraulic radius of each subsection is equal to that of the whole cross section. While this assumption is reasonable for very wide channels of uniform depth, it is not valid for channels with irregular cross sections.

It is interesting to note that the slope of the energy grade line (friction slope) varied from one subsection to the next when computed from the gaged velocity data. This may be due either to the computation method, the accuracy of flow measurements, or it may reflect the effect of unknown secondary currents and form losses.

Research on the subject of composite roughness coefficients is very important to practicing engineers and is appreciated by those who analyze and design channels. It would be helpful if the authors would identify the ranges of channel widths, depths, and velocities that were used in their study, as well as determining if the Horton or Einstein equations had improved results on the wider or more uniform channel cross sections.

Boundary Layers in Developing Open Channel Flow[a]

Discussion by Edward H. Wilson[2]

The boundary layer development region in an open channel of high aspect ratio may be analyzed by use of the equation of gradually varied flow

$$\frac{dD}{dx} = \frac{\alpha - j}{1 - F^2} \quad \ldots \ldots \ldots

Whereas in fully developed flow, j would be evaluated from a resistance formula such as that due to Manning, in boundary layer development it is necessary to evaluate the boundary shear, τ_0, in terms of boundary layer thickness.

In the case of a laminar boundary layer

$$\tau_0 = \mu \left(\frac{\partial u}{\partial y}\right)_{y=0} \quad \text{and} \quad \delta \simeq 3\delta_1 \quad \ldots\ldots\ldots\ldots\ldots\ldots\ldots\ldots (9)$$

and, in the turbulent case

$$\tau_0 = 0.0225\,\rho U^2 \left(\frac{\nu}{U\delta}\right)^{1/4} \quad \text{and} \quad \delta \simeq 8\delta_1 \quad \ldots\ldots\ldots\ldots\ldots\ldots\ldots (10)$$

Provided that some assumption is made concerning the origin of the boundary layer or its displacement thickness then Eq. 7 may be solved to give D as a function of x using Eqs. 9 or 10 to evaluate shear stress.

The merit of the author's approach, which is fundamentally similar to that aforementioned, lies in the use of nondimensional ratios of depth and displacement thickness in a most generalized form. Care would, however, need to be exercised in the use of this approach.

As a rule, the two common examples of open channel boundary layer development are those due to flow from a sluice gate and over a crest.

The writer has experience of boundary layer calculations in the latter case and would point out that streamline curvature causes a free vortex type velocity distribution over the crest.

If displacement thickness is defined by Eq. 2 then, in this case, the result is a negative value for δ_1 because the velocity at the edge of boundary layer is greater than that at the free surface.

The definition of critical depth as given by Eq. 5 is open to criticism. A clear exposition of critical depth is given by Jaeger (10) in terms of discharge, energy, and momentum and he shows that critical depth is unique.

The effect of boundary layer is to distort the velocity distribution, critical depth being modified by use of the usual correction coefficients.

There can be no justification for adding displacement thickness to the critical depth for potential flow. One might just as well add the momentum or energy thicknesses to give three different results, which is unacceptable.

The depth D_c as defined by the author is a useful reference datum but, though close to, is not equal to the critical depth.

Appendix I.—Reference

10. Jaeger, C., *Engineering Fluid Mechanics*, Blackie and Son Ltd., London, England, 1961, pp. 110–112 and 138.

Appendix II.—Notation

j = rate of degradation of mechanical energy;
δ = boundary layer thickness;
μ = dynamic viscosity of fluid;
ν = kinematic viscosity of fluid;
ρ = density of fluid; and
τ_0 = boundary shear stress.

Scour Velocities in Ephemeral Channels[a]

Discussion by Subhash C. Mehrotra[2]

The paper is a welcome addition to the existing literature on scour velocities. It is professedly devoted to "variable short duration discharges as opposed

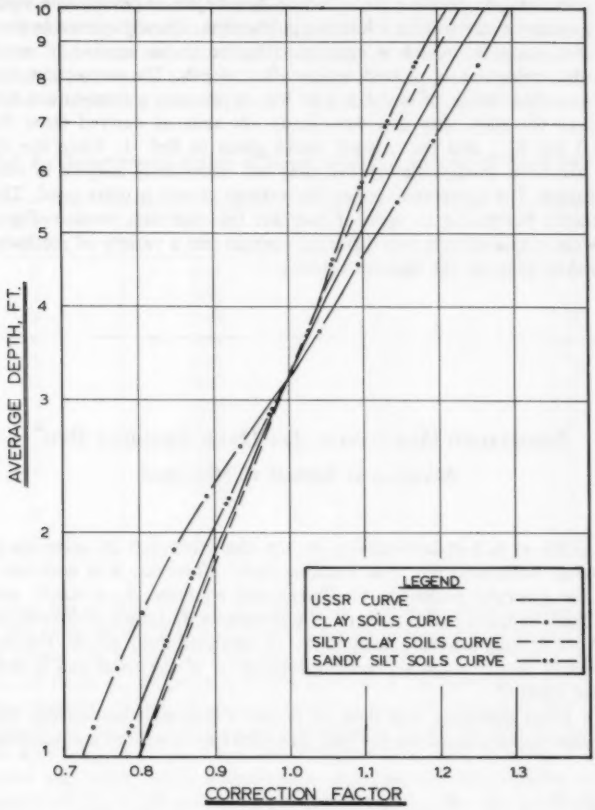

FIG. 4.—Correction Factor for Permissible Velocities as Function of Flow Depth

to long-term constant flows." The writer feels that the distinction between the two types of flows, as far as their eroding potentials are concerned, has not

[a]September, 1980, by William C. Hughes (Proc. Paper 15701).
[2]Engrg. Specialist, Bechtel Inc., Gaithersburg, Md. 20760.

been clarified. Are the variable short duration discharges still in a stage of evolution and therefore unsteady? Or do the channel velocities refer to steady states, however short in duration? From a description given in the paper of the methods employed to estimate these velocities, it would appear that the answer to the latter query is in the affirmative. If this is the case, the duration of flow is of little importance in an ergodic sense. Thus, the results obtained in the paper are to be expected, viz. that "the accepted maximum permissible velocity values appear to be appropriate for channels subject to variable intermittent flow conditions as well as long-term constant flow conditions."

It is interesting to examine the effect of flow depth on permissible velocities. Ref. 1 presents a curve from a Russian publication, already quoted in the paper under discussion, in which a correction factor to be applied to maximum permissible velocities is plotted against flow depth. The correction factor is unity for a flow depth of about 3.2 ft. Fig. 4 presents a comparison between the curves for clay, silty clay and sandy silt soils as derived from Figs. 1, 2, and 3 for $V_{0.01}$ and the original curve given in Ref. 1. Since the derived curves are from small-scale figures, they are necessarily subject to errors of interpolation. The agreement among the various curves is quite good. This fact is especially heartening in view of the fact that the data used in Figs. 1, 2, and 3 were obtained from two different sources and a variety of methods were employed to estimate the channel velocity.

Submerged Horizontal Jet Over Erodible Bed[a]

Discussion by Subhash C. Mehrotra[3]

This paper is rich in information on the characteristics of submerged two-dimensional horizontal jets over erodible beds. However, it is deficient in its use of the powerful technique of dimensional analysis. As a result, some of the conclusions drawn in the paper may be erroneous, and many of the expressions derived are of very limited applicability. To illustrate these points, the authors' investigation of the boundary layer thickness, δ of the sand bed is critically examined herein.

For a given sediment and fluid, a proper functional relationship between steady-state value of δ and the problem variables can be written nondimensionally as:

$$\frac{\delta}{D} = f\left(\frac{U_0}{\sqrt{gD}}, \frac{L}{B_0}, \frac{L}{D}, \frac{x}{L}\right) \quad \ldots \ldots \ldots \ldots \ldots \ldots \ldots \ldots \ldots \ldots \quad (44)$$

Table 3 gives experimental values of the nondimensional parameters (the first three parameters within the parenthesis in Eq. 44) derived from the authors'

[a]November, 1980, by S. S. Chatterjee and S. N. Ghosh (Proc. Paper 15820).

[3]Engrg. Specialist, Bechtel Inc., Gaithersburg, Md. 20760.

data for runs 1–13. Suppose one wishes to examine the dependence of δ/D on $U_0/\sqrt{gD}$ at a fixed x/L. The proper approach to this examination would require that all other nondimensional parameters be held at constant values. One must, therefore, choose runs enclosed within bold lines in Table 3 only for this examination, in which L/B_0 and L/D are held at constant values (L/D actually changes over a small range). It is clear that in no set of such runs the range of variation of $u_0/\sqrt{gD}$ is large enough to enable one to make any general conclusion about the relationship between δ/D and $U_0/\sqrt{gD}$. Similar remarks would apply with respect to L/B_0. Indeed, the independence of δ with respect to B_0 claimed by the authors (Eq. 2) is the more surprising, since it seems intuitively clear that δ should increase with B_0 based on results relating to wall jets. The writer attempted, with considerable strain to his eyes, to discover a discernible pattern in the scatter of experimental points plotted in Fig. 6 with a view to detecting any relationship between δ and B_0 with U_0 kept constant.

TABLE 3.—Experimental Values of Nondimensional Parameters for Runs 1–13

Run number (1)	$U_0/\sqrt{gD}$ (2)	L/B_0 (3)	L/D (4)
1	0.76	33.0	2.31
2	0.92	33.0	2.27
3	1.08	33.0	2.22
4	0.52	22.0	2.31
5	0.67	22.0	2.30
6	0.95	22.0	2.17
7	1.18	22.0	2.21
8	0.31	16.5	2.27
9	0.59	16.5	2.26
10	0.67	16.5	2.24
11	0.42	13.2	2.26
12	0.49	13.2	2.24
13	0.56	13.2	2.22

Comparing run 4 with run 12, for example, could be helpful since U_0 was nearly the same in the two runs and B_0 varies, though not appreciably. With limited number of points to work with, it did appear that δ indeed increased with B_0 for fixed U_0. (Compare Δ with x.) It is to be noted also that because of large steepness of the variation of δ with x over the transition and erodible bed portions of the curve, the actual variation of δ with B_0 may be quite high without appearing to be so. Thus, the dropping of U_0 and B in Eq. 2 appears premature and hasty. Only a systematic experimental investigation covering wide ranges of $U_0/\sqrt{gD}$ and L/B_0 can definitively resolve this question.

Assuming now that δ/D is indeed found to be independent of $U_0/\sqrt{gD}$ and L/B_0, a systematic investigation of the variation of δ/D with x/L would require that it be done over a range of constant values of L/D. The expressions derived by the authors (Eqs. 16–21) are valid only for one value of L/D. (Unfortunately even this value changed at random, though by small amounts, in the authors' experiments.) As such, these expressions and their nondimensional

counterparts (Eqs. 22–27) are of very limited applicability.

In conclusion, the writer believes that the authors' study can be meaningfully extended in light of the foregoing discussion and hopes that they will undertake such an extension. The writer also believes that inclusion of data on scour profiles will greatly enhance the value of the paper.

Technical Papers

Original papers should be submitted in triplicate to the Manager of Technical and Professional Publications, ASCE, 345 East 47th Street, New York, N.Y. 10017. Authors must indicate the Technical Division or Council, Technical Committee, Subcommittee, and Task Committee (if any) to which the paper should be referred. Those who are planning to submit material will expedite the review and publication procedures by complying with the following basic requirements:

1. Titles must have a length not exceeding 50 characters and spaces.

2. The manuscript (an original ribbon copy and two duplicate copies) should be double-spaced on one side of 8-1/2-in. (220-mm) by 11-in. (280-mm) paper. Three copies of all figures and tables must be included.

3. Generally, the maximum length of a paper is 10,000 word-equivalents. As an *approximation*, each full manuscript page of text, tables or figures is the equivalent of 300 words. If a particular subject cannot be adequately presented within the 10,000-word limit, the paper should be accompanied by a rationale for the overlength. This will permit rapid review and approval by the Division or Council Publications and Executive Committees and the Society's Committee on Publications. Valuable contributions to the Society's publications are not intended to be discouraged by this procedure.

4. The author's full name, Society membership grade, and a footnote stating present employment must appear on the first page of the paper. Authors need not be Society members.

5. All mathematics must be typewritten and special symbols must be identified properly. The letter symbols used should be defined where they first appear, in figures, tables, or text, and arranged alphabetically in an appendix at the end of the paper titled Appendix.—Notation.

6. Standard definitions and symbols should be used. Reference should be made to the lists published by the American National Standards Institute and to the *Authors' Guide to the Publications of ASCE*.

7. Figures should be drawn in black ink, at a size that, with a 50% reduction, would have a published width in the *Journals* of from 3 in. (76 mm) to 4-1/2 in. (110 mm). The lettering must be legible at the reduced size. Photographs should be submitted as glossy prints. Explanations and descriptions must be placed in text rather than within the figure.

8. Tables should be typed (an original ribbon copy and two duplicates) on one side of 8-1/2-in. (220-mm) by 11-in. (280-mm) paper. An explanation of each table must appear in the text.

9. References cited in text should be arranged in alphabetical order in an appendix at the end of the paper, or preceding the Appendix.—Notation, as an Appendix.—References.

10. A list of key words and an information retrieval abstract of 175 words should be provided with each paper.

11. A summary of approximately 40 words must accompany the paper.

12. A set of conclusions must end the paper.

13. Dual units, i.e., U.S. Customary followed by SI (International System) units in parentheses, should be used throughout the paper.

14. A practical applications section should be included also, if appropriate.